TECHNOLOGICAL EDUCATIONAL INSTITUTE OF CRETE

SCHOOL OF APPLIED SCIENCES

DEPARTMENT OF NATURAL RESOURCES AND ENVIROMENT
SECTION: WATER RESOURCES AND GEO-ENVIROMENT
LABORATORY: ENVIROMENTAL GEO-INFORMATICS

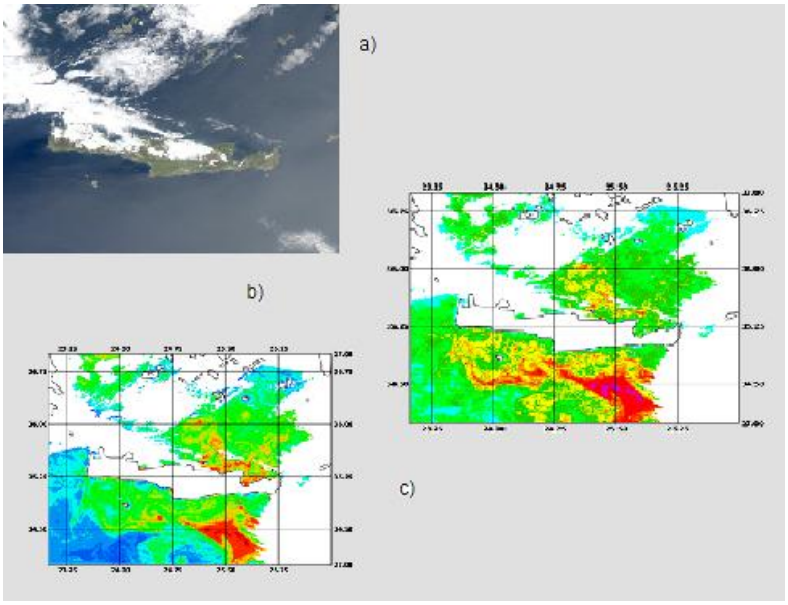

Different views according of 28 of April 2003; a) RGB image acquisition; b) ALICE index map; c) Chl-a concentration map

BACHELOR THESIS

Title:

"Monitoring Crete Coastal sea-water quality by Remote Sensing Techniques"

TOYRNAVITI PARASKEVI

Supervisor(s) Professor(s)

Dr. Lacava Teodosio - Researcher (Italy)
Dr. Kouli Maria - Laboratory Instructor (Greece)

CHANIA 2013

Acknowledgements:

I would like to thank Lapenna Vicenzo director of CNR in Potenza for giving me the opportunity to work into the Research Center for my traineeship. Also special thanks go to Satriano Valeria and Lacava Teodosio for patiently putting up with me and guiding me through the process, without them this thesis wouldn't have been possible.

Examination Committee:

1. **Dr. Kouli Maria**
2. **Dr. Soupios Panteleimon**
3. **Dr. Papadopoulos Ilias**

Περίληψη

Τα υδάτινα οικοσυστήματα είναι τα πιο παραγωγικά και σημαντικά οικοσυστήματα καθώς επίσης και τα πιο ευπαθή σε μεταβολές του περιβάλλοντός τους. Για να τα προστατέψει η Ευρωπαϊκή ένωση εξέδωσε μια οδηγία το 2000 που ορίζει πως όλα τα νερά της Ευρώπης πρέπει να μελετηθούν και να παρακολουθούνται συστηματικά ούτως ώστε να διασφαλιστεί η ποιότητα τους. Αυτή η οδηγία ορίζει πως μέχρι το 2015 το 80% του υδατικού όγκου της Ευρώπης πρέπει να χαρακτηρίζεται ως ¨πολύ καλό¨.

Για αυτό το λόγο το Δεκέμβρη του 2012 ξεκίνησε η ιδέα για ένα ερευνητικό πρόγραμμα συνεργασίας μεταξύ του Εθνικού Ερευνητικού Συμβουλίου της Ιταλίας και του ΤΕΙ Χανίων με το όνομα IOSMOS (IOnian Sea water quality MOnitoring by Satellite data), όπου προβλέπει τη μελέτη και την παρακολούθηση της συγκέντρωσης σε χλωροφύλλη α (chlor-a) στις νότιες ακτές της Ιταλίας και τις ακτές της Κρήτης με δεδομένα που λαμβάνονται από τα αρχεία του προγράμματος Ocean Color (OC) της NASA και τον αισθητήρα MODIS που βρίσκεται αυτή τη στιγμή σε λειτουργία για χάρη του ίδιου προγράμματος (OC).

Για την επεξεργασία και διεξαγωγή των δεδομένων χρειάστηκε η εφαρμογή αυτοσχέδιων προγραμμάτων σε περιβάλλον LINUX, προγράμματα τηλεπισκόπησης (όπως το Geomatica) και προγράμματα GIS (όπως το QGIS). Η καινοτομία που εφαρμόστηκε σε αυτό το πρόγραμμα είναι η εφαρμογή της τεχνικής RST (Robust Satellite Technique), είναι μία στατιστική μέθοδος απαλοιφής του θορύβου από τα δεδομένα και ενίσχυσης του σήματος για την καλύτερη ανίχνευσή του και άρα για καλύτερης ποιότητας αποτελέσματα.

Τα δεδομένα μετά την επεξεργασία τους παρουσιάστηκαν σε χάρτες χρωματικής κλίμακας για την ευκολότερη απεικόνισή τους και κατανόηση τους.

Contents

INTRODUCTION

Coastal ecosystems, defined as those areas which include the coastal lands, the areas of transitional waters, and near shore marine areas, these are among the most productive yet highly threatened systems in the world (EEA, 2006). They provide a wide range of economic benefits to many sectors, such as navigation, fisheries, aquaculture, industries (including oil and gas extraction, wind farms), and recreation activities. This is why population density is higher on the coast than inland; indeed about 25% of the world's population resides in these areas (Small and Nichols, 2003).

On the other hand, coastal ecosystems, being constituted by a wide range of different habitats, are very dynamic and complex systems. The increasing level of urbanization, the ever more irrational exploitation of those areas and, more generally, climate changes are causing severe changes in coastal areas, representing a threat to the present biodiversity as well as for their geo-morphological equilibrium (Small and Nichols, 2003). The European Community, with different actions, such as the Water Framework Directive 2000/60/EC and the Integrated Coastal Zone Management Recommendation 2002/413/EC provided clear indications on the need to prevent the deterioration of water quality in these ecosystems at European level, as well as to maintain and improve their status by 2015.

One of the main constituent of sea water is phytoplankton (i.e., the unicellular microscopic algae living in the upper layer of all water bodies across the world). The phytoplankton through photosynthesis, allows the transformation of inorganic carbon into organic carbon and its storage in biomass; in this way phytoplankton contributes to the carbon cycle and in addition, it is the main element at the basis of marine food chain. It is clear that a variation in phytoplankton may have dramatic consequences on marine environments both at local and global scale. This is why a lot of effort has been made to understand the physical processes affecting the spatial distribution and temporal development of phytoplankton biomass. The growth-limiting factor of phytoplankton is the availability of light and nutrients which depend in turn on physical processes such as general ocean circulation, deep water formation, mixed-layer dynamics, upwelling and the solar cycle. In the framework of a continuous monitoring of the health of coastal ecosystems is therefore also crucial to monitor the content and variability of phytoplankton.

A system that can provide reliable and frequently updated data about its presence and variability might be effective in a timely identification of critical conditions, preventing further situations of degradation. In detail, such a system should be able to observe chlorophyll, which is the most widely used proxy for the study of the distribution of phytoplankton biomass.

Monitoring spatiotemporal variations of chlorophyll by in-situ techniques, based on the collection of the sea water sample and its subsequent laboratory analysis, requires time, effort and high costs; this is why such measurements can be performed only on a small spatial and temporal scale, not ensuring early detection of potentially critical situations.

Satellite data represent an essential observational tool which offers a unique perspective on the natural environment. Thanks to the synoptic view and the high sampling frequency and high spatial resolution, remotely sensed data have been successfully used to provide unique and important information about the phenomena occurring on the sea surface. Data acquired by active and passive sensors in a very large portion of the electromagnetic spectrum (from visible to microwave); have been in fact used to analyze several parameters relate to sea water: temperature, salinity, constituents.

In particular, by using visible radiation, a specific remote sensing discipline, the *Ocean Color* (OC) radiometry, has started. As suggested by the name, OC is focused on deriving sea bio-optical parameters capable to affect the color of the sea water. One of the OC parameters retrievable by satellite measurement is the chlorophyll. Different algorithms for chlorophyll-a (Chl-a) concentration retrieval have been defined and applied on different satellite sensors. In particular in this work we analyzed the Chl-a product obtained by implementing the OC3 algorithm (O'Reilly et al., 1998; 2000) on Moderate Resolution Imaging Spectroradiometer (MODIS) data. MODIS is still operational onboard of Terra and Aqua Earth Observing System (EOS) satellites, the sensor which assures the best trade-off between spatial (up to 250 m) and temporal (up to 3 hours) resolution with a good spectral resolution in the visible region of the electromagnetic spectrum. In addition, more than ten years of nearly continuous, consistent and reliably-calibrated record of remotely-sensed chlorophyll is available at the NASA OC web portal, guaranteeing also long period analysis.

To cover the WFD the IOSMOS (IOnian Sea water quality MOnitoring by Satellite data) project started, the kick off meeting of the project was in December 2012. This project is a collaboration

between CNR ((Consiglio Nationale delle Ricerche)=(National Resaerch Council) of Potenza in Italy and TEI (Technological Educational Institute) of Chania in Greece the starting day for Italy was at February 2013 and in Greece is expected to start at November 2013. The purpose of the project is to monitor the quality of coastal water to detect chlor-a concentration by using remote sensing techniques and also checking the adaption of RST (Robust Satellite Technique) by using OC data, this is a general analysis of Crete Island.

In this thesis ten years (2003-2012) of MODIS OC Chl-a products concerning the sea water surrounding the Crete Island have been analyzed by the Robust Satellite Techniques (RST – Tramutoli, 2005, 2007) approach. RST is a general technique for the analysis of satellite data which have been already successfully applied for the investigation of different natural an environmental processes occurred on the Earth's and Ocean surface. RST, being based only on satellite data, is inherently exportable to different geographic regions and to different satellite data. Crete Island is a good candidate for such an application: about 1,046 km of coastline, with different natural, environmental and climatologically features between the North and South area of the island, an economy based on agriculture and mostly on tourism industry. All these features act together to increase the natural and human pressure on the marine ecosystem, which deserves an adequate system of observation.

By implementing RST on historical series of MODIS OC Chl-a products, the main objectives of this work are:

- The identification of long term (2003-2012) trend of chlorophyll-a variation for the sea water surrounding the Crete Island.
- The identification of possible critical situations at different temporal scale.
- The development of an operational system able to timely identifying any sign of water degradation in terms of chlorophyll-a concentration variation.

Obviously, while trying to reach these objectives, the capability and the limits of the remote sensing observations, to monitor the marine status at short and long time scales will be also investigated.

The thesis is organized as follows: Chapter 1 presents and overview of the problem investigated in this work, namely the monitoring of chlorophyll concentration in coastal waters. In Chapter 2, the basic physical principles of Remote Sensing and the some of the specific concepts of Ocean Color

are described. Moreover a short state of the art of chlorophyll concentration retrieval by satellite oceanography is presented. Chapter 3 presents the Robust Satellite Techniques and its specific implementation to Chl-a analysis. Chapter 4 shows the main results achieved implementing RST on historical series of Chl-a products related to the sea water surrounding the Crete Island. Finally, Chapter 6 draws the main conclusions of this thesis.

Chapter 1 Monitoring Chlorophyll concentration in coastal waters

In this chapter after a brief description of the main features of the coastal ecosystem and of the main regulations at European level concerning sea water quality monitoring, the relevance of the chlorophyll within such an ecosystem will be detailed discussed, providing also a summary about the main methodologies used for its measurement.

1.1 The coastal-marine habitat

Generally speaking the coastal zone is the environment which results from the coexistence of two margins: coastal land, defined as the terrestrial edge of continents; and coastal waters, defined as the littoral section of shelf areas (EEA, 2006). The terrestrial portion of the coastal zone is defined by an area extending 10 km landwards from the coastline. The marine part of the coastal zone is defined as a zone extending 10 km offshore (EEA, 2006).

Estuaries and coastal zones are among the most productive ecosystems in the world, with both high ecological and economic values (EEA, 2010). They provide a wide range of economic benefits to many sectors (Figure. 1.1), such as navigation, fisheries, aquaculture, industries (including oil and gas extraction, wind farms), and recreation activities (EC Guidance on the implementation of the EU nature legislation in estuaries and coastal zones 2001).

Figure 1.1:Several examples of the coastal-marine habitat.

Coastal areas are the place where more than 45 per cent of the world's population lives and works: 75 per cent of the mega-cities with populations over 10 million are located in coastal zones (world ocean review Living with the oceans. 2010). All over the world the population in coastal zones is growing faster than in any other region on Earth.

However, estuaries and coastal zones, being made up of a wide range of different habitats, are very dynamic and complex ecosystems. The above mentioned growing level of urbanization, the irrational exploitation of resources and the climate changes are causing a strong modification of the coastal areas (Figure 1.2), representing a continuous threat to the biodiversity of these zones (EEA, 2010).

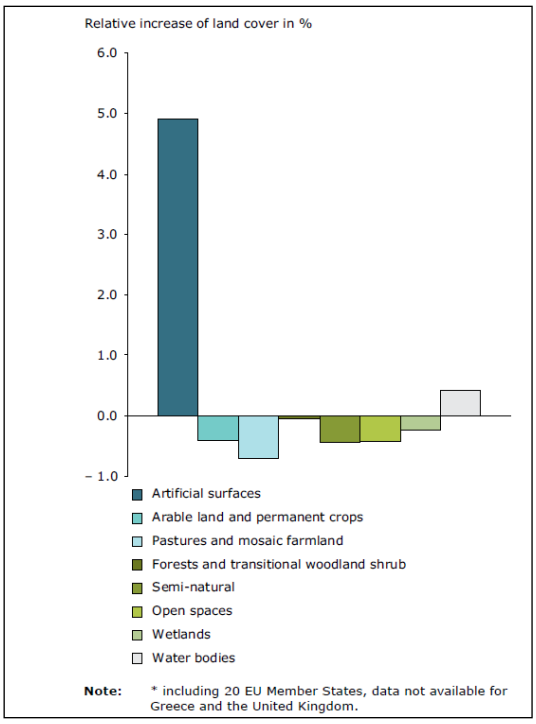

Figure 1.2: Relative change in land cover within 10 km of the coast in 27 European countries * 2000–2006

To preserve the general health of these areas, ensuring the survival of the most threatened coastal and marine species, it is necessary to develop suitable monitoring system, able to provide timely information about the possible changes occurring on these areas. This situation is particularly true in Mediterranean Sea, which is considered the most complex sea, from a biologically point of view, in Europe.

Indeed over than 50% of Mediterranean species comes from the Atlantic Ocean, 17% from the Red Sea, including ancient species and newly discovered ones, also 4% considered as relic species (EEA, 2010). In this framework, European Union, in order to preserve the costal ecosystems, protecting also the citizens who live there and trying to leave a better environment for the next generations, redacted regulations aimed at improving and saving the sea water quality.

1.2 The European Water Framework Directive (WFD)

On 23 October 2000, the "Directive 2000/60/EC of the European Parliament and of the Council establishing a framework for the Community action in the field of water policy" or, in short, the EU Water Framework Directive (or even shorter the WFD) was finally adopted. The Directive was published in the Official Journal (OJ L 327) on 22 December 2000 and entered into force the same

day. The Water Framework Directive establishes a legal framework to protect and restore clean water across Europe and ensure its long-term, sustainable use. The directive establishes an innovative approach for water management based on river basins, the natural geographical and hydrological units, and it sets specific deadlines for Member States to protect aquatic ecosystems. The directive addresses inland surface waters, transitional waters, coastal waters and groundwater, and it establishes innovative principles for water management, including public participation in planning and economic approaches and also the recovery of the cost of water services.

Among the Twelve "Water notes" which intend to give an introduction and overview of key aspects of the implementation of the WFD, the number 6 is focused on Monitor Program. Monitoring is the main tool used by Member States to classify the status of each water body (a water body is a section of a river or other surface water or a distinct volume of groundwater). The directive sets a five-class scale - high, good, moderate, poor and bad status - for surface waters, and two classes - good and poor - for groundwater, and it requires Member States to achieve good status in all waters by 2015. Once Member States have determined the current status of their water bodies, then monitoring helps Member States to track the effectiveness of measures needed to clean up water bodies and achieve good status.

The monitoring of surface waters thus covers their chemical composition, a number of key biological elements, and their hydrological and morphological characteristics in order to provide a comprehensive overview of the health of Europe's waters. Water monitoring programs cover water quality and quantity; the directive specifies three types of monitoring.

Long-term surveillance monitoring provides a broad understanding of the health of water bodies and tracks slow changes in trends such as those resulting from climate change. Operational monitoring focuses on that bodies which do not meet good status and on the main pressures they face – pollution where this is the main problem, water flow where extraction creates risks. Operational monitoring thus tracks the effectiveness of investments and other measures taken to improve the status of water bodies. Member States also undertake investigative monitoring when they need further information about surface water bodies that cannot be obtained via operational monitoring, including information on accidents.

The implementation of the Water Framework Directive raises a number of shared technical challenges for the Member States, the Commission, the Candidate and EEA Countries as well as

stakeholders and NGOs. In addition, many of the European river basins are international, crossing administrative and territorial borders and therefore a common understanding and approach is crucial to the successful and effective implementation of the Directive.

Furthermore, the Directive 2007/60/EC on the assessment and management of flood risks shall be closely coordinated with the Water Framework Directive; in Figure 1.3 the status of the implementation River basin management plans for each European country updated at November 2012 is reported. As you can see, in few European regions, including Greece, the WFD and the Directive 2007/60/EC have been not adopted yet.

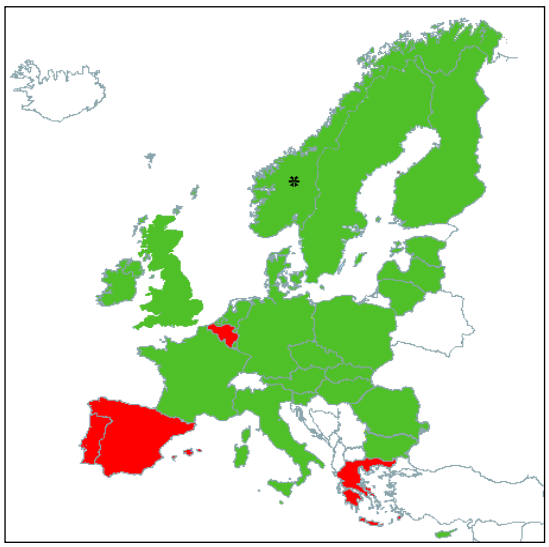

Figure 1.3:The status of the implementation River basin management plans for each European country updated at November 2012 (GREEN - River Basin Management Plans adopted; YELLOW - consultations finalized, but awaiting adoption; RED - consultation have not started

1.3 Chemical and physical properties of seawater

The seawater is a composition of various chemical elements that can be organic, inorganic and ions. The most important ions are are Chloride (Cl^-), Sodium (Na^+), Sulfate (SO_4^{2-}), Magnesium (Mg^{2+}), Calcium (Ca^{2+}) and Potassium (K^+), and represent about 99 per cent of all sea salts.

The other category of dissolved substances in sea water includes inorganic components like carbon, bromide, boron, strontium and fluoride; there are also many minor chemical constituents like inorganic phosphorous and inorganic nitrogen which are important for the growth of organisms, like chlorophyll, that inhabit the sea. Furthermore there are some dissolved atmospheric gases, such can be nitrogen, argon, carbon dioxide and oxygen.

Seawaters compounds are also Dissolved Organic Matter (DOM), that when colored is defined as Colored (or Chromophoric) Dissolved Organic Matter (CDOM) Matter: such substances can be carbohydrates, amino acids and organic rich particulates. They originate primary in the upper 100 meters of the water body, where dissolved inorganic carbon is transformed into organic matter, phytoplankton, through the procedure of photosynthesis (Encyclopaedia Britannica).

Among the elements which are part of seawater system, the phytoplankton (i.e., the unicellular microscopic algae living in the upper layer of all water bodies across the world) is the most relevant one, because it directly influences sea water ecosystem life. A variation in the content of phytoplankton may produce dangerous effect on the whole coastal ecosystem for different reason which will be better described in the next paragraph, where also its main proxy, the chlorophyll, will be also introduced and discussed.

➢ 1.3.1 The Phytoplankton

Phytoplankton is defined as the microscopic photosynthesizing organisms that live in watery environments both salty and fresh. (Figure 1.4). The phytoplankton through photosynthesis, allows the transformation of inorganic carbon into organic carbon and its storage in biomass. The speed with which this biomass is created and made available to the successive trophic levels is called primary production. Phytoplankton growth depends on the availability of sunlight and nutrients. Nutrients (nitrates, phosphates, silicates, etc.) are found in great quantities in the deeper, colder depths of the ocean (NASA website) and they are able also to fix nitrogen and grow in areas where nitrate concentrations are low. Phytoplankton needs also very small amounts of iron, and this can be a limit for its increasing in large areas of the ocean where iron concentrations are not so high. Other factors that influence phytoplankton growth rates are: water temperature and salinity, water depth, wind, and some kinds of predators which are grazing on them.

Figure 1.4: Sample of phytoplankton types

Looking for the phytoplankton large-scale distributions in the ocean, we can see how closely it is related to areas where nutrients are located on the surface water; here the surface appears in greenish color due to the chlorophyll pigment contented in microorganisms.

Microscopic organisms, called zooplankton, grow by feeding from phytoplankton: these little animals are then eaten by larger zooplankton, fish to continue in the food chain till blue whale. It is clear that Phytoplankton represents the first link in the marine food web (Figure 1.5), and this why if it disappears, the food chain is broken with a lot of damages on aquatic flora and fauna. (NASA web-site).

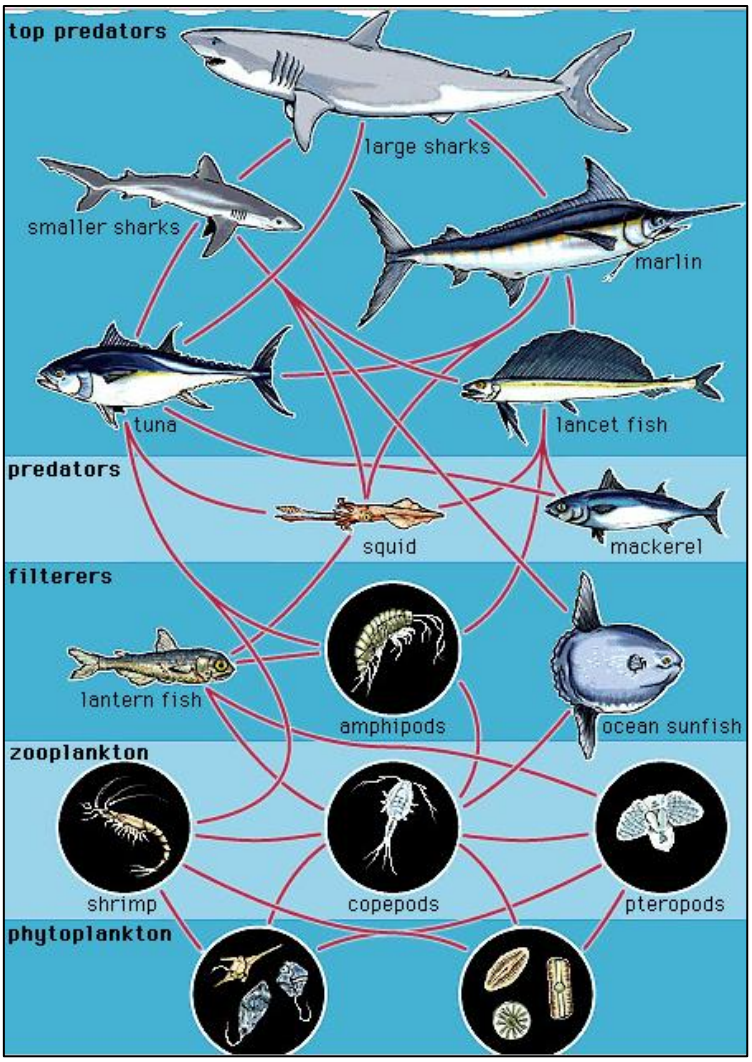

Figure 1.1.5: Marine food chain.

However also an excessive presence of phytoplankton could be dangerous: it produces toxins that can be harmful to marine life and, in some cases, to humans as well. When its growth is stimulated by an overabundance of nutrients from sources such as sewage discharge or runoff of agricultural fertilizers used on land, the consequences can be serious: dense blooms of phytoplankton can essentially block sunlight from reaching the bottom in shallow areas of bays or estuaries and can cause the massive decline in the Submerged Aquatic Vegetation (SAV).

This extreme water condition is called eutrophication, more general defined as the "*process of natural or human enrichment with inorganic nutrient elements, beyond the maximum level of capacity of a given system for a balanced flow and cycling of nutrients*" (Marine Benthic Vegetation, Recent Changes and the Effects of Eutrophication; *Dr. Winfrid Schramm, Dr. Pieter H. Nienhuis, 1996, Springer Publications*). When these blooms die and the plankton sink to the

bottom, bacterial decomposition of all this organic matter essentially strips the water of oxygen. Fish, shellfish and most other living things require oxygen to survive, this is why decaying phytoplankton blooms have been the cause of many massive fish kills over the years.

One of the phytoplankton that can be directly harmful is the *dinoflagellates*, they are the source of red tides (Figure 1.6)

Figure 1.6: Example of Red tide

➢ 1.3.2 Chlorophyll

The chlorophyll is the most widely used proxy for the study of the distribution of phytoplankton biomass. Valuating chlorophyll concentration is a direct way to track algal growth and have an indirect monitoring detection of indicator pollutants, including phosphorus and nitrogen. Chlorophyll is contained in the living cells of algae and other phytoplankton found in surface water; it has an important role in the molecular apparatus that is responsible for photosynthesis, the process in which the energy from sunlight is used to produce life-sustaining oxygen:

$$6CO_2 + 6H_2O \xrightarrow[Chlorophyll]{Sunlight,} C_6H_{12}O_6 + 6O_2 \qquad \text{(Eq.1.1)}$$

Chlorophyll is present in different organisms as algae and bacteria and in different type: chlorophyll-*a* is the most common and gives the green color to the plants; the b, c and d types are rarer and increase the overall fluorescent signal. (The Basics of Chlorophyll Measurement, YSI).

The main difference between chlorophyll *a* and *b* is the portion of the electromagnetic spectrum in which they absorb the radiation (Figure 1.7); the chlorophyll *b* absorption bands coincide with the inflection bands at 460 nm and 650 nm, with a pick in correspondence of 675 nm. On the other

hand the inflection bands at 580 nm, 630 nm and 670 nm coincide with three of the absorption bands of chlorophyll *a*; the 700 nm band is the one that chlorophyll *a* is absorbing less.

For chlorophyll concentration estimation the first one is mostly used, because the rate of photosynthesis was related best to its concentration than the other (Ratio Analysis of Reflectance Spectra (RARS).: An Algorithm for the Remote Estimation of the Concentrations of Chlorophyll a, Chlorophyll b, and Carotenoids in Soybean Leaves; Emmett W. Chappelle, Moon S. Kim and James E. McMurtrey III, 1992, Elsevier Science Publishing).

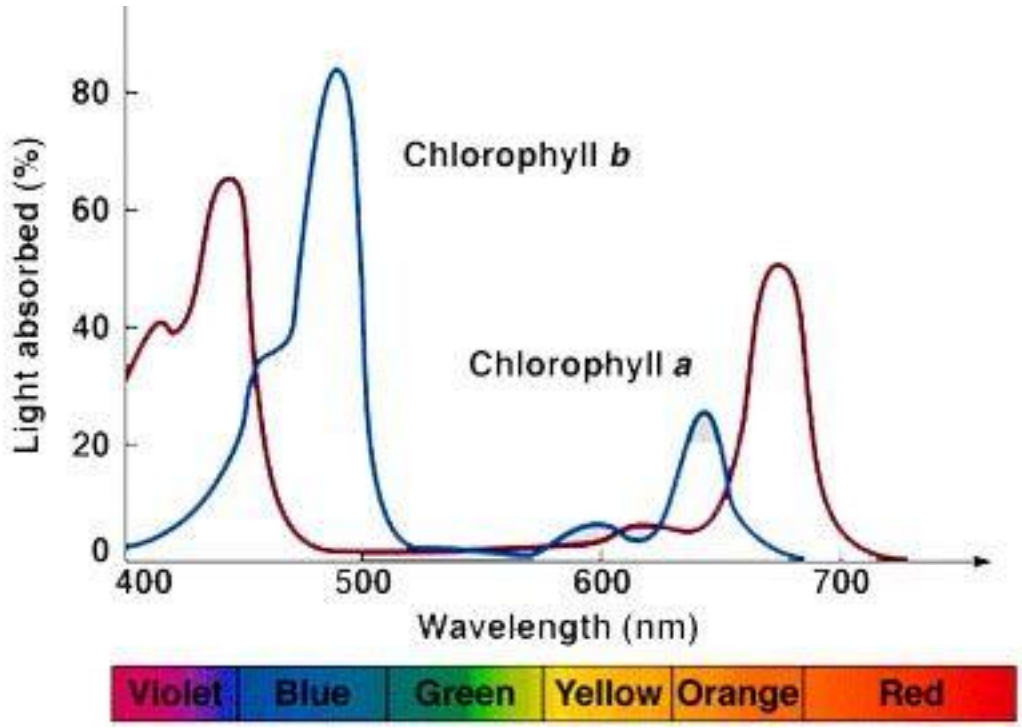

Figure 1.7:absorption spectrum of chlorophyll a and b

These types of chlorophyll can be present in all photosynthetic organisms but vary in concentrations. According to this variability, waters are divided in two categories: Oligotrophic and Eutrophic. The first one is characterized by concentration arriving till 0.3mg/m3 (Validation of empirical SeaWiFS algorithms for chlorophyll-retrieval in the Mediterranean Sea, A case study for oligotrophic seas; Fabrizio D'Ortenzio, Salvatore Marullo, Maria Ragni, Maurizio Ribera d'Alcalà, Rosalia Santoleri, 2002, Elsevier), and is characterized by extremely low nutrient contents. These waters are consequently poor areas for the development of extensive aquatic floras and faunas, on the other side they are very clean thanks to a high dissolved oxygen levels.

The Eutrophic waters have an high level of phytoplankton as a response to increased levels of nutrients, but a very low concentration of oxygen, which induces reductions in specific fish and other animal populations. The nutrients are deposited from the rivers and this is why eutrophism is encountered mostly at coast lines and lakes and during winter months: in that season, in fact, the copious rainwater events generate run-off phenomena and drifts nutrients from the land into the rivers and consequently in the sea. (Eutrophication in the Baltic Sea: An integrated thematic assessment of the effects of nutrient enrichment in the Baltic Sea region; Helsinki Commission Baltic Marine Environment Protection Commission, 2009).

Chlorophyll high concentration indicates high algal bloom activity, which in large scale may destroy the aquatic ecosystem; measuring and monitoring its concentration can give us valuable information about the water's quality and warning in case of peculiar blooming activity, in order to avoid pollution (Chlorophyll-a raw water quality parameter, R. Anne Jones and G. Fred Lee,1982, American Water Works Association).

1.4 Chlorophyll Estimations

Chlorophyll can be measured by two different methodologies. by *in-situ* measurement and by remote sensing techniques.

In situ measurements provide punctual information at high level of accuracy. They are time consuming and costly, especially if large area has to be monitored which a high time frequency. In the following, an example of *in-situ* approach is described.

The procedure requires that researcher retrieves samples from the water body and takes them to the laboratory; here the water can be chemically analyzed in order to verify chlorophyll concentration. It should be stressed that, once acquired, water sample should be kept in dark and refrigerated bottles, in order not to photosynthesize further after they are obtained, and analyzed within 24 hours.

Analytical procedure:

1. Filter 50 to 500mL of a thoroughly mixed water sample through a 0.45 μm pore diameter membrane filter. A distilled water blank should be processed along with each set of samples.

2. When a few milliliters of unfiltered sample are left into the filter funnel, add 0.2 mL of saturated magnesium carbonate solution. Before pipetting the solution shake it to suspend

the precipitated magnesium carbonate; in the blank distilled water should be also add this solution during the filtration.

3. After filtration is complete carefully remove the filter from the holder and place it in a 15mL, graduated, screw-cap centrifuge tube.

4. Add 5 mL of 90% acetone (v/v) to the centrifuge tube, tighten the crew cap, wrap the tube in aluminum foil, for protection from light, and shake it vigorously; afterwards place the tube in the dark at 4˚C, for approximately 24 hours.

5. After the time passes, remove the aluminum foil from the tube and add 90% of acetone to fill the tube (till it reaches the 15mL). Centrifuge in a table-model, clinical centrifuge at 500g for 20 min.

6. Read and record the volume of acetone extract in the tube, then carefully decant the supernatant from the tube into a spectrophotometric cell. Determine the absorbance of the supernatant at 750, 663, 645 and 630nm wavelengths of the spectrum; use the 90% acetone before the measurement to set the zero for each of the wavelengths. Repeat the steps for each supernatant and the blank.

The light path for such spectrophotometric readings should be selected so that the absorbance at 663 nm to be between 0.1 and 0.7, with ideal value around 0.3; if the chlorophyll concentration is low the light path takes more time to cross through the water sample.

7. To correct turbidity, subtract the absorbance readings from the 750 nm from the other three wavelength readings and use the corrected absorbance values to calculate chlorophyll (C_a) from the **Eq. 2**.

$$C_a = 11.64A_{663} - 2.16A_{645} + 0.10A_{630} \qquad \text{(Eq.1. 2)}$$

Where C_a is the concentration of chlorophyll a in the extract and A is the corrected absorbance at a particular wavelength. Use the C_a to **Eq. 3** to calculate chlorophyll-a concentration (Chlorophyll-a raw water quality parameter, R. Anne Jones and G. Fred Lee, 1982, American Water Works Association).

$$\left(chlorophyll\ a, {}^{\mu g}/_{L}\right) = \frac{C_a(volume\ of\ extract, mL)}{(volume\ of\ sample, L)(light\ path, cm)} \qquad \text{(Eq.1. 3)}$$

In this work, chlorophyll-a (that we call by now more simply Chl-a) variations of concentration have been detected by using remote sensing techniques. In the next chapter, basic remote sensing principles and Chl-a retrieval methodologies are described.

Chapter 2 Satellite Remote Sensing techniques for sea water investigation

In this chapter the fundamental elements of Remote Sensing will be first described, after that more details will be furnished concerning its specific application, the Ocean Color radiometry, to sea water investigation.

2.1 Introduction

Generally speaking, Remote Sensing (RS) can be defined as the capability of obtaining information about an object without being in physical contact with it (Gupta, 1991). Hence two are the main aspects to be taken into account: i) the use of a technology able to acquire information through a device which is located at a distance from the object and ii) the analysis of the data for retrieving the physical attributes of the investigated object. The distance which can divide the sensor from the object may vary from few kilometers (airborne platforms) to hundreds kilometers (satellite platforms) (Figure 2.1), in both cases the electromagnetic radiation (em) is the only mean that can link sensor and object. Therefore remote sensing ends up meaning acquisition of electro-magnetic radiation from sensors mounted on aerial (airplane) or space (satellite) platforms, and its interpretation for identifying object characteristics.

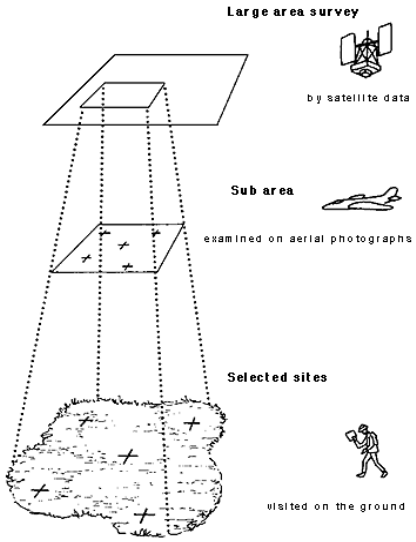

Figure 2.1Different scale of Earth observation: from satellite, airplane and ground

The basic principle of remote sensing is that whatever natural/artificial body emits and/or reflects electromagnetic radiation at different wavelength ranges of the electromagnetic spectrum depending on its own physical/chemical features. So that, provided that devices suitable for

detecting electromagnetic radiation at different wavelength are used, it will be possible to recognize the body that produced them (Rees, 1990).

Remote sensing techniques can be classified in two main categories: passive (Figure 2.2a) and active (Figure. 2.2b). In the latter the investigated object is sensed by an artificial electromagnetic source which belongs to the observational system, while in the first case natural sources of electromagnetic radiation, such as the Sun and the Earth, are used.

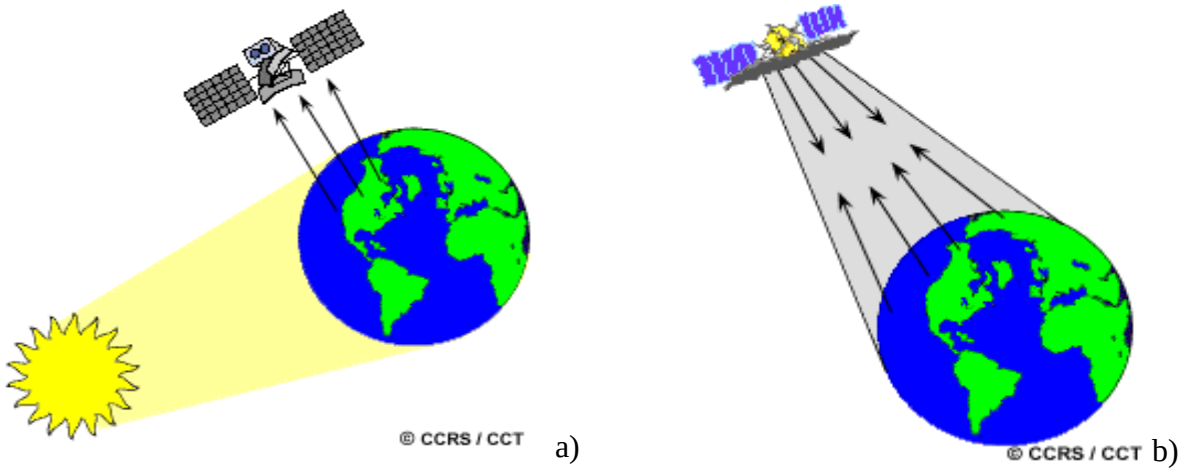

Figure 2.2 Different remote sensing techniques a) passive, b) active.

Compared to the other traditional ground based techniques, Remote Sensing presents a lot of advantages:

- Synoptic Overview: large areas, also poorly or/not accessible from the ground, can be seen during each single acquisition. This allows also studying the correlation among different spatial features and the delineation of regional trends.
- High sampling frequency rate: depending on the platform/sensor system, the same area can be seen in different period, allowing for specific monitoring system program.
- Multi-disciplinary application: on the same platform several sensors acquiring information in different regions of the electromagnetic spectrum can be present; moreover the same data may be used for retrieving different parameters.

On the other side, the main issue of RS techniques is the impossibility of having data both with a high temporal resolution and a high spatial resolution. In addition, often the rate of data acquired is very high, so that, adequate elaboration/archiving systems need.

2.2 Electromagnetic spectrum

As said before, electromagnetic radiations serve as the main connection link between the sensor and the object, all electromagnetic radiation has fundamental properties and behaves in predictable ways according to the basics of wave theory. Electromagnetic radiation consists of an electrical field (E) which varies in magnitude in a direction perpendicular to the direction in which the radiation is traveling, and a magnetic field (H) oriented at right angles to the electrical field (Figure 2.3).

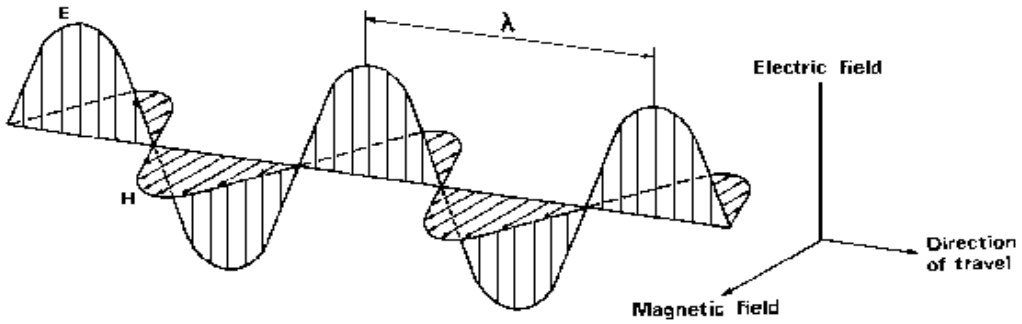

Figure 2.3 Electromagnetic wave

Two characteristics of electromagnetic radiation are particularly important for understanding remote sensing. These are the wavelength and frequency. The wavelength (λ) is the length of one wave cycle, which can be measured as the distance between successive wave crests. Wavelength is measured in meters (m) or some factor of meters such as nanometers (nm, 10^{-9} meters), micrometers (μm, 10^{-6} meters) or centimeters (cm, 10^{-2} meters). Frequency refers to the number of cycles of a wave passing a fixed point per unit of time. Frequency (ν) is normally measured in hertz (Hz), equivalent to one cycle per second, and various multiples of hertz. Wavelength and frequency are related by the following formula:

$$c=\nu\lambda \qquad \text{(eq. 2.1)}$$

Where c is the speed light (2.99793×10^8 m/s), Therefore, the two are inversely related to each other: the shorter (longer) the wavelength, the higher (lower) the frequency.

The electromagnetic spectrum (Fig. 2.4) represents the set of all possible wavelengths (or frequencies) of the electromagnetic radiation. It extends from Gamma Rays ($\lambda < 0.03$ nm) to Radio Wave ($\lambda > 1$ m).

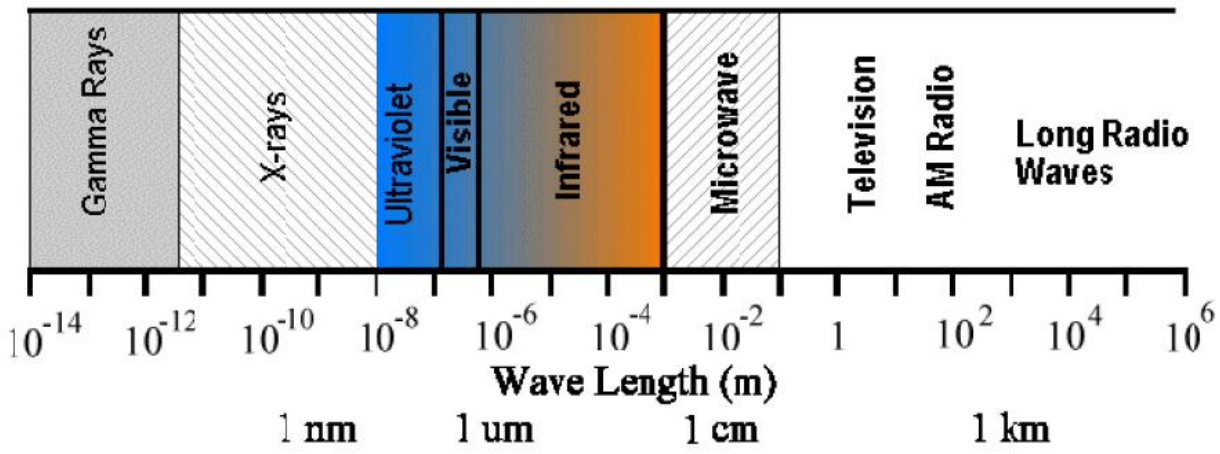

Figure 2.4 Electromagnetic Spectrum

The waves at smallest wavelength are the Gamma rays (λ <0.03 nm) that are completely absorbed by the atmosphere and are not available for the RS; then follow the X-ray (0:03 nm < λ <0.03 μm) which still are not used for RS purposes. Immediately before the area of the visible (VIS), there are the ultraviolet (UV - 0:03 μm < λ <0.4 μm) that are partly transmitted by the atmosphere; then follows the visible, which RS techniques mostly use. After the visible we find the range of the visible infrared (0.7 μm < λ <1 mm) which are divided into two ranges: the reflected infrared and thermal ones (TIR), the first include the sensitive portion of solar radiation reflected from the earth (0.7 - 4 μm, NIR plus SWIR plus MIR), whereas the latter include the spectral bands dominated by the contribution of the radiation emitted from the Earth. For wavelengths longer than 1 mm, we find the microwave (MW), followed by radio waves (Figure 2.4).

Visible range covers the spectral interval between 0.4 and 0.7 μm, the same which is sensitive human eye. It can be divided into smaller portions each corresponding to a particular color (Fig. 2.5).

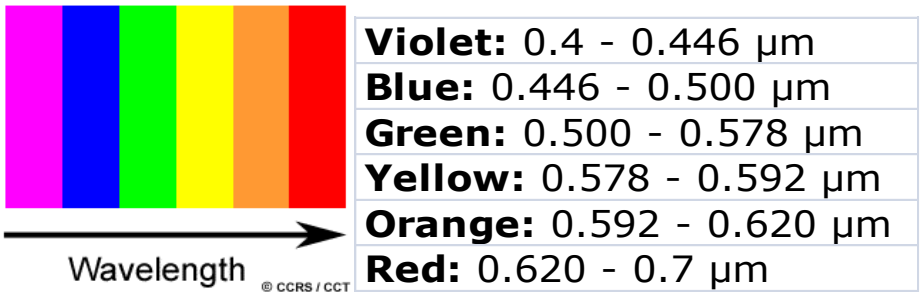

Figure 2.5 Visible range of the electromagnetic spectrum

The energy transfer in the atmosphere essentially occurs in the portion between the ultraviolet rays and microwaves (0:03 μm < λ <1 mm).

The Sun, because of its high temperature, is the main source of energy electromagnetic spectrum. The solar radiation arrives on the Earth's surface and is backscattered (reflected) with a maximum which falls right in the visible range. The Earth itself, being a body with a temperature above 0 Kelvin, emits radiation with maximum the thermal infrared range (Plank's law). These radiations are carrying the information used in the RS by satellite for the determination of the properties of the surface and the Earth's atmosphere. In the visible, infrared and radio regions of the spectrum, the electromagnetic radiation is not or less absorbed by the atmosphere's gases (e.g. the atmospheric radiation transmission is high), hence it can reach the Earth's surface, these regions are called atmospheric windows (Figure 2.6).

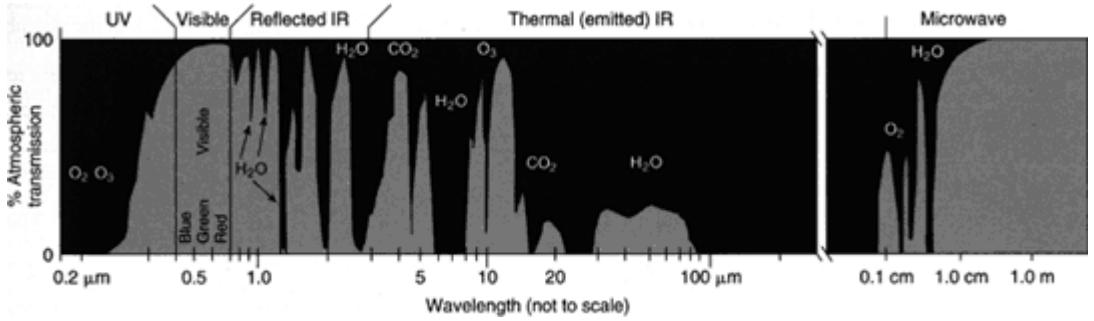

Figure 2.6 Diagram of atmospheric windows. Chemical notation (CO2, O3) indicates the gas responsible for absorbing electromagnetic radiation at a particular wavelength

In addition to absorption and transmission, the other process to which electromagnetic radiation is exposed while crossing atmosphere is the scattering or diffusion. Scattering is a general physical process describing the phenomena of single/multiple reflection of the electromagnetic radiation by the molecular elements present in atmosphere, such as clouds, aerosol, dust etc. These interactions do not cause any change in the wavelength of the incident radiation, and are classified as elastic reactions.

2.3 Matter/radiation interactions

The electromagnetic radiation, once crossed the atmosphere, interacts with the elements present on the Earth's surface, such as land and water (Figure 2.7). In Figure 2.7 the processes occurring as consequence of such an interaction are shown. Like with the atmosphere, three are the main phenomena which may occur: absorption, transmission and reflection which are driven by the following parameters:

reflectance coefficient $\rho = \frac{E_{rif}}{E_i}$ $0 \le \rho \le 1$ (eq. 2.2)

absorbtion coefficient $\alpha = \frac{E_{asb}}{E_i}$ $0 \le \alpha \le 1$ (eq. 2.3)

transmission coefficient $\Im = \frac{E_{tras}}{E_i}$ $0 \le \Im \le 1$ (eq. 2.4)

where: E_i is the incident Energy

E_{rif} is the reflected energy

E_{asb} is the absorbed energy

E_{tras} is the transmitted energy

The three coefficients are linked by the following expression:

$$\rho + \alpha + \Im = 1 \qquad \text{(eq. 2.5)}$$

which describes the principle of conservation of energy. Moreover another important process to consider is the emission of electromagnetic radiation from the Earth that, as already said, it is the most important natural source of electromagnetic radiation in the thermal infrared, with a maximum emission between 9-10 μm. It should also be stressed that the level and the kind of the interactions will change depending on the characteristics of the surfaces and on the specific wavelengths range considered.

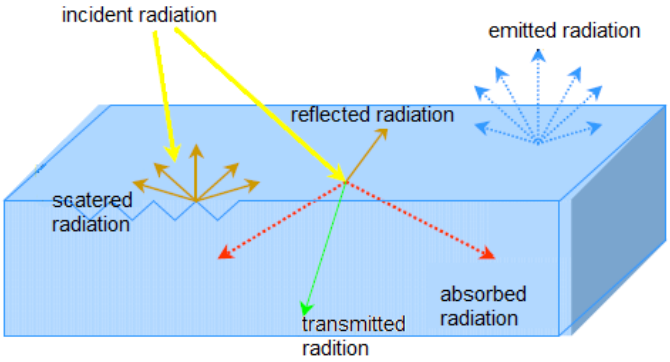

Figure 2.7 Matter/radiation interactions

The kind of reflection depends, in particular, also by the roughness of the surface (Figure 2.8). When the object surface is perfectly smooth a specular reflection will occur, where, according to Snell's law, the angle of reflection is identical to that of incidence (Figure 2.8a). When the surface is rough, the reflection takes place in several directions, so the process of reflection is also defined as diffusion or scattering. An extreme case is represented by a Lambertian surface for which the reflection is isotropic, namely equal in all directions regardless of the radiation angle of incidence (Figure 2.8b). Most of the natural bodies have an intermediate behavior between a specular and a Lambertian reflection, showing a semi-diffuse reflection, i.e. the radiation is diffused in all directions, but with a maximum along a direction coincident with that provided by the law Snell.

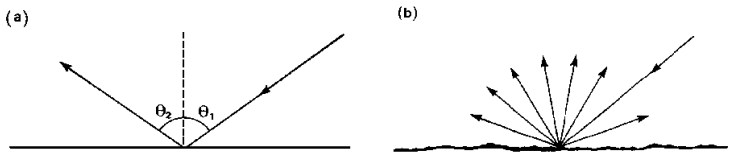

Figure 2.8 (a) Specular reflection, (b) Lambertian or diffuse reflection

The transmission process is not yet completely understood, what it is known is that, if the crossed medium is homogeneous, then the electromagnetic radiation is simply transmitted; on the other hand, if the medium is heterogeneous the transmitted electromagnetic radiation is further spread along the discontinuity surfaces giving rise to the volume scattering. The transmission generally depends on the complex part of the dielectric constant (δ) and the wavelength of the

incident radiation, for example, for sand or clays that have high δ, the EM radiation penetration depth in the visible range is only a few microns, while in the microwave it is larger.

The absorption mechanism is similar to the one found in the atmosphere: if the energy carried by electromagnetic radiation allows for an energy transition at the atomic and/or molecular level of the crossed matter, they are absorbed.

Thus the interactions of the electromagnetic radiation with matter can be described in terms of absorption, reflection and emission, which all depend on the physical-chemical characteristics of the material and the wavelength of electromagnetic radiation considered. The relationship between the intensity of the electromagnetic radiation and the wavelength is defined spectral signature, which is the diagnostic element capable to permit the identification of the type of material (and of its chemical and physical conditions) responsible for the particular process of interaction considered. In the framework of remote sensing, three different kinds of spectral signatures may be analyzed: in terms of reflectance, emission and absorption (Figure 2.9).

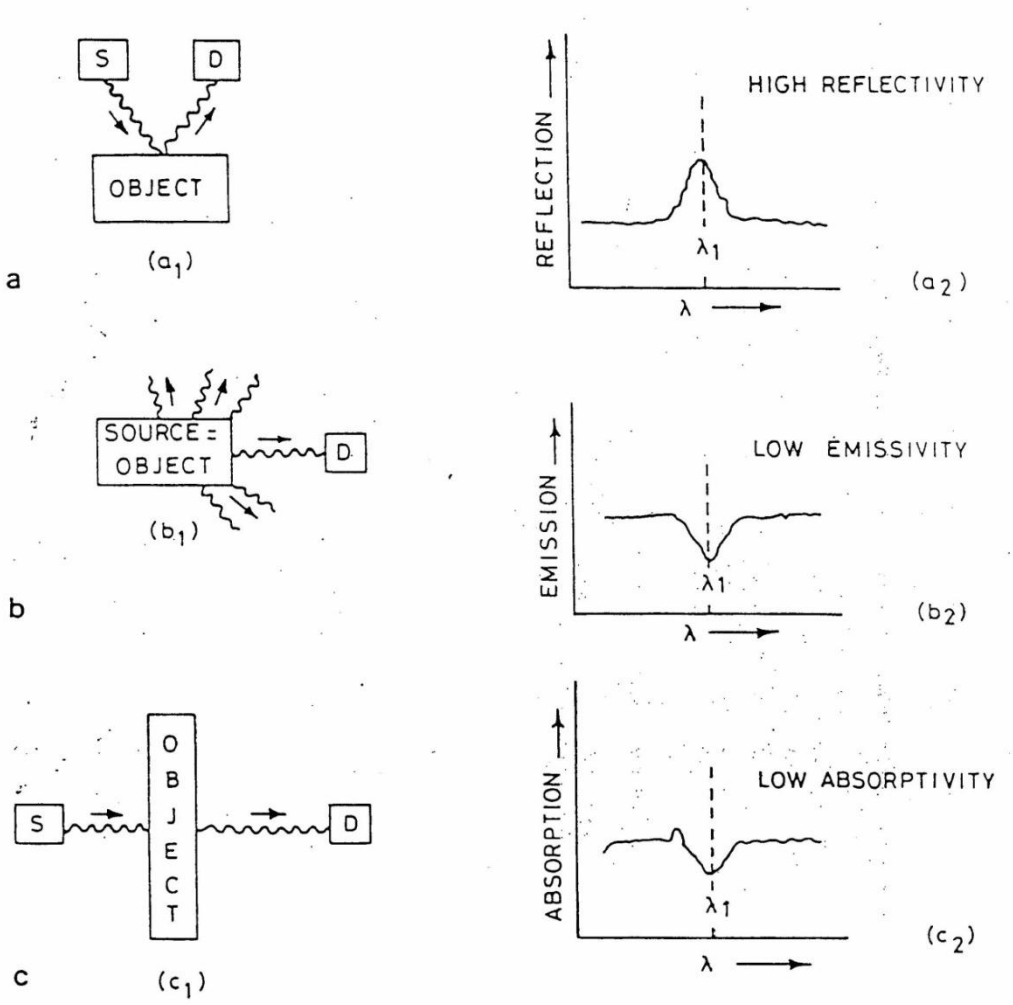

Figure 2.9 Analysis of spectral signature

The Figure 2.10 represents a typical spectral signature in reflectance which provides an indication about the amount of the electromagnetic radiation reflected from the surface of the investigated object at different wavelengths. The emission one furnishes a measurement of the amount of the energy emitted from an object at different wavelengths, while the absorbing signature provide information about the amount of energy absorbed by the object which is located between the source and the sensor.

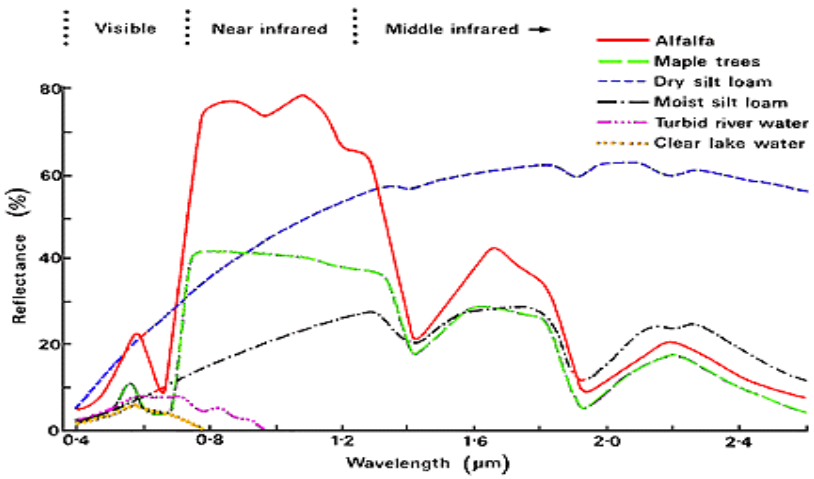

Figure 2.10 Spectral signature, in reflectance, of different materials

Object showing at a specific λ a maximum in reflectivity, have at the same wavelength a minimum both in absorption and emission, minimum which generally are defined as "absorption bands", whether speaking of absorption, emission or reflection.

2.4 Remote sensing Parameters/Definitions

Before moving to the specific remote sensing application of this thesis, it is important to remind some basic parameters and characteristics, both for satellites and remote sensing. Satellite platforms are classified on the basis of their orbit, namely the path they follow in the space while acquiring information about the Earth's surface and atmosphere. Orbit classification can be done in terms of altitude (the satellite's height above the Earth's surface), orientation and rotation relative to the Earth. A geostationary orbit is a circular orbit located at about 35000 kilometers above the Earth's equator and following the direction of the Earth's rotation. An geostationary satellite has an orbital period equal to the Earth's rotational period (about 24 hours), and thus appears motionless, fixed into position in the sky, to ground observers. This allows the satellite to observe and collect information continuously from that specific area without assuring a global coverage (Figure.2.11a).

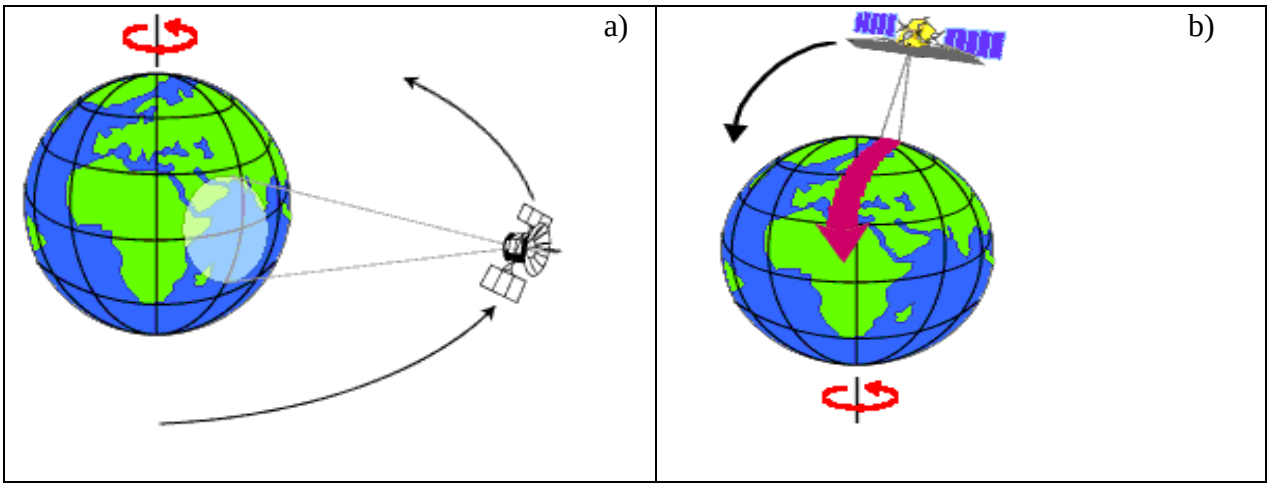

Figure 2.11a) Geostationary orbit; b) Near-polar orbit

Those satellites that are moving around the Earth and passing over the poles (from North to South and the contrary) are following a near-polar orbit (Figure 2.11b). The plane of this orbit is usually slight inclined respect to the polar plane. The distance from the Earth's surface varies from 500 to 1000 km. The orbit movement coupled with the Earth's rotation (from West to East) allows for a global coverage. A specific near-polar orbit is the one defined as Sun-synchronous: the satellite passes over the same area at the same local mean solar time, providing consistent illumination conditions.

Data acquired by satellite sensors are a bi-dimensional array of values of the energy measured in each element of this matrix (Figure 2.12), which usually is defined as pixel.

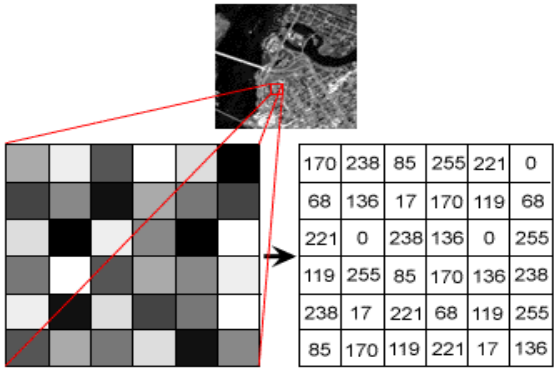

Figure 2.12 Representation of digital image

The data collected by each satellite sensor can be described in terms of spatial, spectral, radiometric and temporal resolution

The **spatial resolution** specifies the pixel size of satellite image covering the Earth surface. Higher the spatial resolution, higher the details of the acquired image (Figure 2.13).

The classification of the satellite data on the basis of their spatial resolution is:

High spatial resolution: 0.6 - 4 m

Medium spatial resolution: 4 - 250 m

Low spatial resolution: 250 - > 1000 m

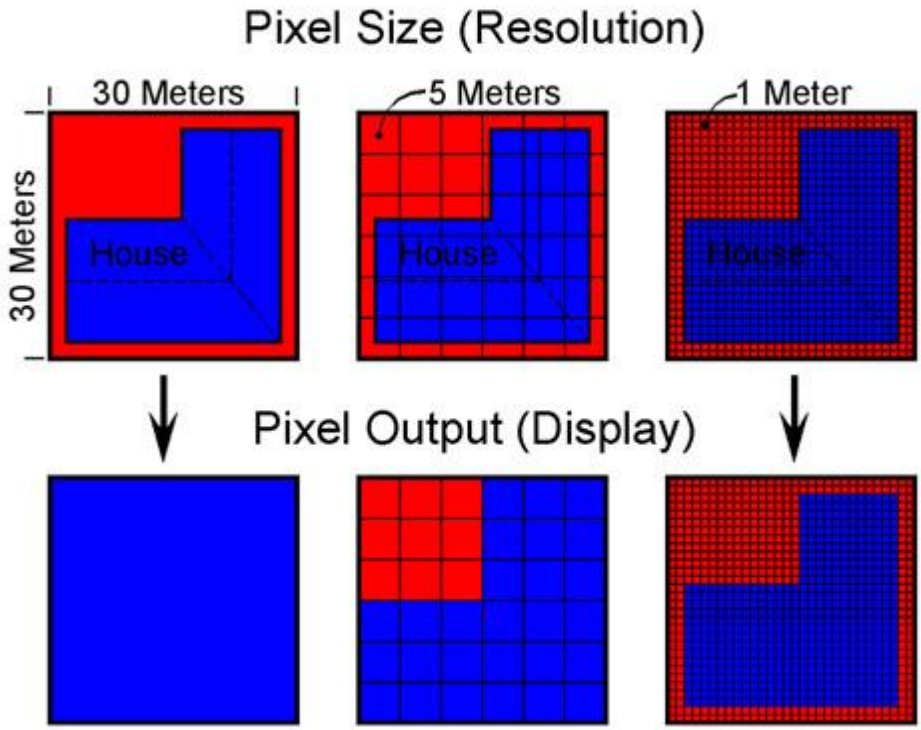

Figure 2.13 Spatial Resolution

The **temporal** resolution specifies the revisiting temporal frequency of a satellite sensor for a specific location.

Satellite data on the basis of their temporal resolution are classified as:

Very high Temporal resolution: < 1 hours

High temporal resolution: < 24 hours - 3 days

Medium temporal resolution: 4 - 16 days

Low temporal resolution: > 16 days

The **spectral resolution** specifies the number of spectral bands in which the sensor can collect the energy (Figure 2.14).

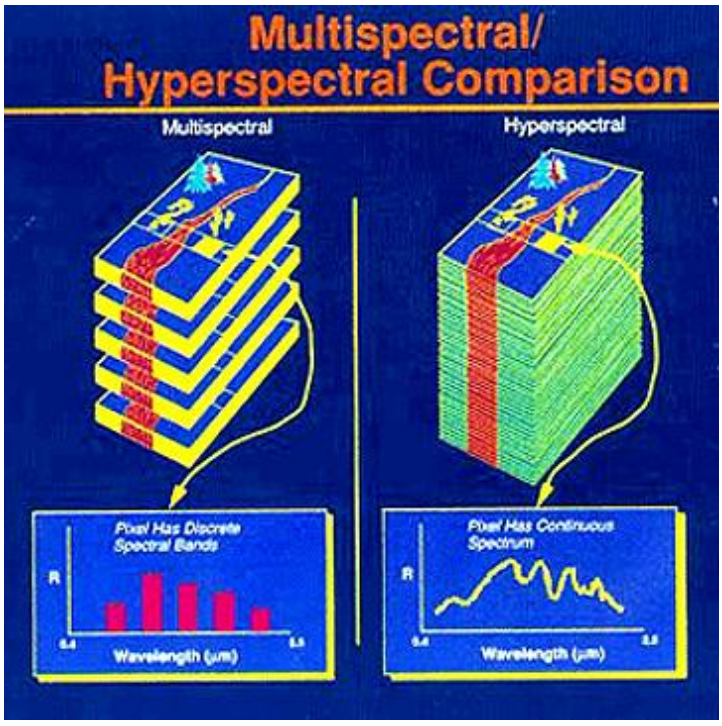

Figure 2.14 Comparison between Multi and Hyper spectral imagery

Satellite data on the basis of their spectral resolution are classified as:

High spectral resolution: > 100 bands (hyper-spectral sensor)

Medium spectral resolution: 3 - 30 bands (multi-spectral sensor)

Low spectral resolution: 1- 3 bands

The **radiometric resolution** of an imaging system describes its ability to discriminate very slight differences in energy. The finer the radiometric resolution of a sensor the more sensitive it is to detecting small differences in reflected or emitted energy (Figure 2.15).

Figure 2.15 Spectral resolution

Imagery data are represented by positive digital numbers which vary from 0 to (one less than) a selected power of 2. This range corresponds to the number of bits used for coding numbers in binary format. Each bit records an exponent of power 2 (e.g. 1 bit=2 1=2). The maximum number of brightness levels available depends on the number of bits used in representing the energy recorded. Thus, if a sensor used 8 bits to record the data, there would be 28=256 digital values available, ranging from 0 to 255. However, if only 4 bits were used, then only 24=16 values ranging from 0 to 15 would be available. Thus, the radiometric resolution would be much less. Image data are generally displayed in a range of grey tones, with black representing a digital number of 0 and white representing the maximum value (for example, 255 in 8-bit data).

2.5 RS techniques for sea water investigation: the Ocean Color radiometry

The main objective of this work is the investigation and monitoring of Crete island sea-coastal waters quality by satellite techniques. Generally speaking, satellite and/or aircraft data have been already used for this kind of applications. The possibility to observe large areas with high temporal

resolution and relatively low costs has encouraged the use of satellite techniques for the analysis of phenomena occurring on the sea surface. Data acquired by active and passive sensors in a very large portion of the electromagnetic spectrum (from visible to microwave) have been in fact used to analyze several parameters relate to sea water: temperature, salinity, constituents, etc.

In particular, by using visible radiation, a specific remote sensing discipline, the Ocean Color (OC) radiometry, has started (Platt et al., 2008). As suggested by the name, OC is focused on deriving sea bio-optical parameters capable to affect the color of the sea water.

The bulk or large-scale optical properties of water are conveniently divided into two mutually exclusive classes: inherent and apparent (Mobley et al., 2013). Inherent optical properties (IOPs) are those properties that depend only upon the medium, and therefore are independent of the ambient light field within the medium. The two fundamental IOPs are the absorption coefficient and the volume scattering function.

Apparent optical properties (AOPs) are those properties that depend both on the medium (the IOPs) and on the geometric (directional) structure of the ambient light field, and that display enough regular features and stability to be useful descriptors of the water body. Commonly used AOPs are the various reflectance values, average cosines, and diffuse attenuation coefficients. Considering that IOPs measurement are difficult to achieve, the bulk optical properties of water bodies are usually expressed in terms of the above mentioned AOPs. Among them, the various reflectance ranges are probably the most commonly used apparent optical properties because they are fundamental to remote sensing of the oceans (Mobley et al., 2013).

➢ 2.5.1 Theoretical background of OC

The concepts already discussed in the paragraph 2.3 Radiation/Matter Interaction, will be here detailed for radiation/sea water interaction. In the early days of ocean color remote sensing, algorithms were developed to relate the irradiance reflectance R to quantities such as absorption and backscatter coefficients and chlorophyll concentrations (e.g., Morel and Prieur, 1977; Gordon and Morel, 1983). More recently, the remote-sensing reflectance R_{rs} has become the choose AOP for remote sensing of ocean properties (e.g., O'Reilly et al. (1998); Mobley et al. (2005)).

The *spectral irradiance reflectance* (or *irradiance ratio*), $R(z,\lambda)$, is defined as the ratio of spectral upwelling to down-welling plane irradiances:

$$R_{(z,\lambda)} \equiv \frac{E_u(z,\lambda)}{E_d(z,\lambda)} \qquad \text{(eq. 2.6)}$$

$R(z,\lambda)$ is a measure of how much of the radiance traveling in all downward directions is reflected upward into any direction, as measured by a cosine collector. This is illustrated in Figure 2.16. Depth z can be any depth within the water column, or in the air just above the sea surface.

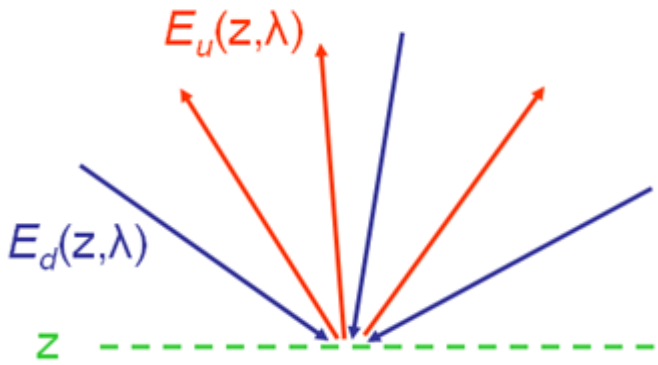

Figure 2.16 : Illustration of light rays contributing to the irradiance reflectance R.

Irradiance reflectance has the virtue that it can be measured by a single, un-calibrated, plane irradiance detector. The down-welling irradiance E_d can be measured, and then the detector can be turned "upside down" to measure E_u.

The *spectral remote-sensing reflectance* R_{rs} is defined as:

$$R_{rs}(\theta,\varphi,\lambda) \equiv \frac{L_w(in\ air,\theta,\varphi,\lambda)}{E_d(in\ air,\lambda)} \ \left(sr^{-1}\right) \qquad \text{(eq. 2.7)}$$

Here the depth argument of "in air" indicates that R_{rs} is evaluated using the water-leaving radiance L_w and E_d in the air, just above the water surface. The remote-sensing reflectance is a measure of how much of the down-welling radiance that is incident onto the water surface in any direction is eventually returned through the surface into a small solid angle $\Delta\Omega$ centered on a particular direction (θ,ϕ), as illustrated in Figure 2.17.

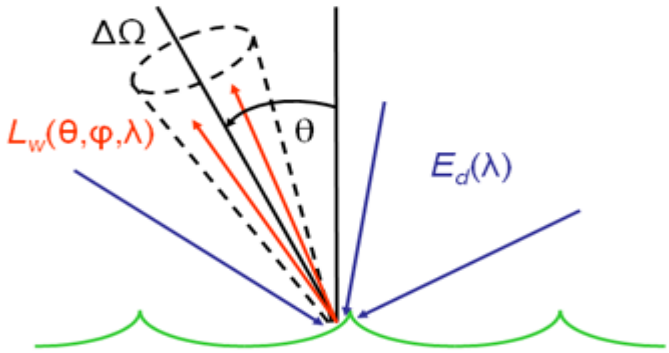

Figure 2.17 Illustration of light rays contributing to the remote-sensing reflectance Rrs

Although R_{rs} is often computed for nadir-viewing direction's only, in actual remote sensing it is usually an off-nadir direction that is being observed by an airborne or satellite remote sensor. As shown next, R_{rs} is less sensitive to environmental conditions such as sun angle or sky conditions than is R. This is the reason that it has replaced R for remote sensing. However, determination of R_{rs} is more difficult than R. First, the measurements of L_u and E_d require different sensors, which must be accurately calibrated. Second, the water leaving radiance L_w cannot be measured directly; Only the total upwelling radiance L_u above the surface can be measured. This L_u is the sum of the water-leaving radiance L_w and the downward sun and sky radiance that is reflected upward by the sea surface, L_s, as illustrated in Figure 18. Therefore L_w must be *estimated* either from a measurement of the total upwelling radiance L_u made above the sea surface, or from a measurement of L_w made at some distance below the sea surface and extrapolated upward through the surface. Each of these estimation methodologies are followed by arguments against their use (e.g. Mobley (1999); Toole et al. (2000)) (Figure 2.18).

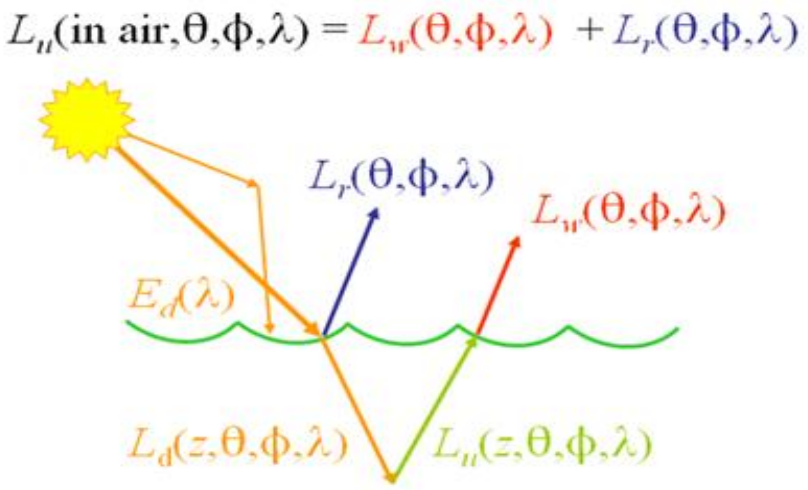

Figure 2.18 Illustration of light rays contributing to Lu as measured above the sea surface

2.6 Optical Constituents of the Ocean water

Several studies have been conducted to evaluate the parameters that influence the optical behavior of sea water. In Figure 2.19 the water absorbs and diffuses solar light, but its color depends by dissolved and suspended substances, which absorb and transmit the light. In particular these parameters are:

- Phytoplankton;
- Non-phytoplankton organic (non-algal) particles (sometimes referred to as NAP, detritus or tripton).;
- Colored (or chromophoric) dissolved organic material (CDOM).

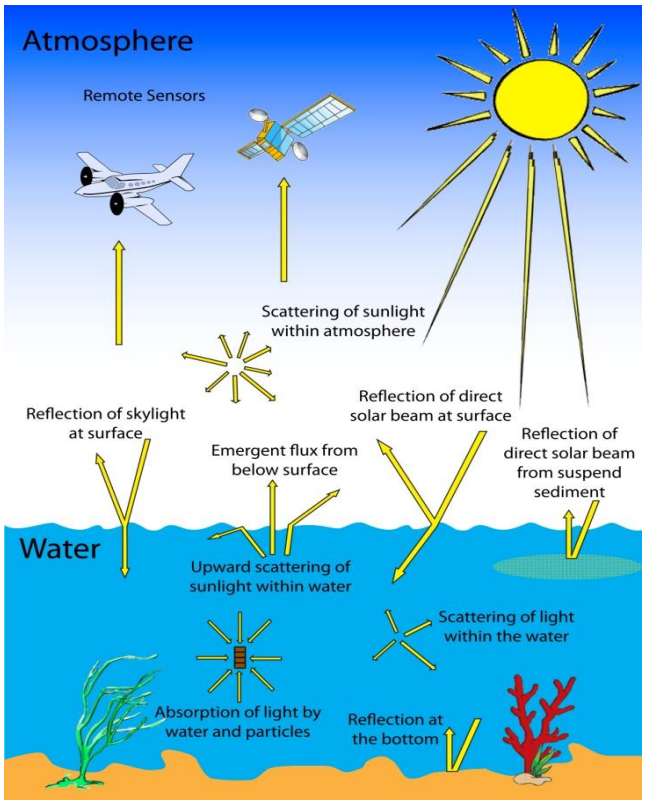

Figure 2.19 Interaction among visible radiations and sea water consituents

According to the concentration of the parameters above, sea waters was classified in two categories: waters case 1 and waters case 2 (Morel and Prieur, 1977). To the first one belong waters whose color depends only by chlorophyll concentration and to the second, belong those that are influenced also by terrigenous particles, material dissolved, suspended sediment, CDOM, or by bacterial blooms.

The Figure 2.20 shows the main spectral features of the deep clear water in the VIS-SWIR range of the electromagnetic spectrum. Pure sea water exhibits usually a relatively high reflectance in the blue region of visible range, which decreases moving to high wavelengths. In the NIR no more reflection is present: the radiation is fully absorbed by water, as better evident in Figure. 2.21.

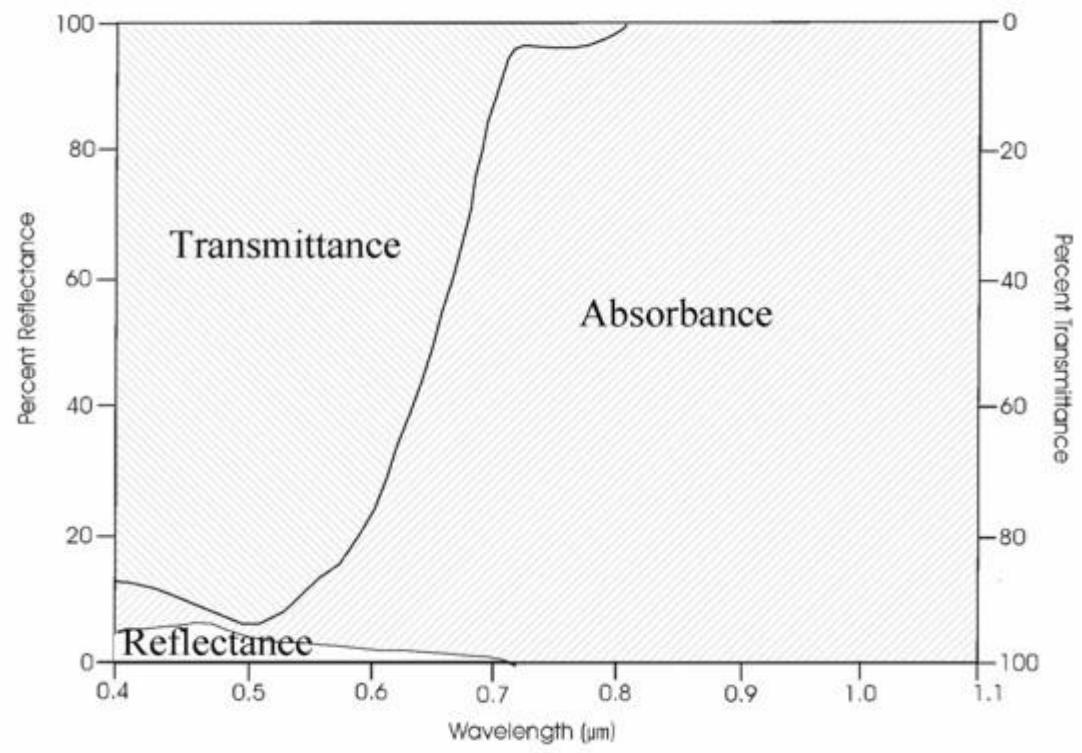

Figure 2.20 Spectral reflectance characteristics of deep, clear water

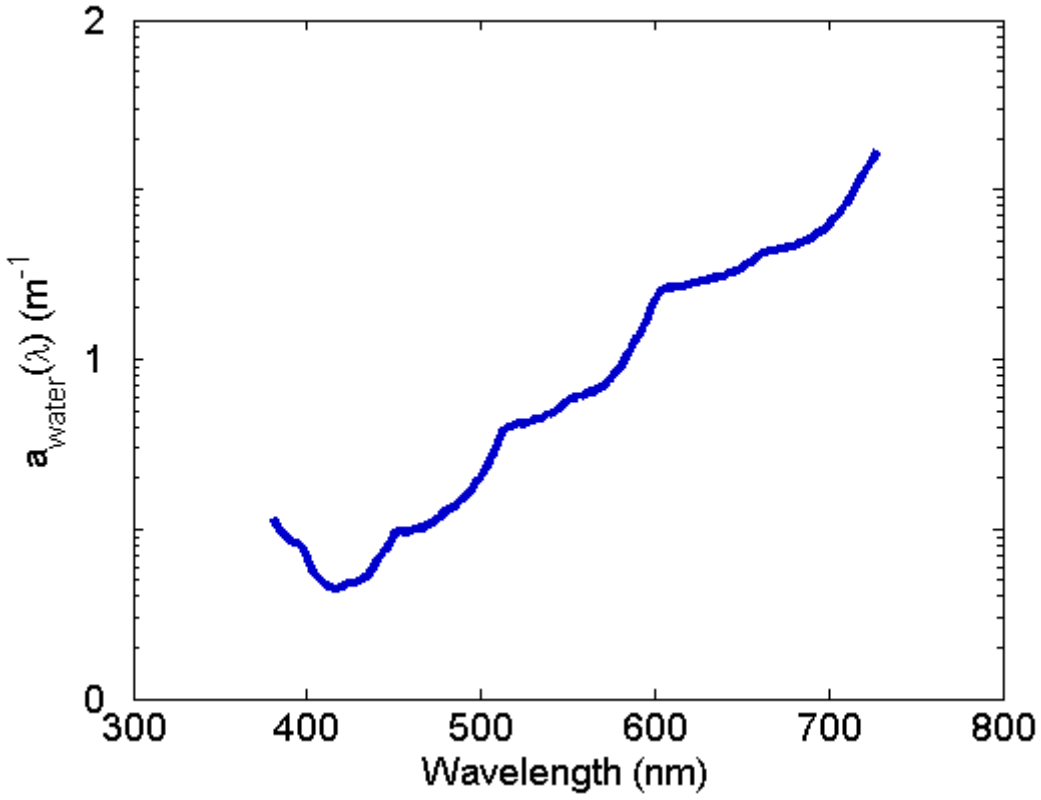

Figure 2.21 Pure water absorption of the spectrum on a semi-log scale (data from Pope and Frye, 1997).

The effect of the other water constituents in terms of absorption are shown in Figure 2.22. In the blue-green portion of the spectrum, absorption is dominated by particulate and dissolved substances, while at wavelengths between ~600 nm and ~650 nm, water absorption is strongest. Further in the red, the strong chlorophyll-a absorption peak centered near 676 nm can reach or even exceed absorption by seawater in the most productive waters and can often be observed as a trough in the spectral remote sensing reflectance. In turbid coastal waters or river plumes, particulate and dissolved absorption at 555 nm is significantly higher than those of water. Even in areas of lower productivity, high concentrations of NAP (predominantly sediment) and CDOM typical of the region cause absorption in the green to be dominated by the particulate and dissolved components.

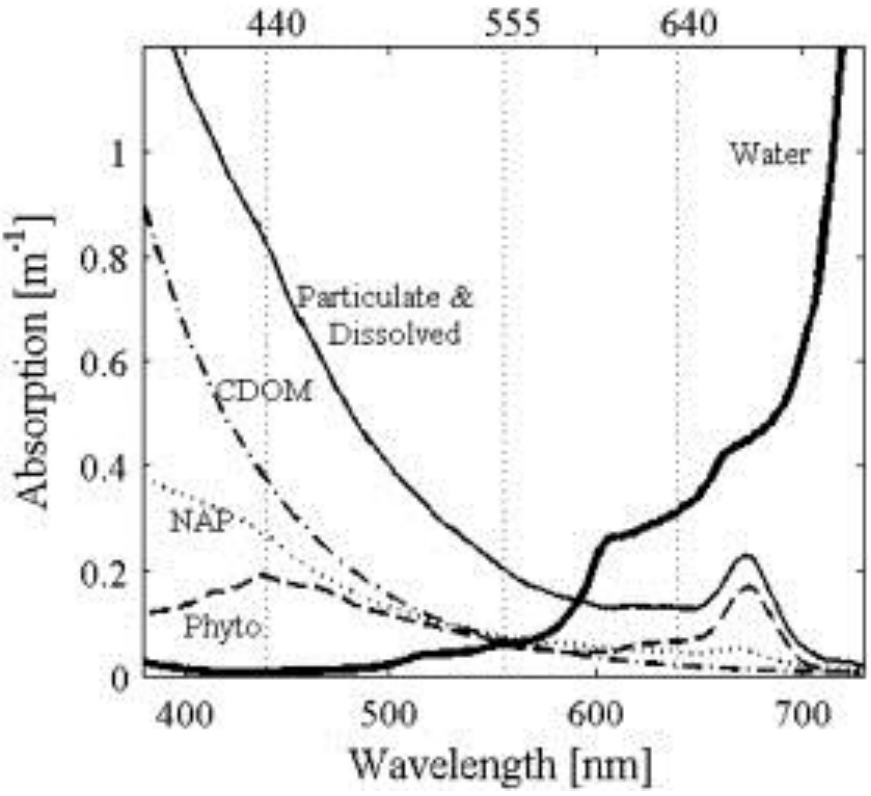

Figure 2.22 Typical water constituent absorption spectra (Aurin et al, 2012)

The whole of these effects, expressed in terms of reflectance, influence the specific color shown by sea water. On the basis of this consideration, it is clear why each satellite sensor able to acquire data in the VIS-SWIR region of the electromagnetic spectrum could be used for OC application. Table 2.1 summarizes all the sensors that starting from the Coastal Zone Color Scanner (CZCS) on board Nimbus 7 from 1978 to 1986 has been used for such a kind of application.

Table 2.1 Ocean Color Sensors, through the years, and their Characteristics

Sensor	Agency	Satellite	Operating dates/Launch date	Swath (km)	Spatial Resolution (m)	# of Bands	Spectral Coverage (nm)	Orbit
CZCS	NASA (USA)	Nimbus-7 (USA)	24/10/78-22/6/86	1556	825	6	433-12500	Polar
CMODIS	CNSA (China)	SZ-3 (China)	25/3/02-15/9/02	650-700	400	34	433-12500	Polar
COCTS CZI	CNSA (China)	HY-1A (China)	15/5/02-1/4/04	1400 500	1100 250	10 4	402-12500 420-890	Polar
GLI	NASDA (Japan)	ADEOS-II (Japan)	14/12/02-24/10/03	1600	250/1000	36	375-12500	Polar
MERIS	ESA (Europe)	ENVISAT (Europe)	1/3/02-9/5/12	1150	300/1200	15	412-1050	Polar
MOS	DLR (Germany	IRS P3 (India)	27/01/99-16/6/04	200	500	18	408-1600	Polar
OCI	NEC (Japan)	ROCSAT-1 (Taiwan)	27/1/99-16/6/04	690	825	6	433-12500	Polar
OCM	ISRO (India)	IRS-P4 (India)	26/5/99-8/8/10	1420	360/4000	8	402-885	Polar
OCTS	NASDA (Japan)	ADEOS (Japan)	17/8/96-26/6/97	1400	700	12	402-12500	Polar
OSMI	KARI (Korea)	KOMPSAT-1 /Arirang-1(Korea)	20/12/99-31/1/08	800	850	6	400-900	Polar
POLDER	CNES (France)	ADEOS (Japan)	17/8/96-29/6/97	2400	6 km	9	443-910	Polar
POLDER-2	CNES (France)	ADEOS-II (Japan)	14/12/02-24/10/03	2400	6000	9	433-910	Polar
SeaWiFS	NASA (USA)	OrbView-2 (USA)	01/08/97-14/02/11	2806	1100	8	402-885	Polar
COCTS CZI	CNSA (China)	HY-IB (China)	11/4/07	2400 500	1100 250	10 4	402-12,500 433-865	Polar
GOCI	KARI/KORDI(South Korea)	COMS	26/6/10	2500	500	8	400-865	Geostationary

HICO	ONR and DOD Space Test Program	JEM-EF Int. Space Stn.	18/9/09	50 km Selected coastal scenes	100	124	380-1000	51.6˚ 15.8 orbits p/d
MERSI	CNSA (China	FY-3A (China)	27/5/08	2400	250/1000	20	402-2155	Polar
MERSI	CNSA (China	FY-3B (China)	5/11/10	2400	250/1000	20	402-2155	Polar
MODIS-Aqua	NASA (USA)	Aqua (EOS-PM1)	4/5/02	2330	250/500/ 1000	36	405-14,385	Polar
MODIS-Terra	NASA (USA)	Terra (EOS-AM1)	18/12/99	2330	250/500/ 1000	36	405-14,385	Polar
OCM-2	ISRO (India)	Oceansat-2 (India)	23/9/98	1420	360/4000	8	400-900	Polar
POLDER-3	CNES (France)	Parasol	18/12/04	2100	6000	9	443-1020	Polar
VIIRS	NOAA /NASA (USA)	NPP	28/10/11	3000	370/740	22	402-11,800	Polar

Each of the above showed sensor has different spectral/spatial/temporal characteristics and thus could be useful for different application also taking into account both the data deliver and distribution policy and, with the aim of a continuous monitoring, the observing temporal continuity and global coverage of the satellite mission. Under these considerations, for this study the Moderate Resolution Imaging Spectroradiometer MODIS (Figure 2.23) has been selected. It allows for the best trade-off between spatial and temporal resolution for coastal water application, providing free global data since 2000. MODIS is a spectrometer mounted on NASA's satellites Terra (Figure 2.24a) and Aqua (Figure 2.24b).

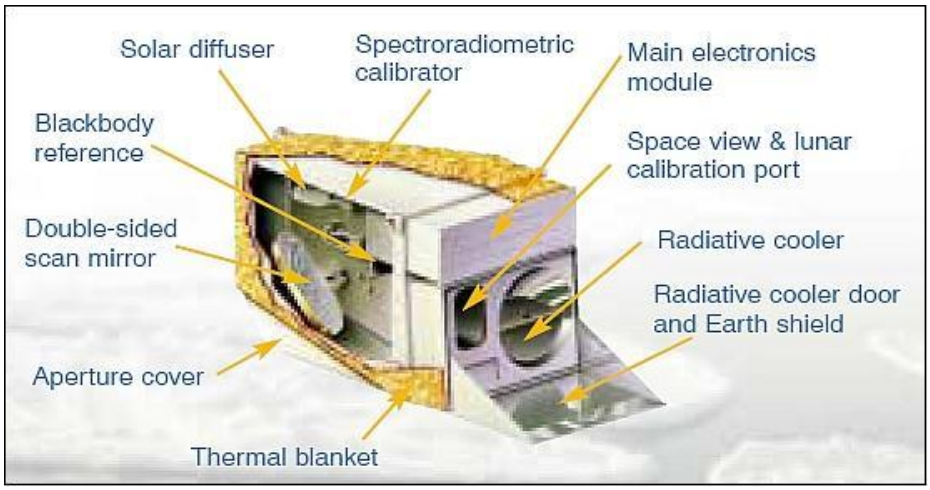

Figure 2.23 MODIS sensor

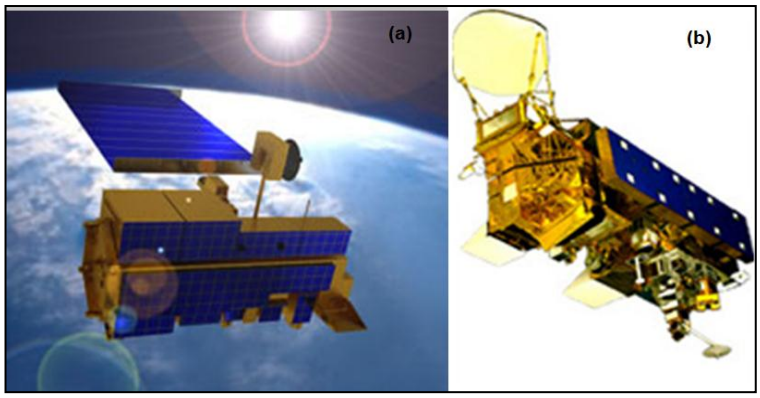

Figure 2.24 a)Terra and b) Aqua satellites

Both satellites follow a sun-synchronous orbit, crossing the equator at the same local time every day (e.g. 10:30 for Terra and 13:30 for Aqua) and their contemporary use allows to ensure global Earth coverage every 12 hours, with a temporal resolution during the day up to 3 hours. MODIS measures data in 36 spectral bands in the wavelength range between 400nm and 14.4μm, at different spatial resolutions.

- Bands 1-2, spatial resolution of 250m
- Bands 3-7, spatial resolution of 500m
- Bands 8-36, spatial resolution of 1km

Thanks to all these features MODIS has been already applied for studying coastal water, providing operational Level 2 products. After each sensor acquisition, a MODIS Ocean Color (OC) Level 2 product is produced and delivered by NASA Ocean color web site (http://oceancolor.gsfc.nasa.gov/), where it is also possible to access to the whole archive of the historical acquired data. The contents of each of its product is delivered in HDF format and shown in tab. 2.2. Several "water quality parameters" are distributed; among them also the Chlorophyll concentration, which is the investigated signal of this work.

Table 2.2 Products of MODIS NASA_L2_LAC_OC

Aerosol optical thickness at 869 nm	
Aerosol Angstrom Exponent, 443 to 865 nm	
Remote Sensing Reflectance	MODIS (412, 443, 469, 488, 531, 547, 555, 645, 667,678 nm)
Chlorophyll concentration, *OC3 algorithm*	
Diffuse attenuation coefficient at 490 nm, *KD2 algorithm*	
Calcite Concentration, *Balch and Gordon*	
Particulate Organic Carbon, *D.Stramski 2007*	
CDOM index, *Morel 2009 algorithm*	
Instantaneous Photosynthetically Available Radiation	
Normalized Fluorescence Line Height	
Photosynthetically Available Radiation, *R.Frouin*	

2.7 Chlorophyll concentration: the OC3 algorithm

Since the Coastal Zone Color Scanner launched in 1978, Chl-a has been derived from satellite data and used to assess phytoplankton biomass and primary production. (Longhurst et al., 1995). Empirical approaches are used for chlorophyll a concentration retrieval because an analytical solution to the problem requires an assessment of the entire radiance distribution, and such measurements are not possible with satellite data (Zaneveld et al., 1973).

All empirical algorithms establish a relationship between optical measurements and the concentration of constituents based on experimental data sets, for example between measurements of above or below-surface reflectance (or radiance) and coincident measurements of in situ concentrations. The most common relationship makes use of the so-called "colour ratio" as described by the equation below:

$$\hat{p} = \alpha\left(\frac{R_1}{R_2}\right)^{\beta} + \gamma \qquad \text{(eq.2.7)}$$

where $\hat{p}$ is the physical quantity to be estimated (e.g. chlorophyll concentration) and *Ri* is the reflectance (or radiance) in spectral channel *i*. The coefficients α, β and γ are derived from regressions between the radiance ratios and the desired property and are based on experimental data. The advantages of empirically-derived algorithms are that they are simple, easy to derive even

from a limited number of measurements (provided they cover the desired range of measurements), and easy to implement and test.

There are, however, several limitations to empirical algorithms: the derived relationships are valid only for data having statistical properties identical to those of the data set used for the determination of the coefficients. These algorithms are thus particularly sensitive to changes in the composition of water constituents (e.g. regional or seasonal effects) (IOCCG Report Number 3, 2000).

The current empirical algorithms have been applied to case 1 water (Gordon et al., 1983), where, as already said, sea-surface optical properties are primarily dominated by changes in terms of chlorophyll concentration.

These algorithms make use of the different absorption of phytoplankton in the blue (maximum at 443 or 490 nm) and green (minimum at 555 nm) to obtain estimates of chlorophyll. Using simple linear regression of log-transformed data, the power equation has been widely used to relate water-leaving radiances to chlorophyll concentrations. Based on a large set of field data, empirical algorithms have been developed for the SeaWiFS and MODIS satellite sensor wavebands. The two widely used algorithms are the Ocean Chlorophyll 2 (OC2) and the Ocean Chlorophyll 4 (OC4) maximum band ratio algorithms (O'Reilly et al., 1998; O'Reilly et al., 2000).

During the years different versions of these two algorithms have been developed, with a gradually increasing of in situ measurements of chlorophyll concentration (version 1 N = 919; version 2 N = 1174; version 4 N = 2853).

The OC2 uses the reflectance of two bands, combined in a single band ratio R490/R555 and it is given by the following relation:

$$C_a = 10^{\left(0.319 - 2.336R_2 + 0.879R_2^2 - 0.135R_2^3\right)} - 0.071 \quad \text{(eq.2.8)}$$

where: R2 = log10 (R490/R555)

Instead OC4 was derived from an optical dataset of the world's ocean spanning Chl-a concentrations from 0.02 to 50 mg/m3 , and it uses the reflectance of four bands combined in three possible band ratios R443/R555, R490/R555, R510/R555; in the fourth order polynomial, that characterizes the OC4, the highest ratio among the three above-mentioned ratio bands is used

(Maximum Band Ratio: MBR). OC4v4 algorithm has been implemented on SeaWiFS sensor and is given by this relation:

$$C_a = 10^{\left(0.366-3.067R_4+1.930R_4^2+0.649R_4^3-1.532R_4^4\right)} \quad \text{(eq.2.9)}$$

where: R4 = log10 (R443/R555 > R490/R555 > R510/R555)

In this thesis the reference algorithm is the OC3M (Ocean Color 3 Bands MODIS, O Really et al., 2000), which was implemented on MODIS sensor; it uses three reflectance bands R443, R488 and R547 combined in two possible band ratios R443/R547, R488/R547, according to MBR, as in the previous algorithm OC4. The analytical equation is the following:

$$[Chl] = 10^{\left(C_0+C_1R_3+C_2R_3^2+C_3R_3^3+C_4R_3^4\right)} \quad \text{(eq.2.10)}$$

where: R3 = log10 (R443/R547 > R488/R547)

In particular, in this work, OC3Mv6 has been implemented, and the values of the coefficients used are: C_0=0.2424, C_1=-2.7423, C_2=1.8017, C_3=0.0015, C_4=-1.2280 .

From the analysis of these algorithms, based on the MBR, it is clear that the concentration of chlorophyll is a function of the blue and green reflectance in the visible domain. Remote sensing reflectance (Rrs) in relation to the Chl-a concentration values is plotted in Fig. 2.25.

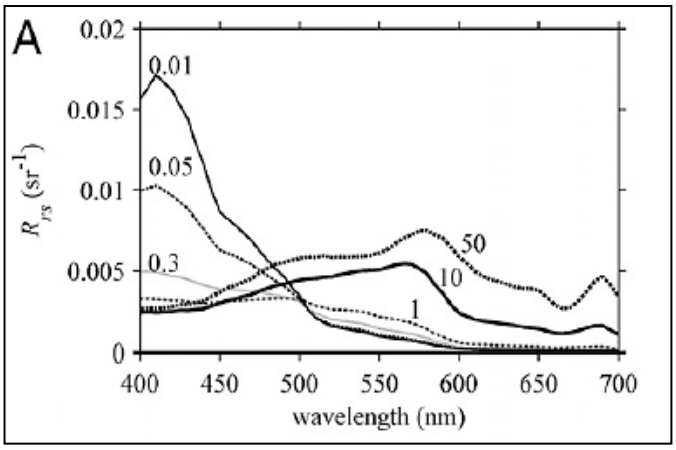

Figure 2.25 Rrs in relation with Chl-a value curves

This figure shows how Rrs changes from blue peaked to green peaked with the increasing of chlorophyll. According to MBR, for Chl-a <0.7 mg/m3, R443/R547 band ratio is used, because around this value (443 nm) there is the reflectance peak. When concentration increases, R488/R547 band ratio is used, because for high values of Chl-a concentrations (from 1 to 10, 50 mg/m3) the reflectance peak is shifted from the end of blue band to the beginning of green one.

The algorithm OC3M considered in this thesis sometimes overestimates the concentration of chlorophyll, especially in oligotrophic conditions, as well as for the previous OC2 and OC4 algorithms developed by NASA (Volpe et al., 2007)

Chapter 3 The Robust Satellite Techniques (RST) approach for chlorophyll analysis

In this chapter the methodologies used for the analysis of Chl-a NASA MODIS data will be described. After a brief description of the general methodology, its specific application for the analysis carried out in this work will be presented.

3.1 The Robust Satellite Techniques (RST)

The methodology used in this work is based on the Robust Satellite Techniques (RST) approach (Tramutoli, 2005, 2007), a general technique for the analysis of satellite data which have been already successfully applied for the investigation of different natural an environmental processes occurred on the Earth's surface (Tramutoli et al., 2001; N.Pergola et al.; 2001; N.Pergola et al., 2004; G.Di Bello et al., 2004; R.Corrado et al., 2005; T. Lacava et al., 2005, 2006; C.Filizzola et al., 2007; N. Genzano et al., 2007; D.Casciello et al., 2007; Mazzeo et al., 2007; C.S.L.Grimaldi et al., 2008; N.Pergola et al., 2008). In particular, a few applications have been focused on the analysis of phenomena in progress on sea surface, such as oil spill detection and mapping (Grimaldi, Casciello) and suspended sediment material detection (Mirauda, Lacava)

RST is actually a change detection algorithm, based on the analysis at pixel level of historical (multi-year) series of homogeneous (in the spatial/temporal domain) satellite data. Such an analysis allows for a preliminary characterization of the investigated signal in terms of the value expected for a specific localization and condition of observation (i.e. time of day, month of the year) and its normal variability. These two values, which are usually expressed by the temporal mean and the standard deviation, are finally compared with the signal at hand to automatically identify possible statistically significant anomalies at different level of confidence. Three are the phases of the RST approach (Figure 3.1).

The **first step** deals with the generation of a dataset of historical satellite imagery co-located over the area of interest. To reduce the noise related to the variability of the conditions of observation, these images must be acquired under observing conditions as uniform as possible with

respect to the image to be investigated. The homogeneity in the time domain is achieved by selecting all images acquired by a specific sensor in the same month of the year and at the same time of day.

In detail, after the calibration of the raw data (i.e the transformation of digital data in radiance), the procedures of navigation and re - projection ensure that the data extracted by the orbit are always the ones that concern the same region of interest, with an accuracy no less than the typical spatial dynamics of the studied process. This means that all the portions extracted always represent the same area, with the same number of pixels and lines, and each pixel (x, y) of the image is always same point of geographic coordinates (i, j) on the ground.

STEP 1

Creation of the co-located (in the spatiotemporal domain) dataset of satellite data

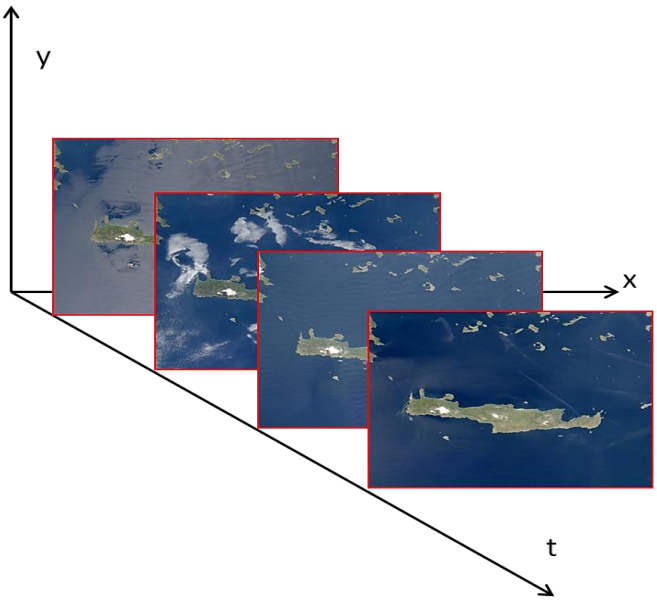

STEP 2

Reference fields computation

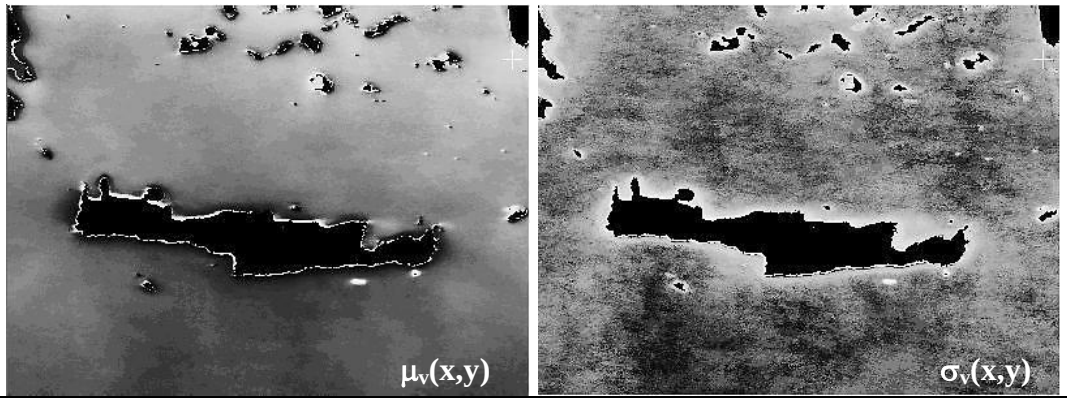

STEP 3

Anomaly detection by the *ALICE* (*Absolutely Local Index of Change of the Environment*)

$$\otimes_V (x,y,t) = \frac{V(x,y,t) - \mu_V(x,y)}{\sigma_V(x,y)}$$

Figure 3.1 RST phases

In the **second step**, starting from the previously identified dataset, for each pixel of the scene, the expected value of the investigated signal V(x,y) under normal conditions (i.e. in the absence of events known or not, able to modify these conditions), is computed, taking also into account its natural variability. Typically, the normal conditions are expressed, for each pixel of the scene considered, from the value of the temporal mean ($\mu_{V_{(x,y)}}$), representative of the behavior of the signal in unperturbed conditions, while the measure of the deviation of the natural signal from the expected behavior for those observation conditions is expressed by the relative standard deviation ($\sigma_{V_{(x,y)}}$). For an adequate statistical characterization of the signal investigated the time series must include at least five years of data.

To reduce the effect of random signals, known or not, that could affect the identification of the unperturbed conditions of investigated signal, a reiterative procedure named k_σ clipping has been used. This procedure is a statistical method that iteratively updates the number of measurements of the time series V(t) (with μ_V and standard deviation σ_V), saving only the elements for which the condition: $|V(t) - \mu_V| < k\sigma_V$ (symmetrical clipping) is verified; at each iterative process it calculates

the new values for μ_V and σ_V considering the elements that remain from the previous step of k_σ clipping. The process terminates, and μ_V and σ_V are determined, when the clipping does not find any other values more to discard.

For the same reason and every time it is necessary, also cloudy pixels have selected and excluded before computing reference fields. The cloud detection is made by a procedure called OCA (One-channel Cloud-detection Approach) (Tramutoli 1998; Cuomo et al. 2004) which exploits the spectral properties of the clouds (i.e. clouds show high reflectance in the VIS and NIR and low brightness in the TIR), to identify and eliminate cloud affected pixels.

At the end of this second step, the reference fields are the products obtained, in particular two matrixes with size equal of the analyzed scene, in which the values μV and σV have been calculated for each clear pixel of the scene. The reference fields describe the behavior of the investigated signal over a long period, so that, especially when each calendar month of the year is analyzed by RST, they could be useful to identify possible trend in the analyzed signal, as well as areas characterized by specific spatial and/or temporal features. In this view, reference fields represent themselves a first import outcome of the RST approach, every time is applied.

The **third and final step** is the change detection one: after the identification of the the "normal" behavior of the signal in the place (x,y) at time (t), an anomalous signal will be detected when the signal at hand exceed such normal condition, teaking into account also its natural variability. In particular, the identification of the anomalies is achieved by implementing an index named ALICE (Absolutely Local Index of Change of the Environment):

$$\otimes_v (x, y, t) = \frac{V(x,y,t) - \mu_v(x,y)}{\sigma_v(x,y)} \qquad \text{(Eq. 3.1)}$$

Where V(x,y,t) is the investigated signal relative to the pixels (x,y) at time (t), $\mu_V(x,y)$ and $\sigma_V(x,y)$ are the reference fields previously computed. The robustness of RST is intrinsic, an anomalous signal will be detected only when the deviations of the investigated signal from its expected values is higher than the historical variability $\sigma_V(x,y)$. The signal V(x,y,t) is defined according to the studied parameter and it can be associated to a measurement carried out in a specific band, or deriveded from the combination of different channels (Tramutoli, 1998).

The ALICE index is a standardized variable, which tends to have a Gaussian distribution, with mean equal to zero and sigma equal to one. Thus, the probability of occurrence of values above/below 2 sigma ($x>\mu_v \pm 2\sigma_v$) is about 2.5%, and decrease to 0.13% for values above/below 3 sigma. This means that a deviation of the investigated signal from the mean value of at least twice its normal variability (i.e. Signal to Noise ratio -SN - equal to 2) allows for the identification of anomalies statistically significant, with a level confidence growing by increasing SN ratio.

3.2 Using RST for analyzing chlorophyll

In this work, as before stated, the investigated signal is the chlorophyll a (Chl-a) product produced by NASA starting from MODIS acquisition. This means that the equation 3.1 turns in:

$$\otimes_{Chl-a}(x,y,t) = \frac{Chl-a(x,y,t)-\mu_{Chl-a}(x,y)}{\sigma_{Chl-a}(x,y)} \qquad \text{(Eq. 3.2)}$$

where $\mu_{Chl-a}(x,y)$ and $\sigma_{Chl-a}(x,y)$ where the two reference fields computed analyzing historical series of Chl-a NASA MODIS product. We expect to observe high (low) values of such an index in correspondence of a statistical significant increase (decrease) of the Chl-a concentration. It should be stressed that such an index can be computed considering as investigated signal both daily Chl-a values and monthly ones, depending on the time scale at which the change detection analysis is carried out.

To implement the Eq. 3.2, according to RST prescriptions, one fundamental element is represented by the historical dataset of the specific data/product to be analyzed. As already mentioned in chapter 2 and also before, in the analysis here performed, we are using MODIS NASA Level 2 Ocean Color product. NASA delivers such data from the Ocean Color portal (http://oceancolor.gsfc.nasa.gov/) where data can be searched specifying different criteria, such as sensor, temporal range and the geographical coordinates of the area of interest (Figure 3.2). Starting from these indications, the system returns the list of total orbits, relative to all acquisitions available in the specified temporal range, within which for sure falls a small portion of the area of interest at least (Figure 3.3).

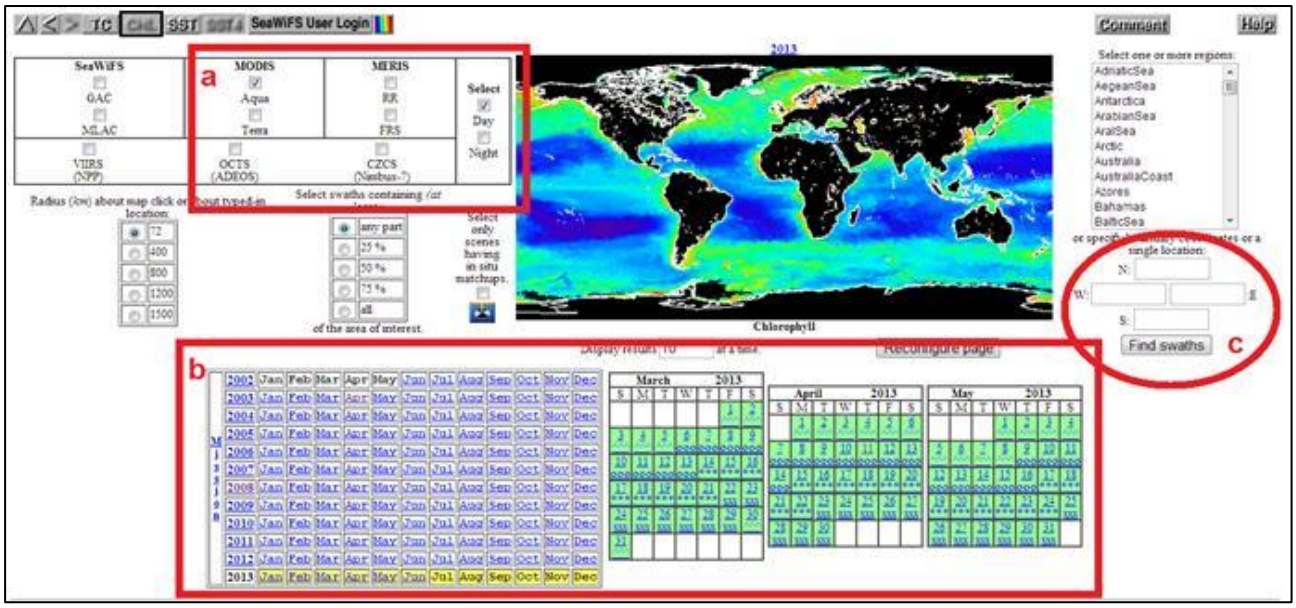

Figure 3.2 NASA portal (search criteria: box a: sensors; box b: temporal range; circle c: area of interest)

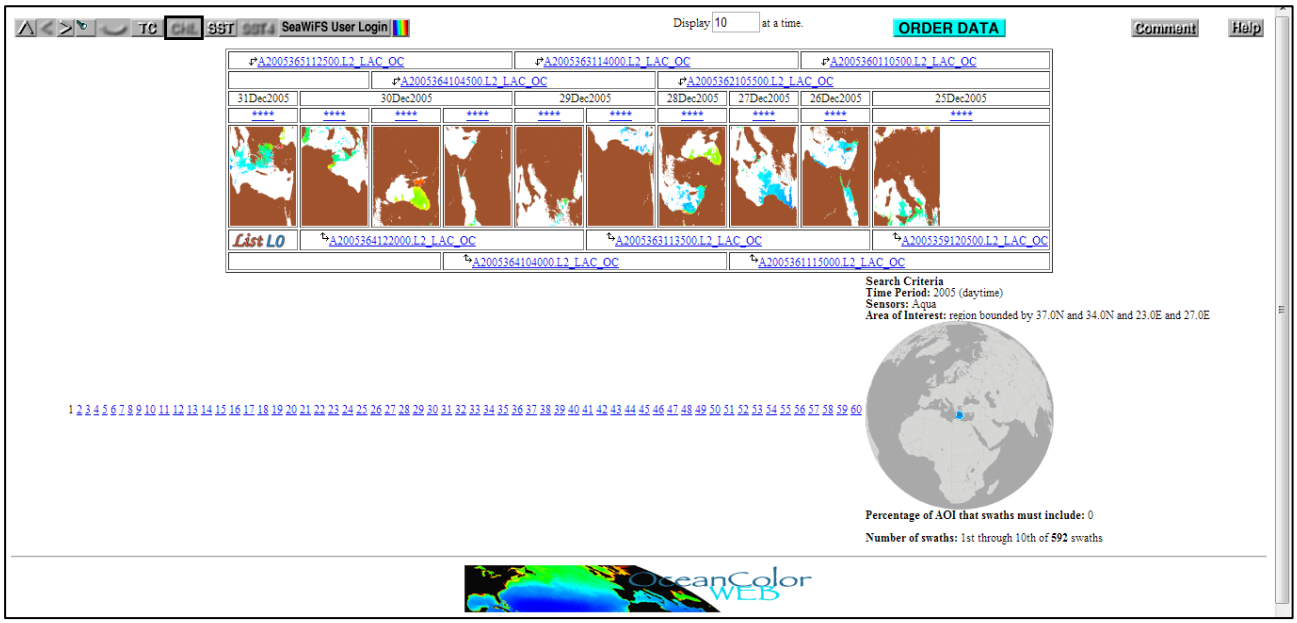

Figure 3.3 NASA portal (products available)

Once found, data are available for download, when the temporal range is too large, the system will provide a link by mail where downloading them. Once the full orbit of each level 2 data is available, a spatial and "spectral" subset have to be carried out. The spatial subset is fundamental for generating co-located series of data, where each pixel concerns always the same ground cell moving from one image to another. Obviously the spectral subset allows for the extraction of the

same channel (if talking about a multispectral satellite data) or the same parameter, when a higher product level is analyzed (i.e. the Chl-a in this case). Both these operations have been carried out using the HDFlook software (http://www-loa.univ-lille1.fr/Hdflook/hdflook_gb.html), by writing several ad hoc routines in bash shell language. Finally these co-located series of data have to be stratified on the basis of their calendar month of acquisition, to produce for each of them its multi-year temporal dataset which is the input for the reference fields generation. A program written in C++ has been used for this purpose.

In the next chapter the results achieved by applying RST on historical series of Chl-a MODIS Level 2 Ocean Color products concerning the Crete Island sea water will be shown and discussed.

Chapter 4 RESULTS

In this chapter the results obtained applying the RST approach for the study of Crete island sea-costal water, concerning in particular the chlorophyll-a parameter, will be described. RST allows for achieving different outputs depending on the kind of analysis carried out: the first ones come from a multi-year long term analysis where the chlorophyll-a concentration trend for the investigated area has been recognized. During the second analysis short (monthly-daily) temporal scales have been studied, looking for anomalous chlorophyll-a concentration values.

4.1 The investigated area: Crete island sea-coastal water

The island of Crete is the biggest in Greece and the second larger one in East Mediterranean after Cyprus; it is located in the south of the Aegean Sea (Figure 4.1) and covers an area of 8.366 km^2, it spans 260 km from east to west, it is 60 km at its widest point, and narrows to as little as 12 km. Crete's coastline is more than 1,000 km. The South part of the island is characterized by shallow coasts as the African tectonic plate slips beneath the Eurasian tectonic plate and it is forcing the island to lift on its Southern part; on the other hand the northern part of the island is characterized by deeper sea water.

Figure 4.1 The location of Crete in Aegean Sea

From a geomorphological point of view (Figure 4.2), Crete can be considered as extremely mountainous with a series of mountains which range from the West to East part of the island. In particular, from West to East three are the main mountain groups: i) the Lefka Ori (White Mountains) which reaches a height of 2.452 m above sea level; ii) the Ida mountain range where the Mount Psiloritis is the highest (2.456 m) and iii) the Mount Dikti with highest top Spathi at 2.148 m. Several plateaus are also present: Omalos, Nidha and Lasithi's Platue, or caves such as Diktaion and Ideon Andros, and also different rivers and gorges. One of the most famous gorges is Samaria Gorge (16 km long), that, from 1962 has been declared as National Park since it hosts numerous endemic species of birds and other animals, such as Kri-Kri and Wild Goat.

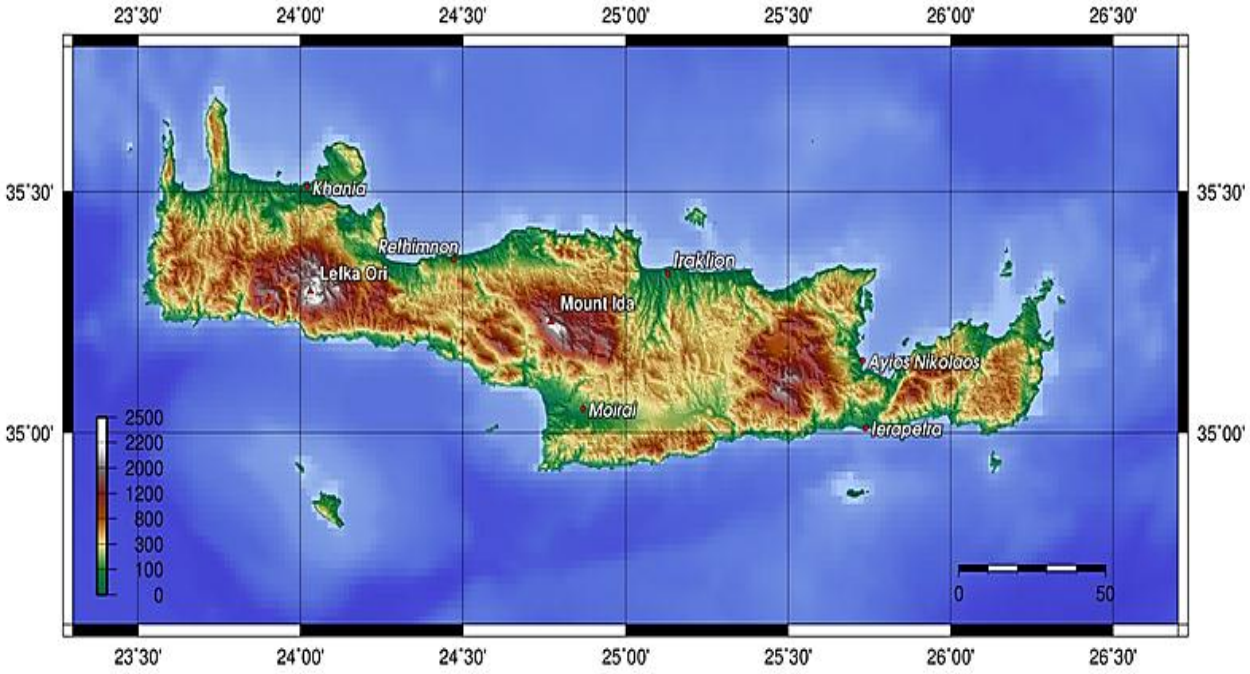

Figure 4.2 The Island of Crete

Because of the small width of the island there are a few rivers that start from the mountains and off at the Libyan Sea (South) or Cretan Sea (North); most of them during the winter months have a very low water level and in summer are completely dry. Among them, the Anapodiaris River is the biggest river of the island; it is located in south-central prefecture of Heraklion. More specifically, it starts gathers water from east-central Heraklion and southern Dikti, with smaller rivers (eg Baritis) flowing into it. It carries 40 million cubic meters of water into the Libyan Sea every year (CB 2013). Another one is the river Giofyros or Diakoniaris which is located in the northern prefecture of Heraklion and it is one of the longest rivers of the island. The river is watered by several

tributaries close to the village of Profitis Ilias (Prophet Elijah) and flows next to the Pancretan Stadium, in Heraklion city (CB 2013).

From a climatologically point of view, even if southern part of the island falls in the North African climate zone, Crete is characterized by a Mediterranean climate; the atmosphere can be pretty humid, according to the distance from the sea, and this makes the winter to be mild and humid with a lot of rains mostly in the West of the island; snowfall at the plateaus is rare, but it is usual on the mountains; during the summer the mid temperature is between 25-30˚C.

The Island is composed by four regional units, Chania, Rethymno, Heraklion and Lasithi, from West to East; the Capital and biggest city is Heraklion with a population of 304.270 (as to 2011) citizens, second city in population is Chania with (156.220 inhabitants - 2011), third is Rethymno 85.160 inhabitants - 2011) and finally Lasithi (75.690 inhabitants - 2011). More than 50% of Cretan people leave in coastal areas. The northern part of the island is more appropriate for water sports and water activities, resulting to be extremely crowded, and urbanized, while the southern part is more quiet and unorganized. Except for the native population, every year the island gets visited by about 3 million people that makes Crete one of the most popular tourist destinations in Greece; 15% of the total tourist arrivals are at the harbor or airport of Heraklion. (Interkriti 2013)

4.2 RST implementation for the analysis of Crete island coastal water

Before going ahead with the analysis, following the procedures described in the previous chapter, the multi-year historical dataset of NASA MODIS Chl-a Level 2 OC product for the Crete island region of interest were generated. Table 4.1 reports the number of images covering the investigated area that have been acquired by NASA portal for each calendar month of the year, in the period 2003-2012. Both Terra and Aqua OC product have been collected, for a total of about 10000 imagery.

Table 4.1 Number of images downloaded month by month

Months	Number of image (2003-2012)
January	868
February	772
March	853
April	818
May	848
June	818
July	853
August	852
September	826
October	852
November	812
December	835
Total	**10008**

For each of these data, the Chl-a concentration map have been generated by applying the subset spectral and spatial procedures. In particular, an area of 400 pixel x 300 lines (Corner: UL 37N23E; LR 34N27E) re-projected in the WGS84 reference system (Figure 4.3) has been extracted from each single orbit.

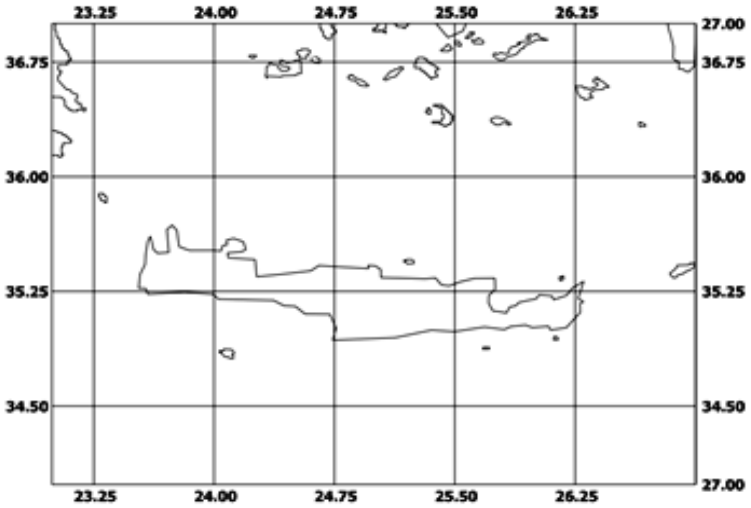

Figure 4.3 Area of interest

Finally, by exploiting these 12 datasets, the RST approach have been applied, generating in the first phase, 24 reference fields (one temporal mean + one standard deviation for twelve calendar months) related to the period 2003-2012.

4.3 Long term trend Analysis

The long term trend analysis has been carried out at two different temporal scales; first the ten-year period has been investigated and then the yearly trend has been analyzed.

➢ 4.3.1 Multi-year investigation

This first analysis was carried out on the results achieved by applying the RST multi-year approach. As above said, at the end of this phase, one temporal mean and one standard deviation map of chlorophyll-a concentration are available for each calendar month, and they refer to a 10 year period (2003-2012) of investigation. Such maps are shown in Figure 4.4 and 4.5, Chl-a concentration values are depicted in different color depending on its intensity. Land areas have been masked in white.

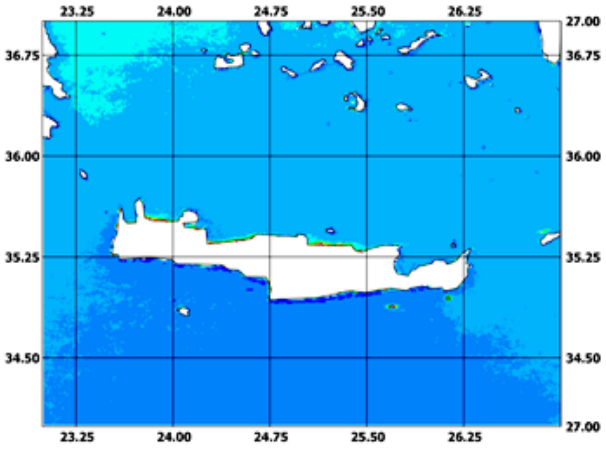

January

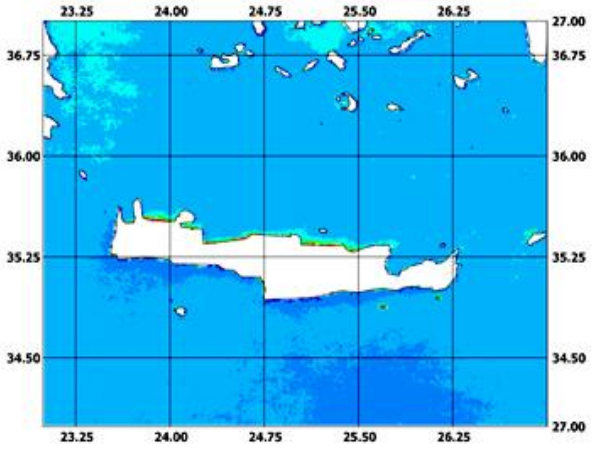

February

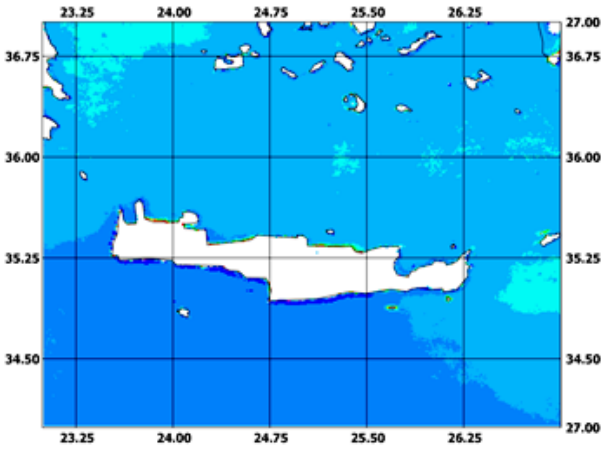

March

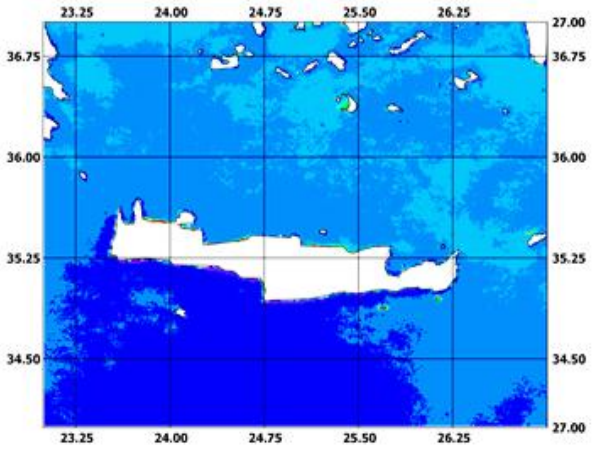

April

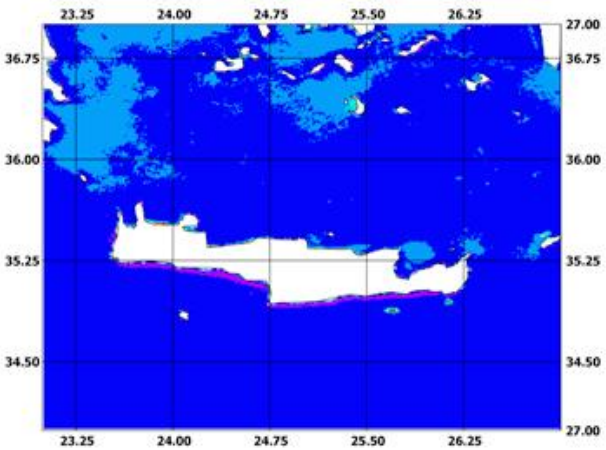

May

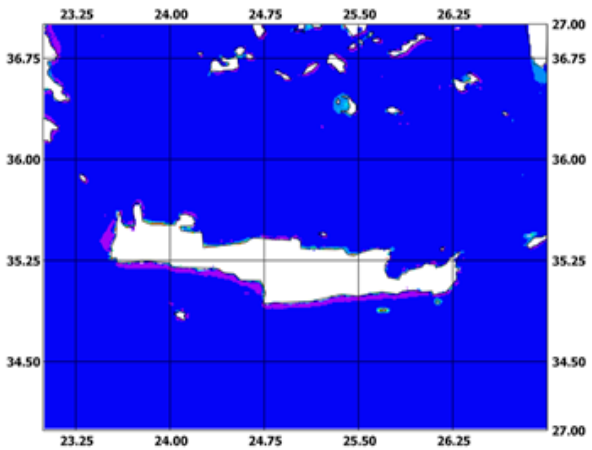

June

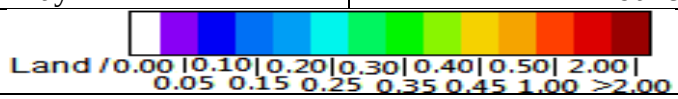

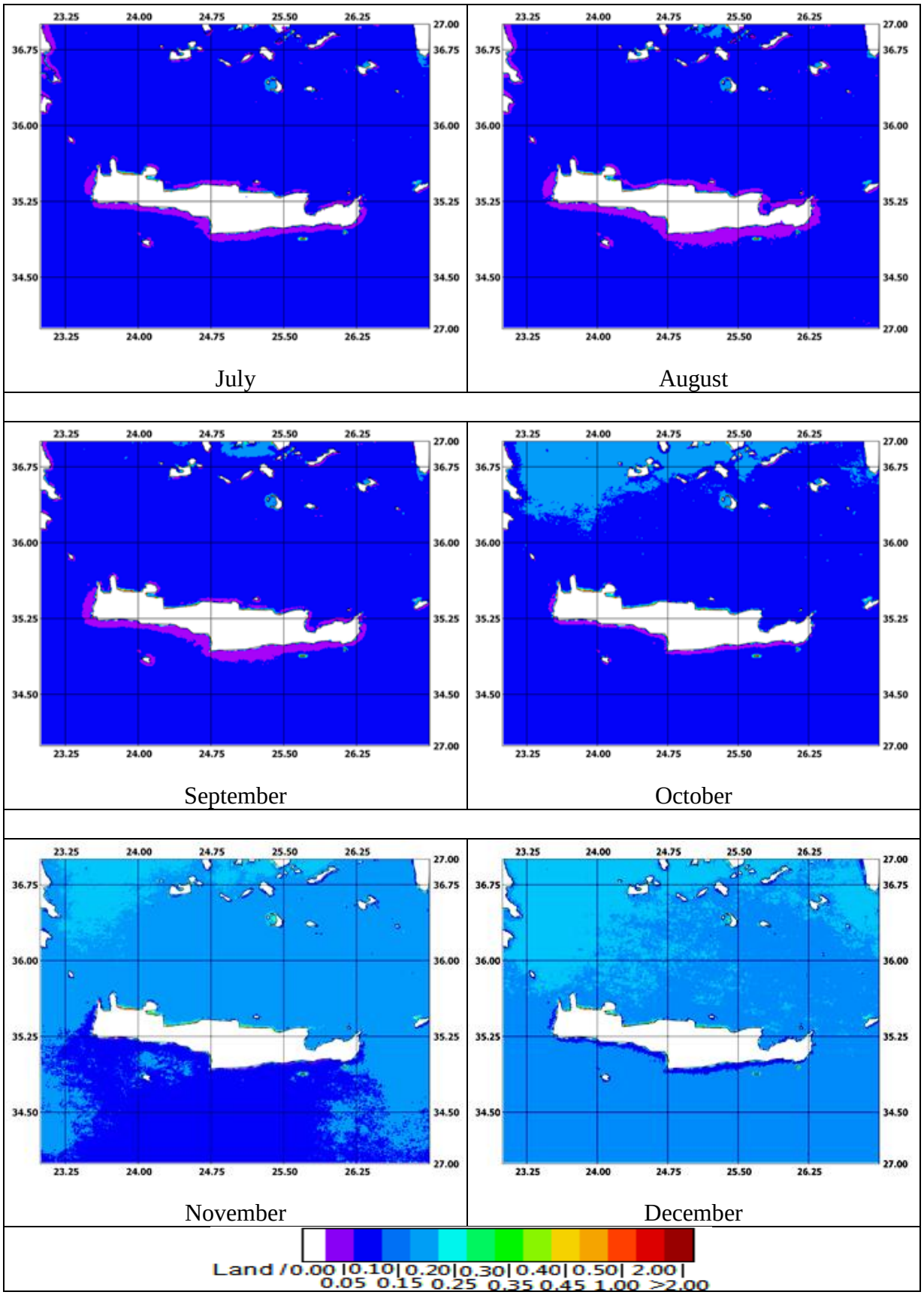

Figure 4.4Monthly temporal mean chlorophyll-a concentration (mg/m3) maps generated by the long term (2003-2012) RST analysis

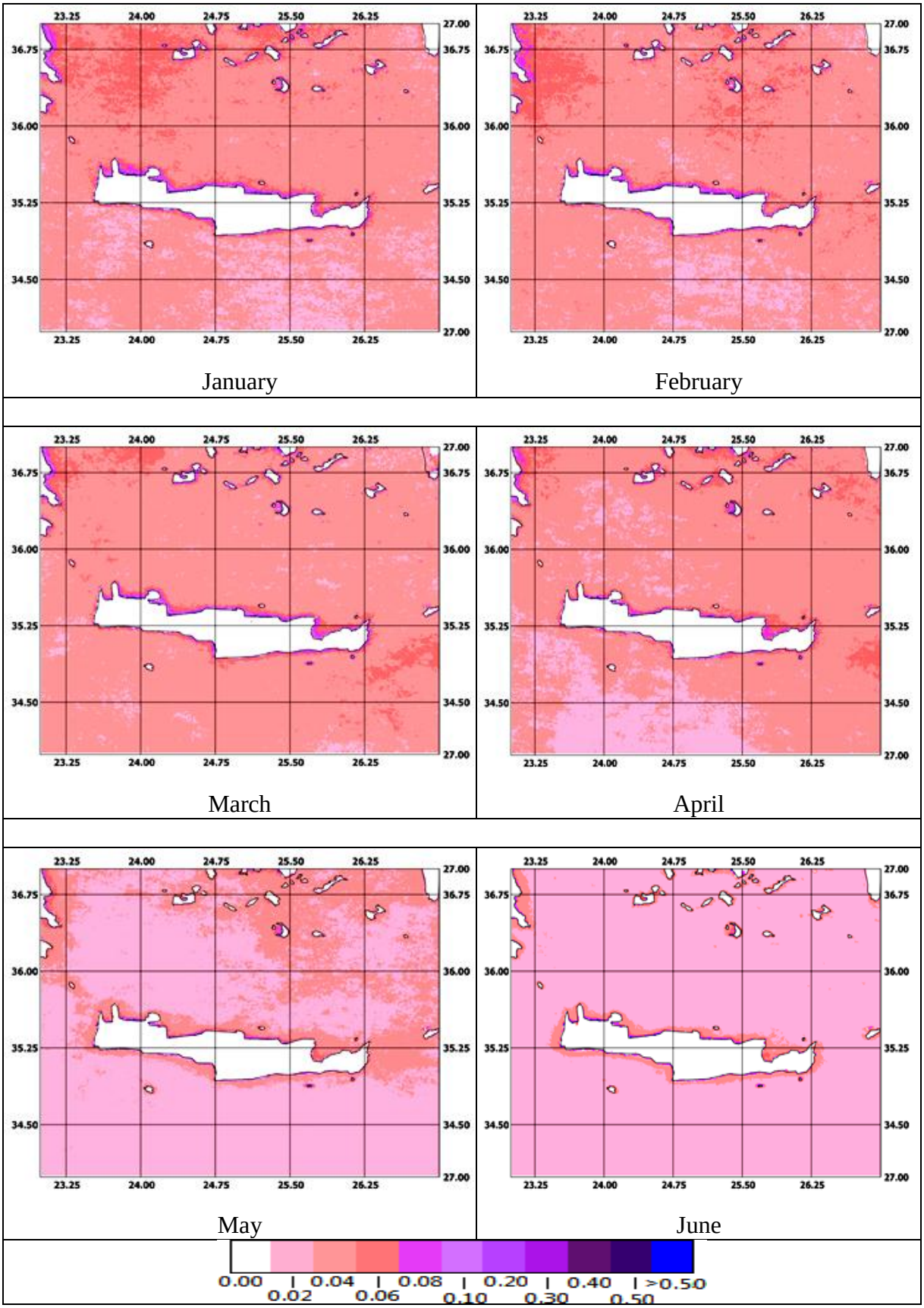
23.25
24.00
24.75
25.50
26.25
27.00
36.75
36.00
35.25
34.50
January
February
March
April
May
June
0.00
0.02
0.04
0.06
0.08
0.10
0.20
0.30
0.40
0.50
>0.50

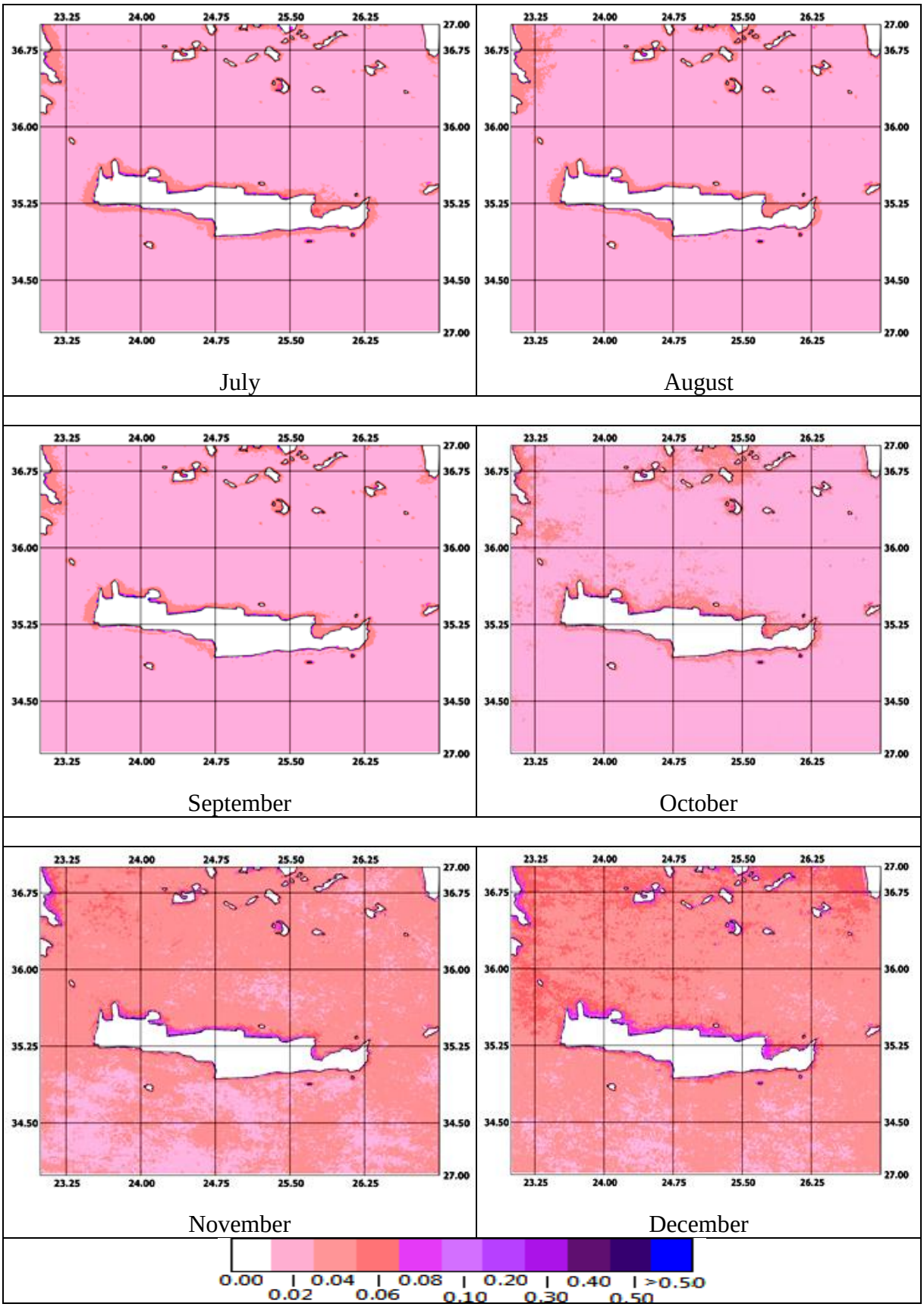

Figure 4.5 Monthly standard deviation chlorophyll-a concentration (mg/m3) maps generated by the long term (2003-2012) RST analysis

Looking at the maps shown in figure 4.4 and 4.5 some considerations may be done:

- the Chl-a concentration values around Crete Island range in a very short interval, between 0.05 – 0.30 mg/m^3, with very low fluctuations. These values are those typical measured for oligotrophic conditions, in good agreement with previous achievements (Lazzari at al., 2012);
- The highest variability, as expected, is achieved close to the coast, where human activities and the increased presence of nutrient influence inevitably the chlorophyll concentration. It seems that costal water in northern part have a dynamic higher, in terms of chlorophyll-a concentration values, than in the southern area: this is due by the high number of cities present along the northern coastline.
- A clear difference between cold and hot season is achievable: relatively high Chl-a concentration values are present during winter and fall, while low amount of chlorophyll-a have been detected during summer. Again, this results is well in agreement with previous work (Lazzari at al., 2012) and it is due to the high nutrient contribution by rivers as well the high vertical instability of water during winter season;
- In all the maps, the northern part of the investigated region shows chlorophyll-a concentration values higher than the southern area. The reason for this lies in the marine circulation: the northern part, in fact, belongs to a closed area in which waters are less subject to sea current producing an increase of chlorophyll-a.
- Santorini island coastal water have a behavior different from the surrounding sea water, showing always high concentration values. Again, the peculiar shape of the island, which promotes a stability of sea water, is responsible of this value increase.

To better characterize the detected multi-year trend, for each monthly maps (both temporal mean and standard deviation) the spatial average over the investigated waters has been computed. The results are shown in Table 4.2 an used to build the temporal 2003-2012 trend (Figure 4.6), where the blue line represents the mean trend of Chl-a while black lines show the range of fluctuation in terms of two times the standard deviation value. As already said, following RST philosophy, about the 98% of possibly Chl-a values should fall within such an interval.

Table 4.2 Spatially averaged values of Chlorophyll concentration over the Crete Island area

MONTH	Spatial average of temporal mean values 2003-2012 (mg/m^3)	Spatial average of standard deviations values (mg/m^3)
JAN	0,150578	0,029059
FEB	0,158867	0,029312
MAR	0,153683	0,028872
APR	0,116936	0,026120
MAY	0,080295	0,017667
JUN	0,067717	0,013022
JUL	0,063744	0,012934
AUG	0,060504	0,013862
SEP	0,064426	0,014241
OCT	0,078204	0,015706
NOV	0,110079	0,025025
DEC	0,125465	0,030034

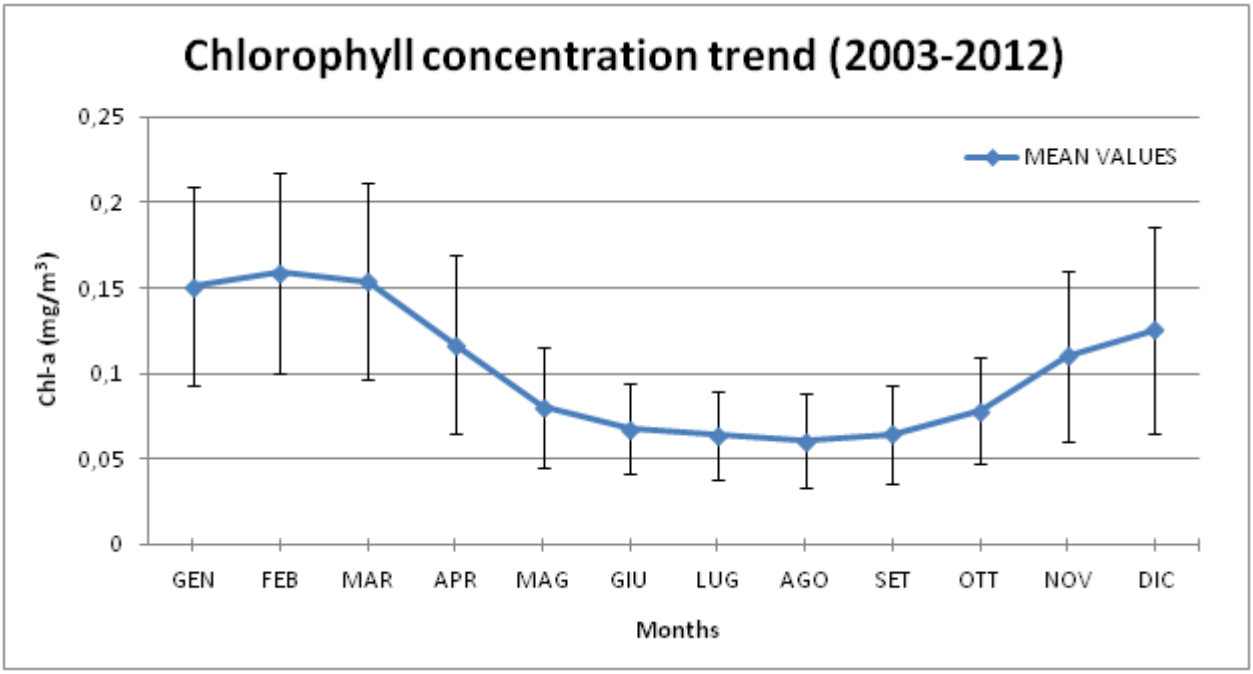

Figure 4.6 Multi-year (2003-2012) Chlorophyll-a trend for Crete island sea water

The analysis of Figure 4.6 confirms the previous consideration. Over the investigated ten-year period, the values of Chl-a concentration for the water surrounding Crete Island are almost low and quite stable in time. A clear seasonal trend is detectable, with high value and a high variability during winter. Definitively such sea water may be described as oligotrophic.

This first relevant result represents the basis of the next analysis: only after the exact characterization of the "normal" behavior of the investigated parameter, both in term of expected value and normal variability, possible critical/anomalous situation can be identified.

➢ 4.3.2 Yearly investigation

The same procedure applied before was carried out also at annual temporal scale. By such an investigation, we would like to better characterize the behavior of Chl-a concentration for the Crete island sea water, trying to identify possible deviations from the long term trend previously identified.

In the Figure 4.7 - 4.16 are shown, for each year from 2003 to 2012, both the chlorophyll concentration values (spatial average of temporal mean image) and the relative graph (red line) overlapped on previously identified multi-year trend.

a/a 2003	Chl-a (mg/m^3)
JAN	0,132335
FEB	0,143957
MAR	0,159441
APR	0,167441
MAY	0,099181
JUN	0,076521
JUL	0,069625
AUG	0,066629
SEP	0,070252
OCT	0,077747
NOV	0,102977
DEC	0,119707

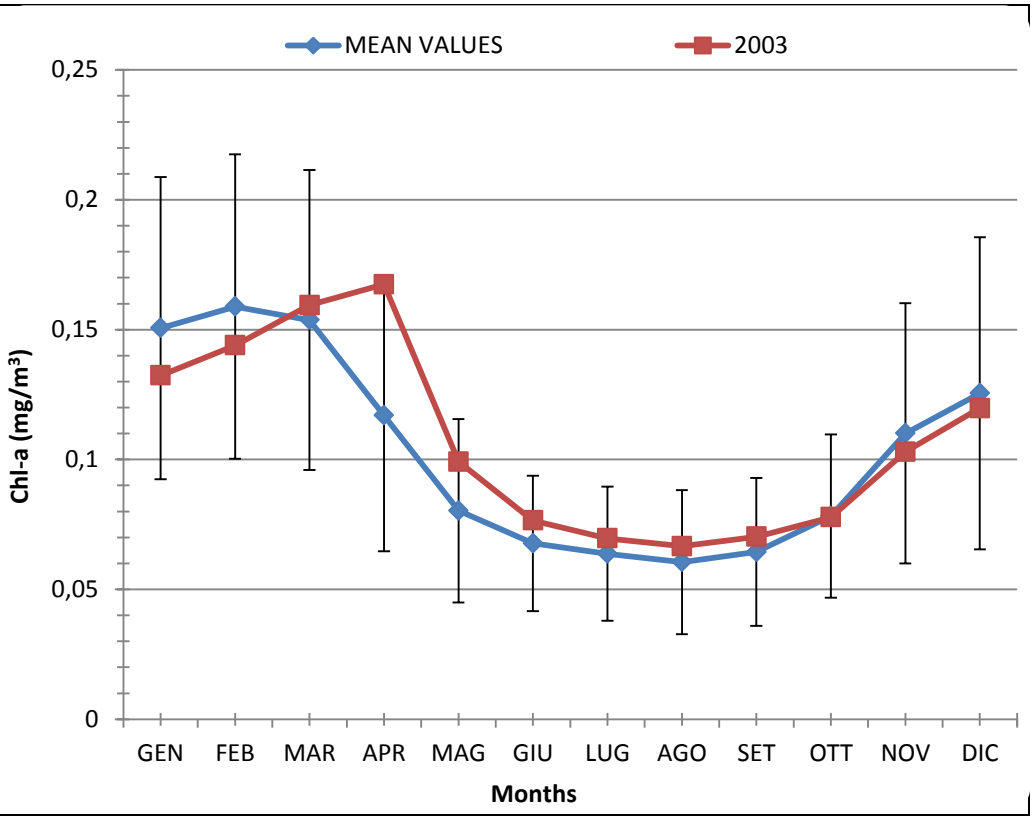

Figure 4.7 On the left: Spatially Averaged monthly Chl-a concentration for 2003. On the right, in red, 2003 Chlorophyll-a trend for Crete island sea water, in blue the multi-year (2003-2012) Chlorophyll-a trend already shown in figure 4.6

a/a 2004	Chl-a (mg/m^3)
JAN	0,153293
FEB	0,164967
MAR	0,168802
APR	0,119231
MAY	0,090589
JUN	0,072592
JUL	0,067829
AUG	0,062454
SEP	0,064836
OCT	0,070978
NOV	0,102610
DEC	0,115576

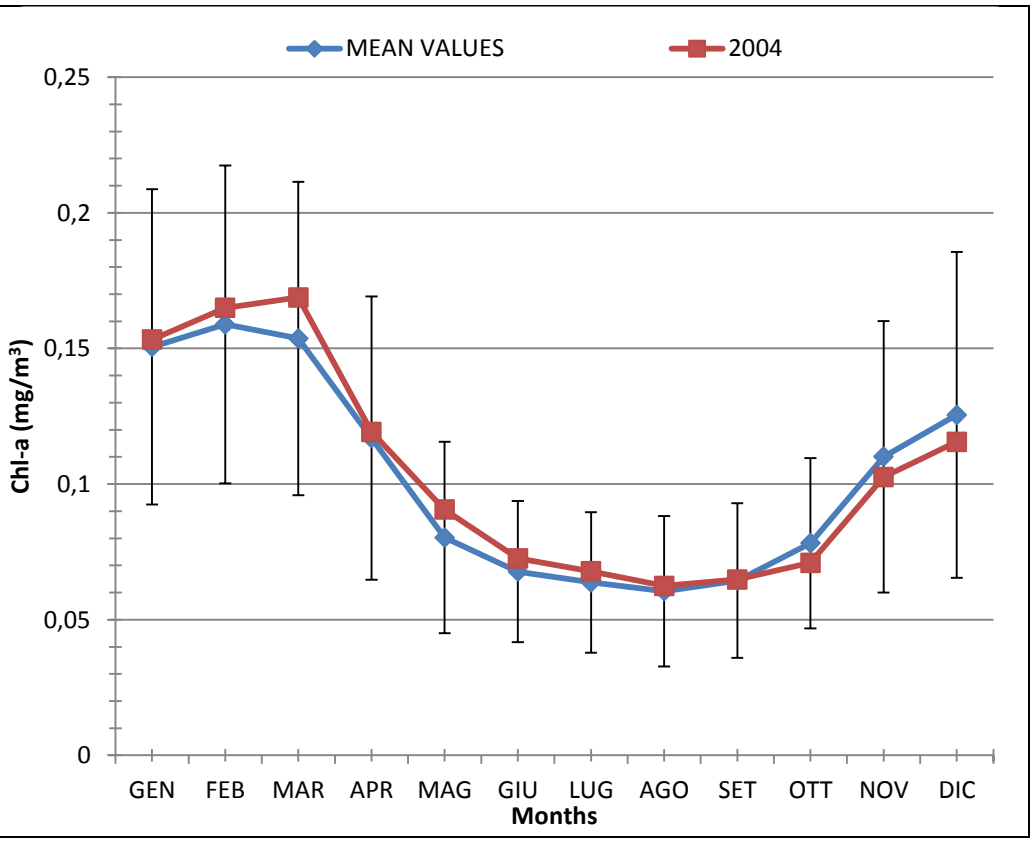

Figure 4.8 As figure 4.7 for 2004

a/a 2005	Chl-a (mg/m^3)
JAN	0,146015
FEB	0,150831
MAR	0,156591
APR	0,120612
MAY	0,073099
JUN	0,065601
JUL	0,062092
AUG	0,059133
SEP	0,060356
OCT	0,076501
NOV	0,093100
DEC	0,117262

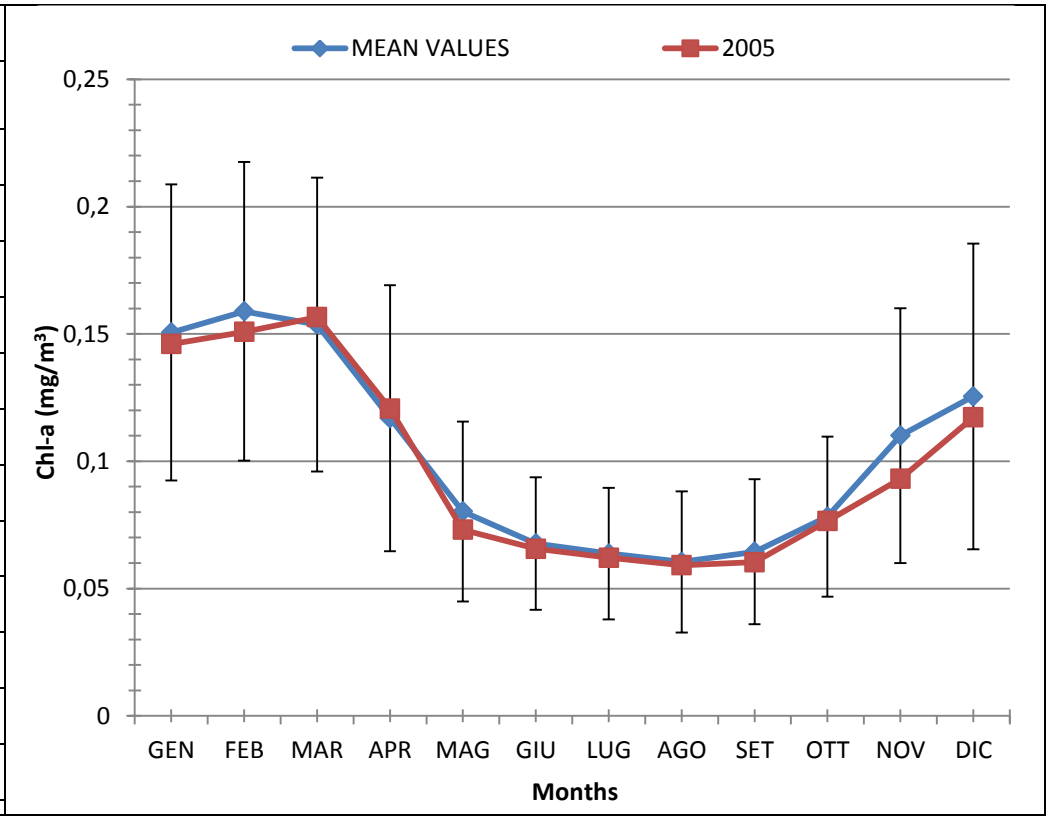

Figure 4.9 As figure4.7 for 2005

a/a 2006	Chl-a (mg/m^3)
JAN	0,148626
FEB	0,173262
MAR	0,158964
APR	0,119345
MAY	0,080910
JUN	0,065563
JUL	0,065407
AUG	0,064996
SEP	0,071886
OCT	0,090806
NOV	0,138976
DEC	0,139551

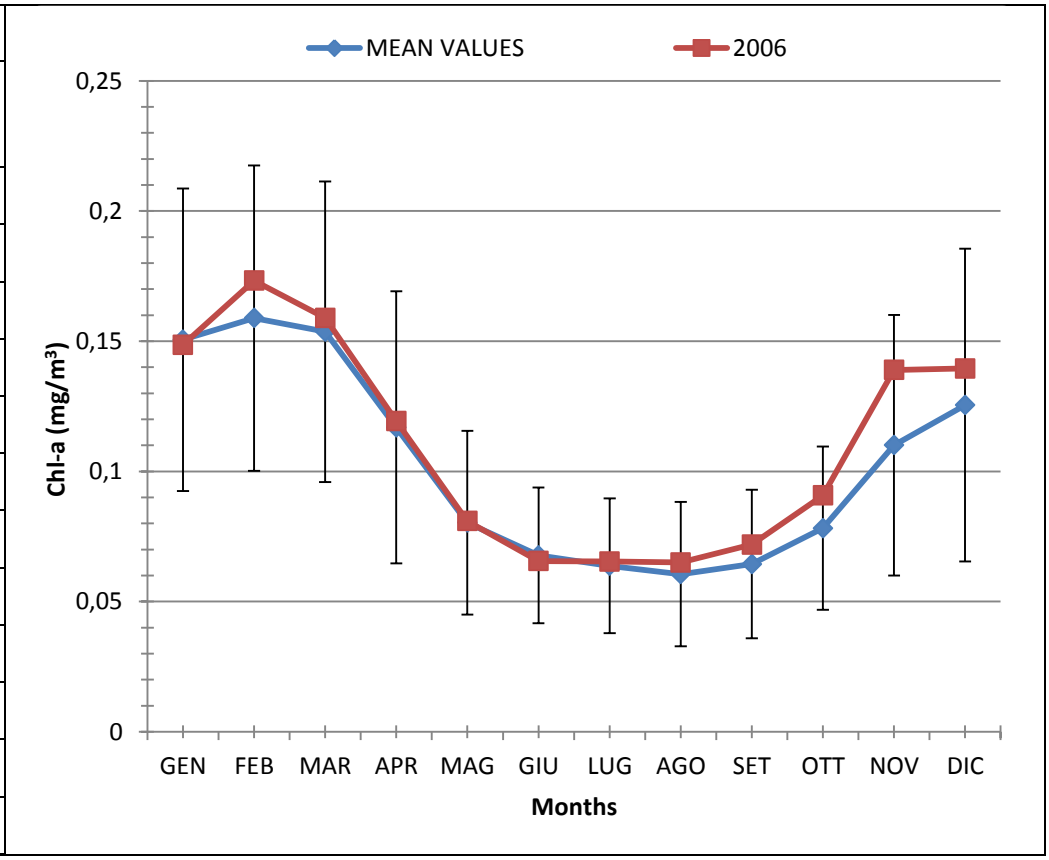

Figure 4.10 As figure 4.7 for 2006

a/a 2007	Chl-a (mg/m^3)
JAN	0,171843
FEB	0,156628
MAR	0,164318
APR	0,125390
MAY	0,095649
JUN	0,087574
JUL	0,069819
AUG	0,065156
SEP	0,067282
OCT	0,077769
NOV	0,111551
DEC	0,122807

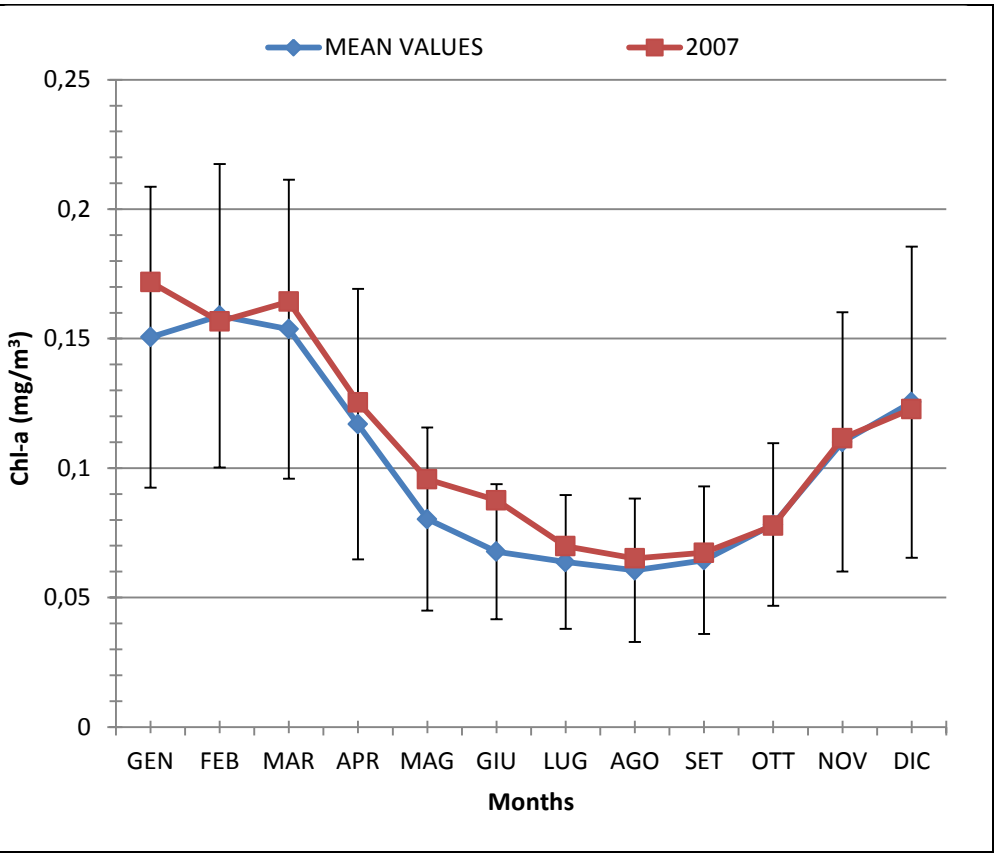

Figure 4.11As figure 4.7 for 2007

a/a 2008	Chl-a (mg/m^3)
JAN	0,148284
FEB	0,164296
MAR	0,156766
APR	0,140388
MAY	0,069494
JUN	0,062074
JUL	0,061234
AUG	0,058512
SEP	0,063852
OCT	0,087025
NOV	0,101034
DEC	0,130250

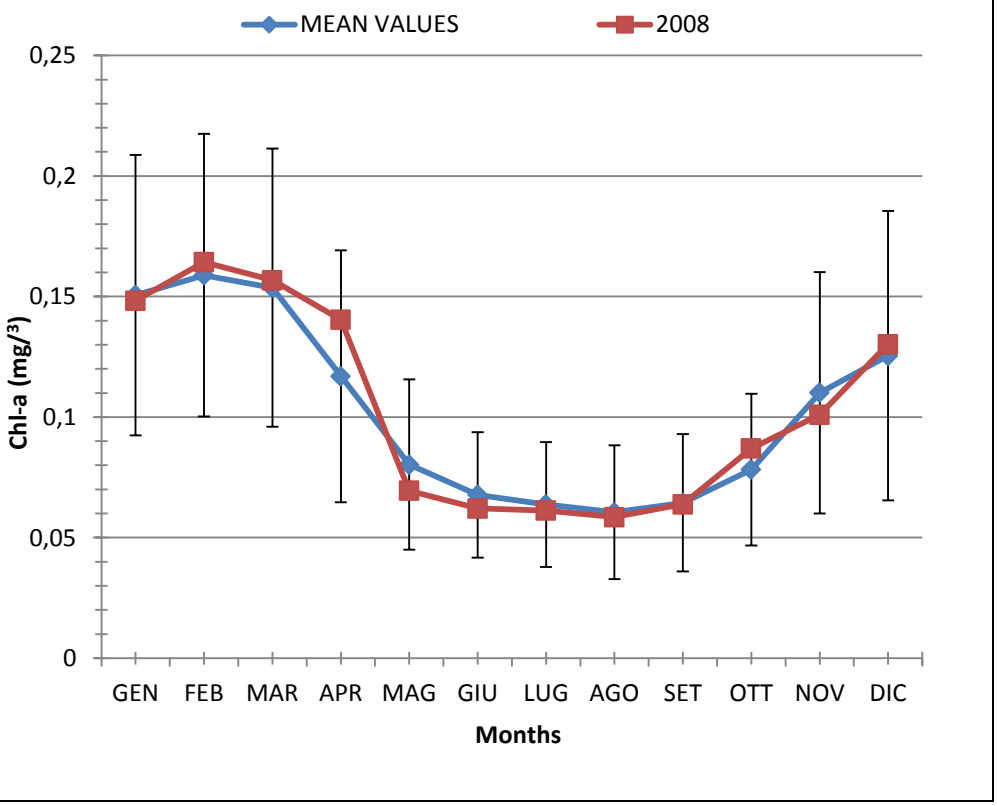

Figure 4.12As figure 4.7 for 2008

a/a 2009	Chl-a (mg/m^3)
JAN	0,162500
FEB	0,158746
MAR	0,153941
APR	0,102446
MAY	0,069846
JUN	0,057730
JUL	0,056761
AUG	0,056583
SEP	0,061514
OCT	0,078939
NOV	0,121270
DEC	0,141181

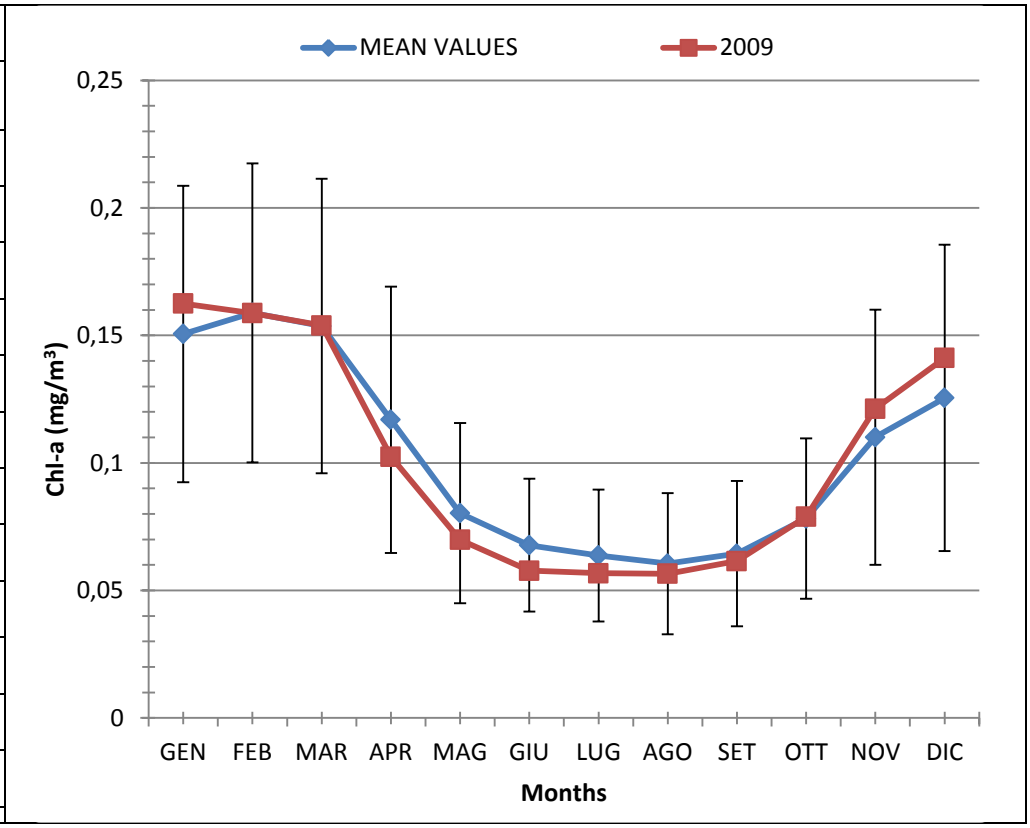

Figure 4.13 As figure 4.7 for 2009

a/a 2010	Chl-a (mg/m^3)
JAN	0,141510
FEB	0,164399
MAR	0,159954
APR	0,103868
MAY	0,080258
JUN	0,063879
JUL	0,059145
AUG	0,051788
SEP	0,053551
OCT	0,070727
NOV	0,097667
DEC	0,097390

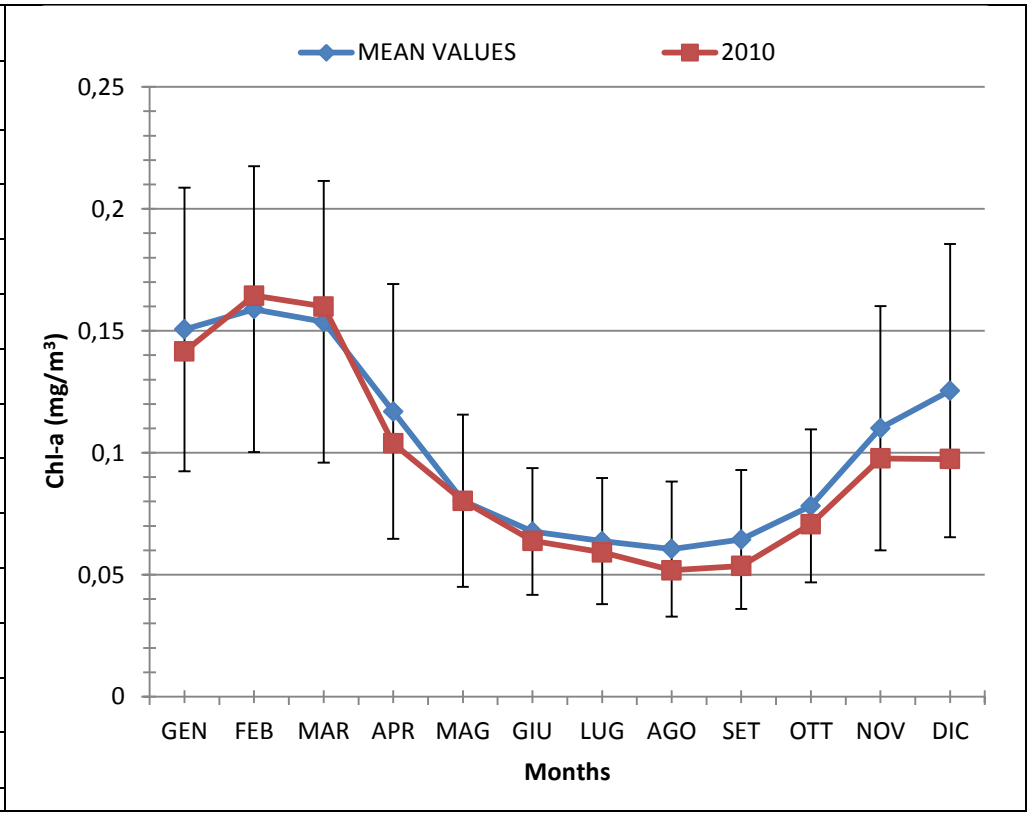

Figure 4.14 As figure 4.7 for 2010

a/a 2011	Chl-a (mg/m^3)
JAN	0,115480
FEB	0,146067
MAR	0,139286
APR	0,113523
MAY	0,087868
JUN	0,064668
JUL	0,054044
AUG	0,051020
SEP	0,055548
OCT	0,080671
NOV	0,107378

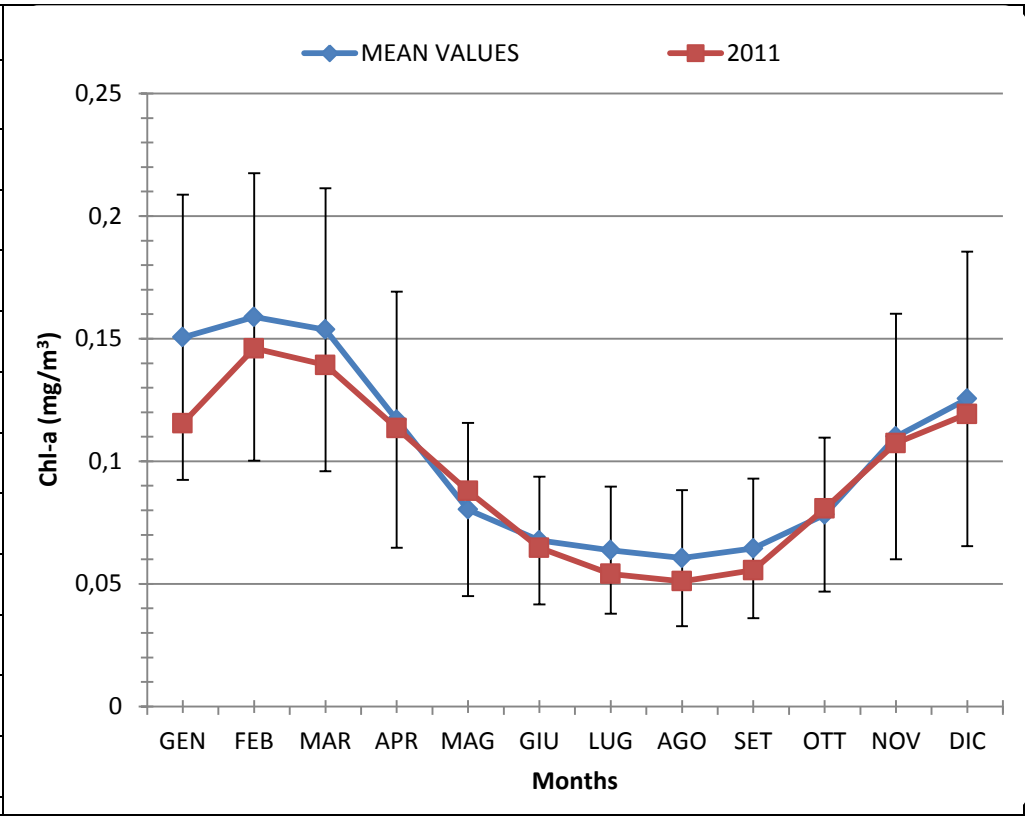

Figure 4.15 As figure 4.7 for 2011

a/a 2012	Chl-a (mg/m^3)
JAN	0,145495
FEB	0,147898
MAR	0,144707
APR	0,119090
MAY	0,078676
JUN	0,067284
JUL	0,061740
AUG	0,061348
SEP	0,064690
OCT	0,067356
NOV	0,094014
DEC	0,118618

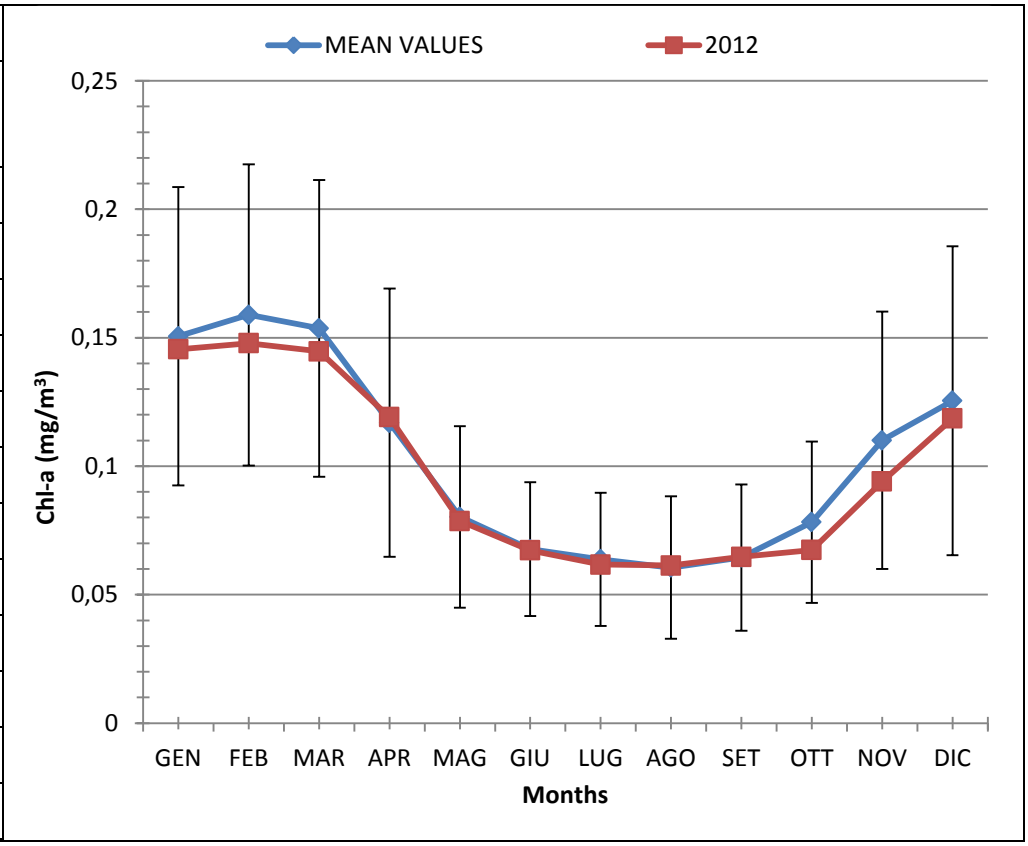

Figure 4.16 As figure 4.7 for 2012

Analyzing the results, the first thing that can be noted is that in every year a chlorophyll-a trend almost similar to the long term trend has been detected; this seems to indicate that the sea conditions have been almost stable in time, even if the 2003 shows a strange feature. Looking at Figure 4.7, in fact, it can be seen that the spatially averaged Chl-a concentration value for April 2003 does not follow the expected trend, resulting higher (and not lower, as usually) than the one measured in the previous month (i.e. March 2003) and the highest among all the other April months that have been analyzed. Figure 4.17 provides a summary of this achievements showing the temporal trend of spatially averaged Chl-a concentration values for the month of April in the period 2003-2012, plotted together with long term mean value and the two times standard deviation interval.

As it is possible to observe, the Chl-a value achieved for April is almost out of the natural "normal" confidence interval. Considering that such a value has been obtaining by averaging an area of almost 120 km^2, it is clear that something perturbed the Chl-a map achieved for April 2003.

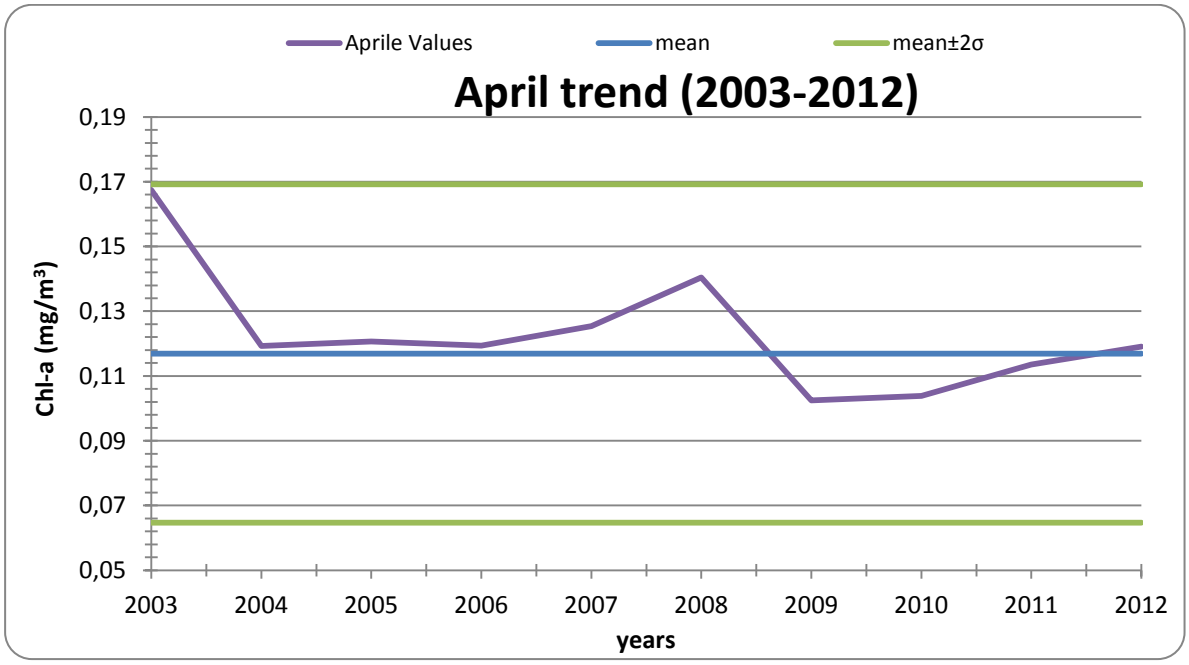

Figure 4.17 Analysis of a partially averaged Chl-a concentration (mg/m3) for the month April, from 2003 to 2012. Blue line: mean multi-year value; purple line: mean yearly value; green lines: two times standard deviation interval

The Chl-a concentration map of April 2003 is plotted in Figure 4.18 and the corresponding monthly Chl-a ALICE map in Fig. 4.19. This last map has been obtained applying equation 3.2, using as image at hand the April 2003 Chl-a map, which has been compared with the Chl-a multi-year (2003-2012) temporal mean and standard deviation maps.

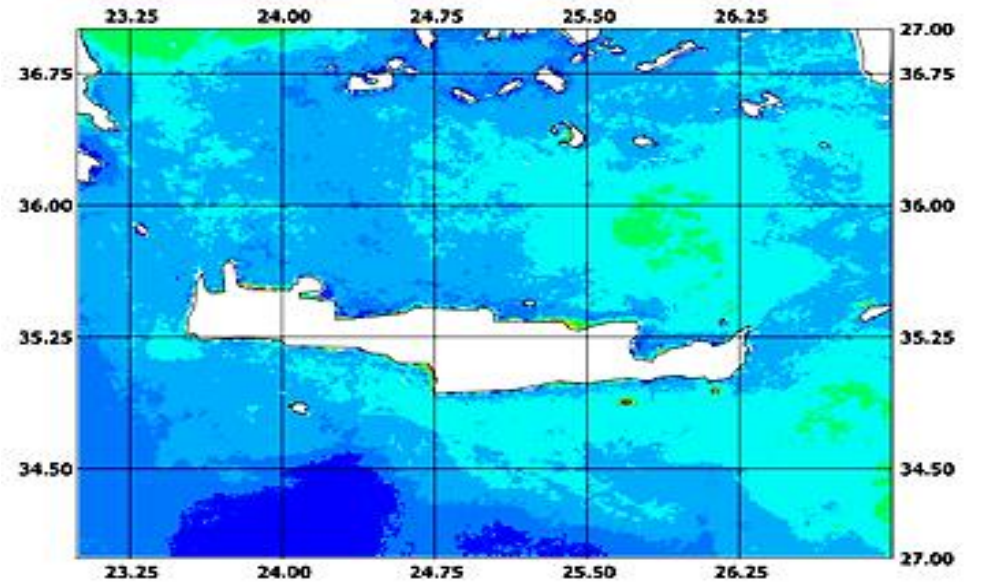

Figure 4.18 Chlorophyll concentration (mg/m3) map of April 2003

Looking at Figure 4.18, it is possible to note as Chl-a values are almost in line with we expected. Values mainly range between 0.10 and 0.30 mg/m^3, with some area interested by values up to 0.40 mg/m^3. The map itself is not describing an extreme situation in term of chlorophyll-a concentration values. They could be identified as excessive only thanks to the previous carried out RST analysis, where we discovered that for April, "normal" values are in the range 0.07 and 0.17 mg/m^3. Figure 4.19 describes graphically the concept just exposed. Also low absolute values of chlorophyll-a concentration, may represent significant statistically deviation from expected values. This is even more important when the investigated signals shows low "normal" values and low natural fluctuation, as in the case of chlorophyll-a concentration for Crete Island sea-water. In Figure 4.19, the anomalous pixels (those having a Chl-a concentration higher than 25 mg/m^3) have been detected at medium intensity (>6) Chl-a ALICE index.

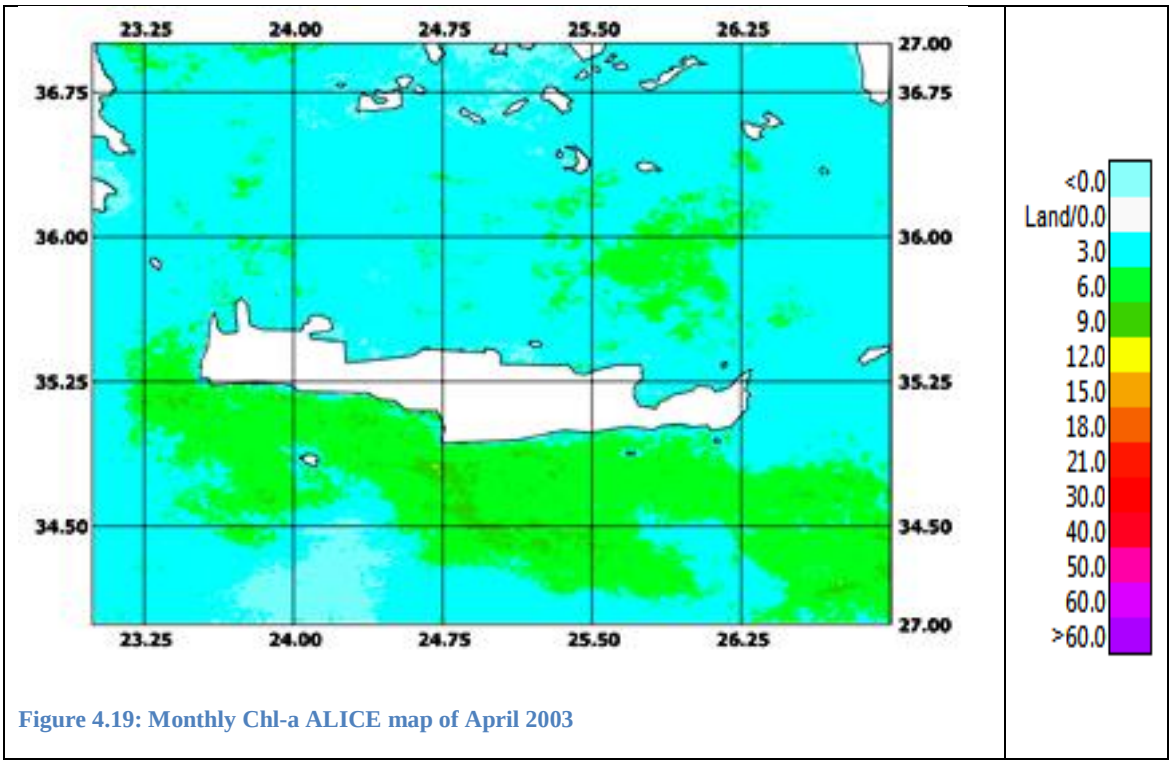

Figure 4.19: Monthly Chl-a ALICE map of April 2003

➢ 4.3.3 Short time investigation

The results just showed highlighted the capabilities of RST in detecting long term trend as well as possible critical spatial/temporal features, working at long/medium temporal scale. In this paragraph we will analyze its potential in identifying short temporal scale variations which are, obviously, fundamental when monitoring activities are in progress. The timely identification of critical situation may be crucial in order to limit the effects of the phenomena in progress and of its consequence.

Starting from the achievements reached in the previous paragraph, the ALICE index (**Eq. 3.2**) was computed for all the daily Chl-a maps of April 2003, looking for the possible source of the anomalous monthly behavior. In this case, the Chl-a concentration values measured in each image acquired during April 2003 represents the image at hand to be compared with the multi-year April temporal mean and standard deviation maps. The index was computed only for the "clear" (without clouds coverage or with poor cloud coverage) imagery of the month (in total twelve images); in this way it will be possible to check if there was a particular event that influenced April 2003 behavior much more than the others.

Chl-a ALICE maps for each day are shown in Figure 4.20 - 4.31 together with relative chlorophyll maps and RGB image. This last image provides the view of the region of interest with the cloud coverage. Clouds, land pixels, as well as areas outside of MODIS swath have been depicted in white in the chlorophyll and ALICE map. Also those areas for which NASA algorithm fails in detecting Chl-a concentration are in white in both the maps. Failures of the Chl-a algorithms may be due by high atmospheric contribution, as well as by the presence of turbid water (O'Really et al., 1998; 2000).

a)

b)

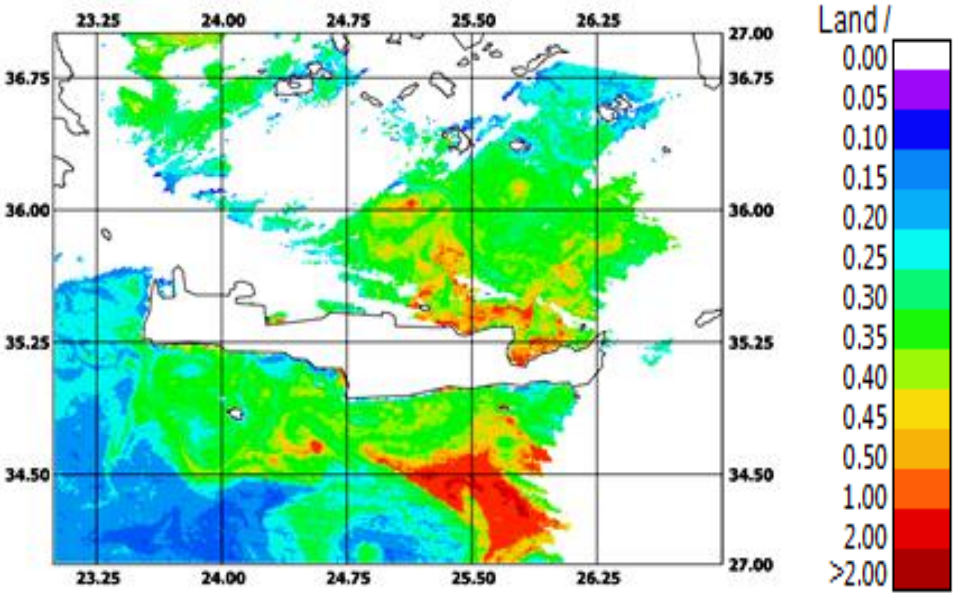

c)

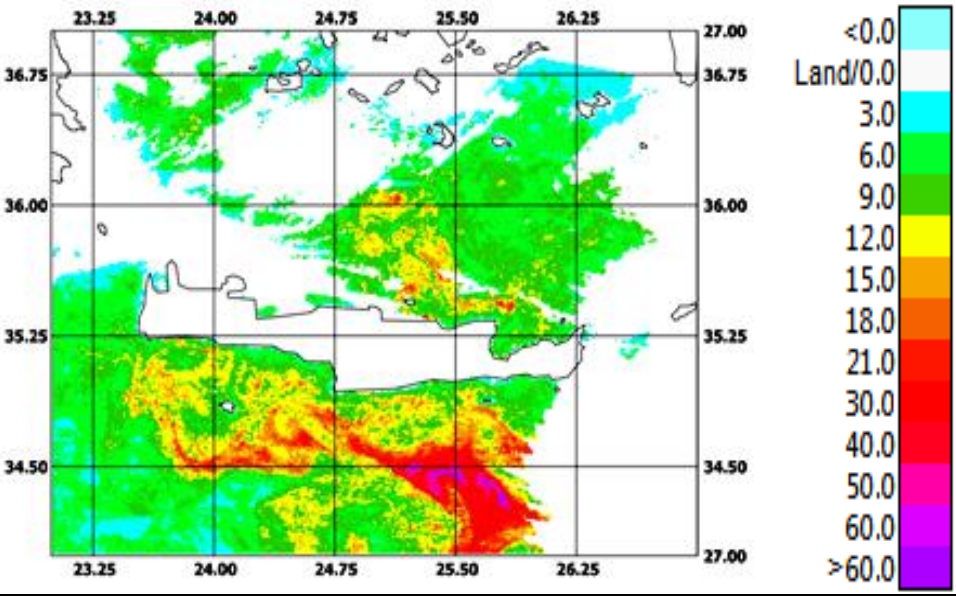

Figure 4.20 a) RGB of the MODIS acquisition of 4th April 2003 at 9:15am GMT; b) the correspondent chlorophyll-a map produced by NASA (OC3 algorithm - O'Really et al., 1998; 2000; c) the correspondent Chl-a ALICE map

a)

b)

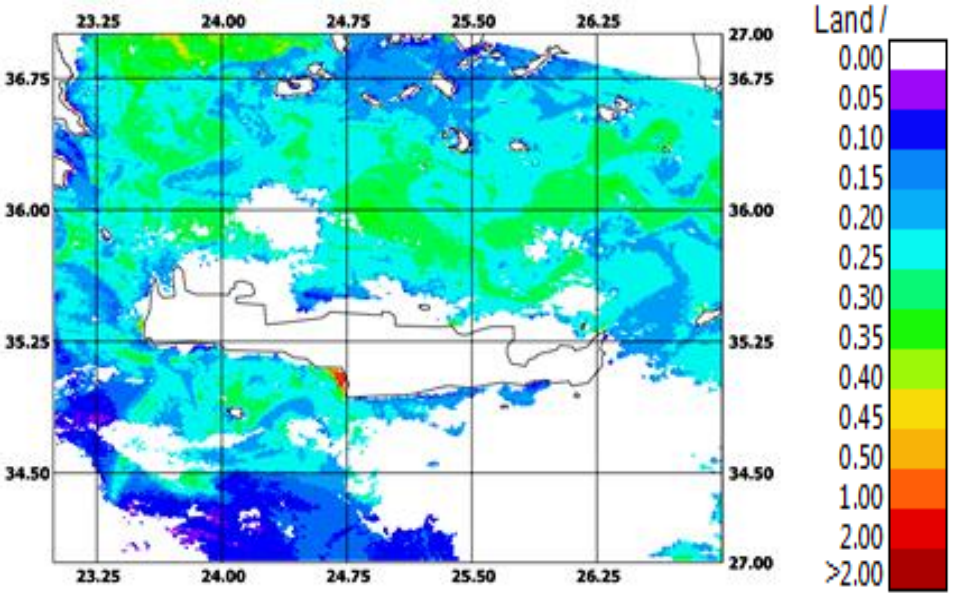

c)

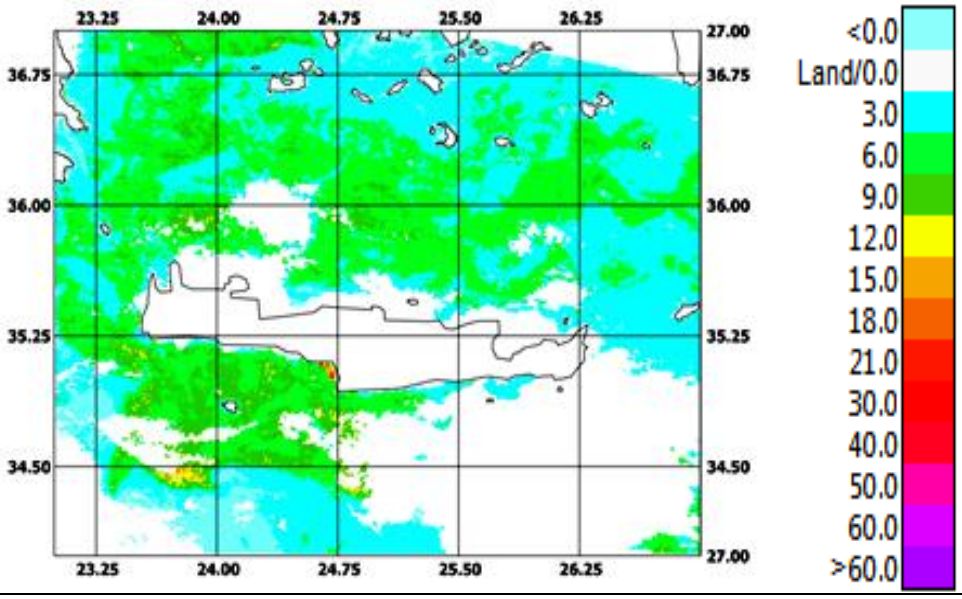

Figure 4.21as figure 4.20 for the MODIS acquisition of 9th April 2003 at 9:35am GMT

a)

b)

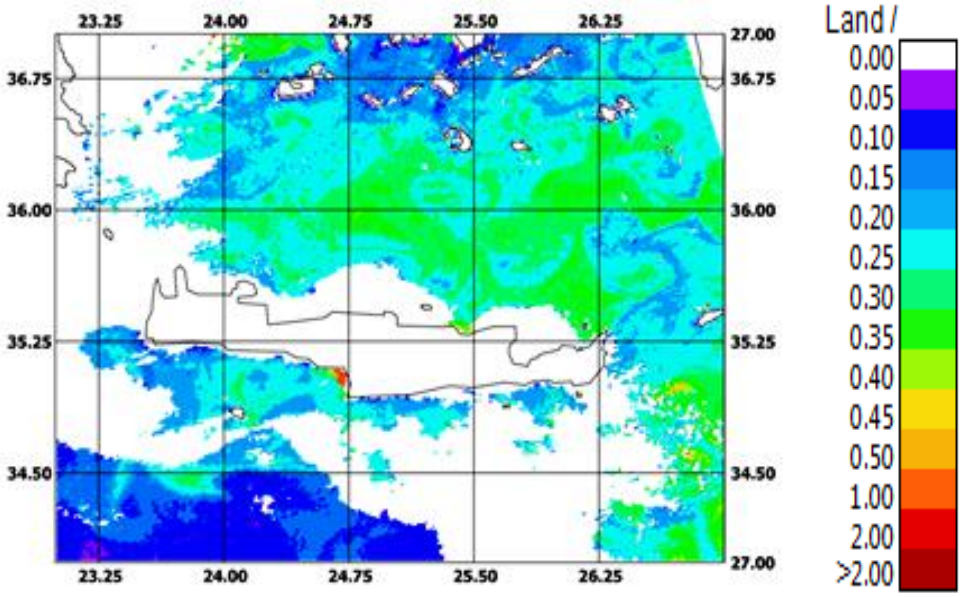

c)

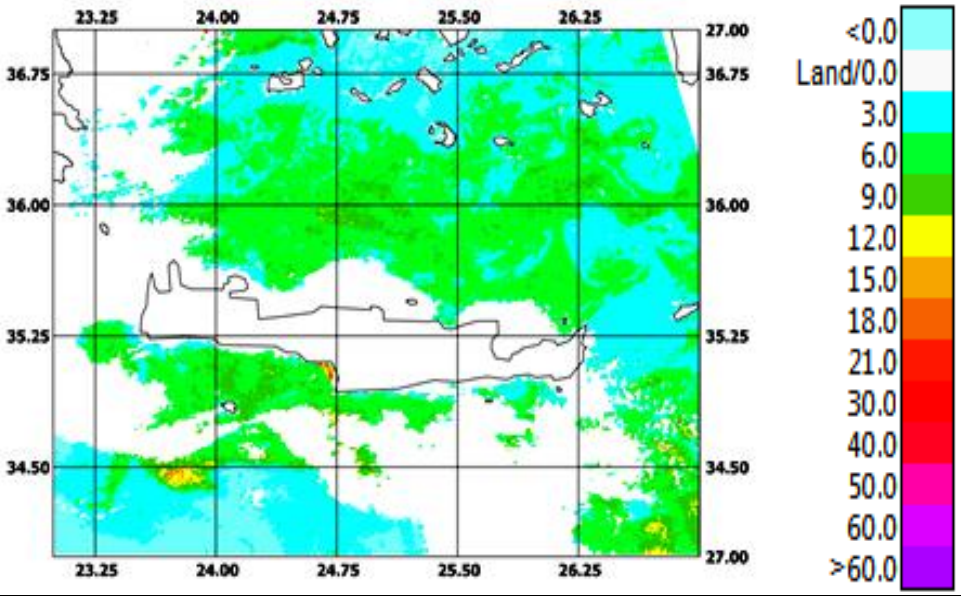

Figure 4.22 as figure 4.20 for the MODIS acquisition 9th April 2003 at 11:05am GMT

a)

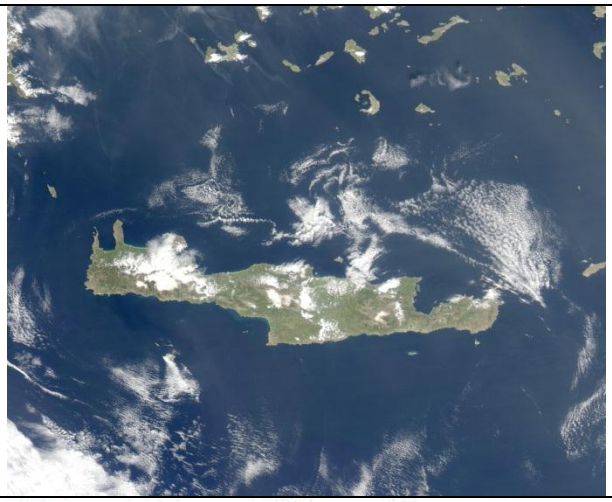

b)

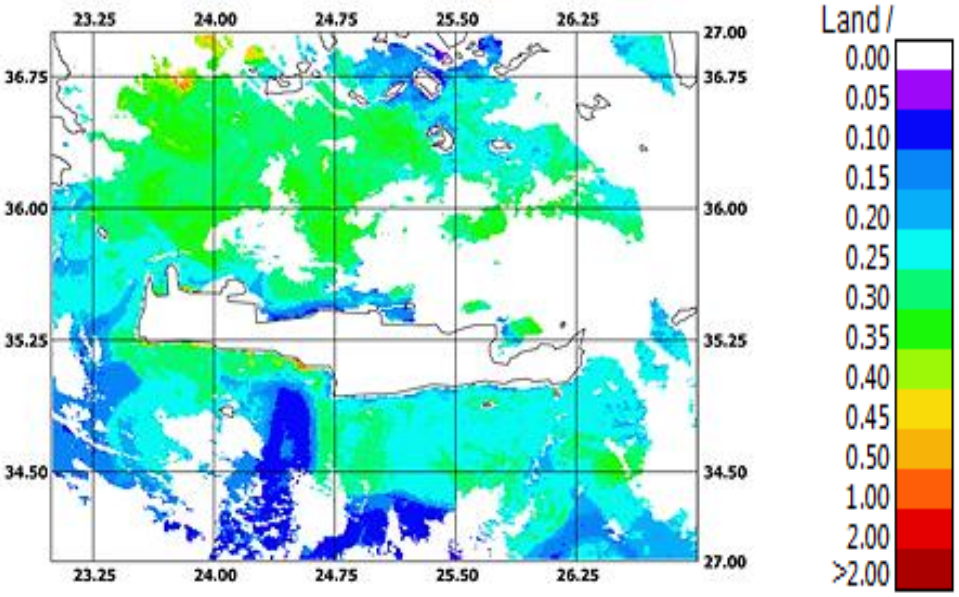

c)

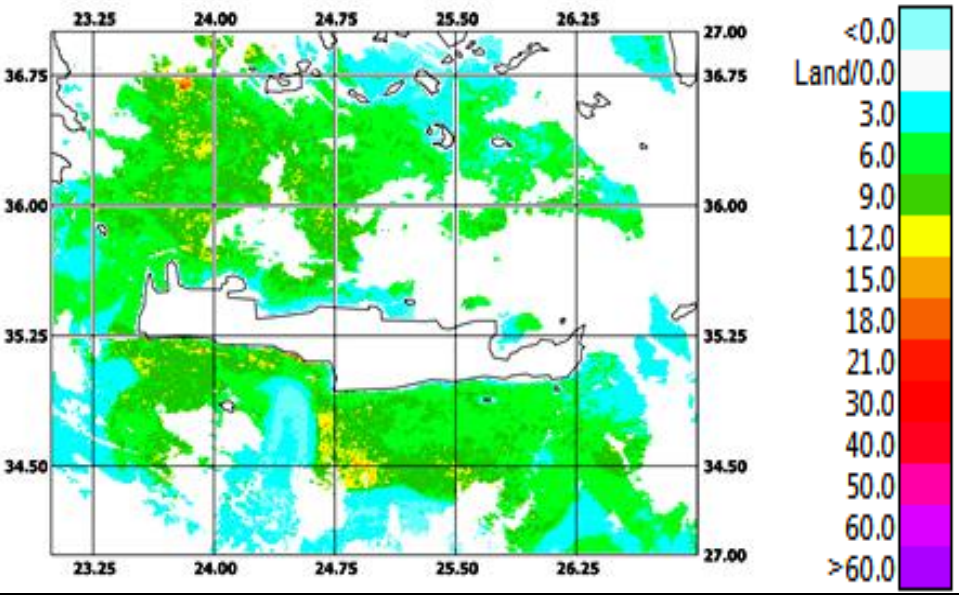

Figure 4.23 as figure 4.20 for the MODIS acquisition of 12th April 2003 at 11:35am GMT

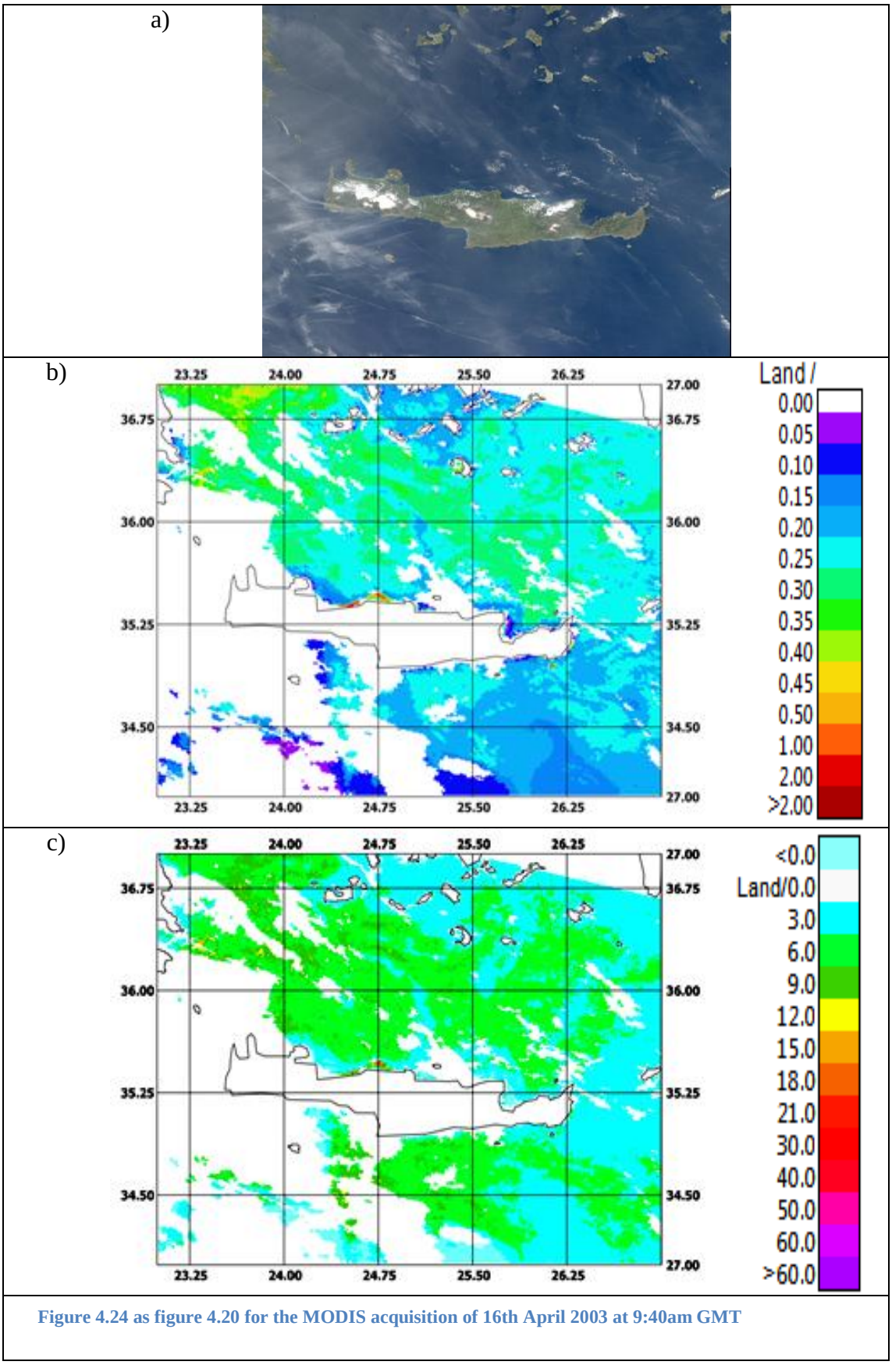

Figure 4.24 as figure 4.20 for the MODIS acquisition of 16th April 2003 at 9:40am GMT

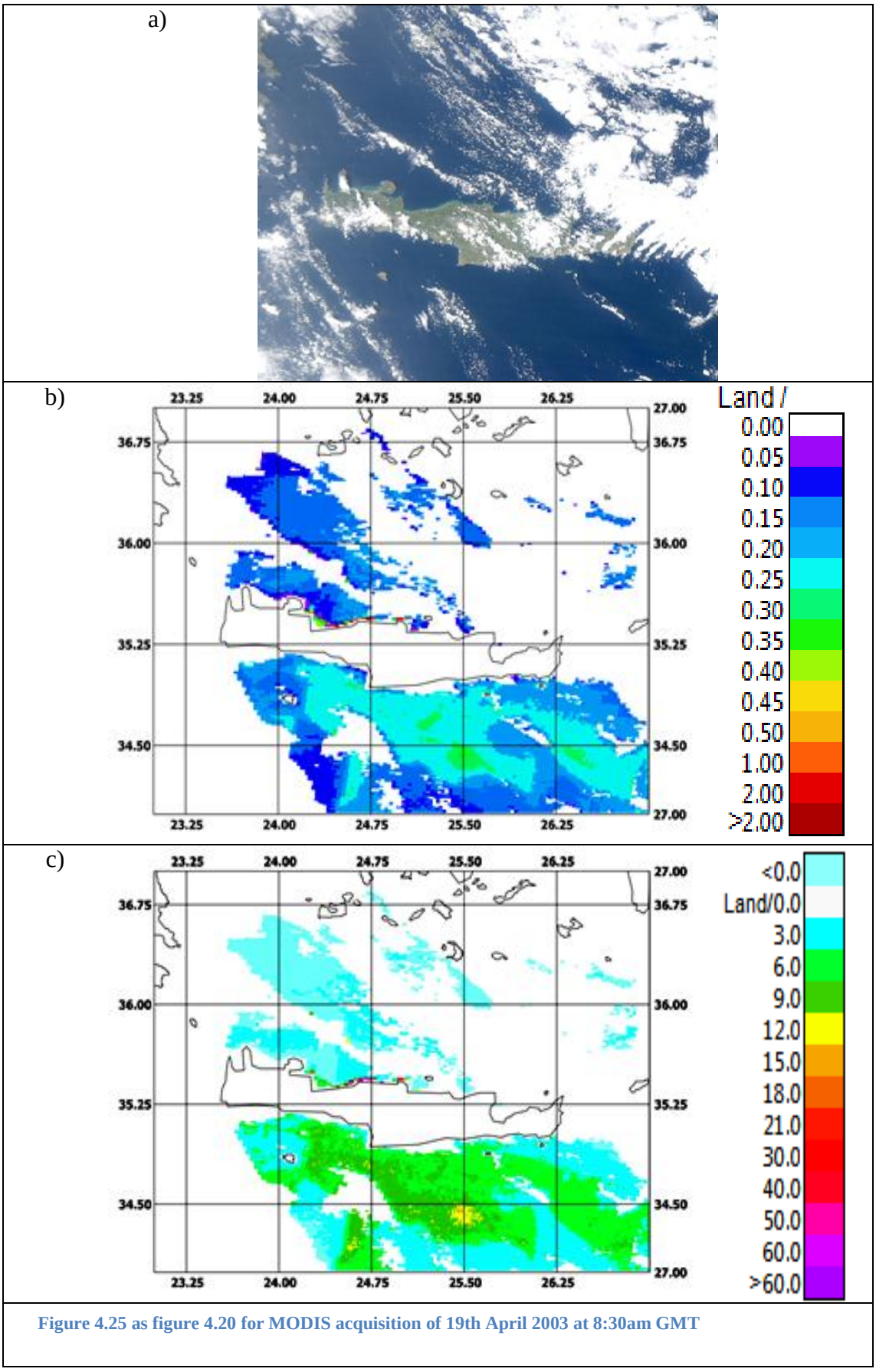

Figure 4.25 as figure 4.20 for MODIS acquisition of 19th April 2003 at 8:30am GMT

a)

b)

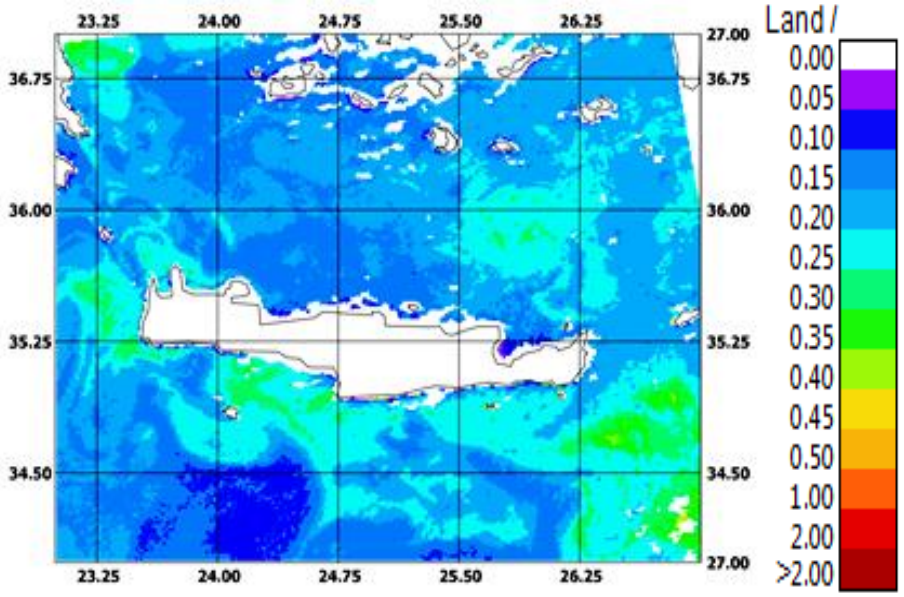

c)

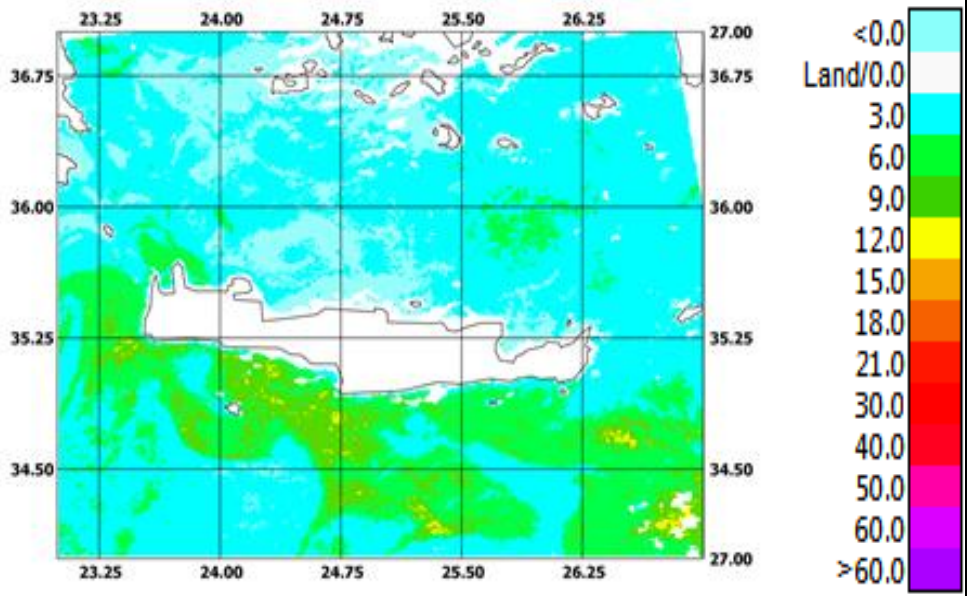

Figure 4.26 as figure 4.20 for MODIS acquisition of 26th April 2003 at 11:50am GMT

a)

b)

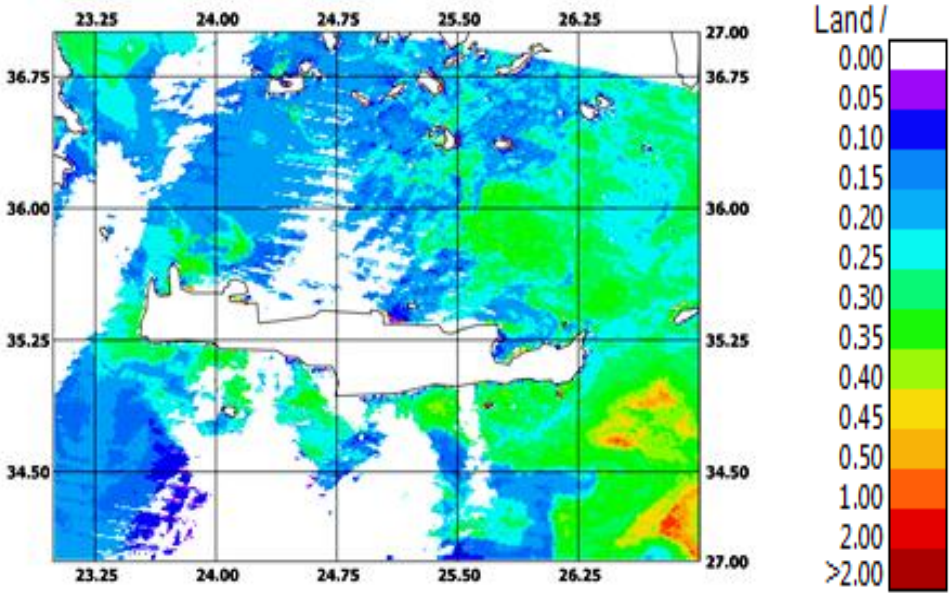

c)

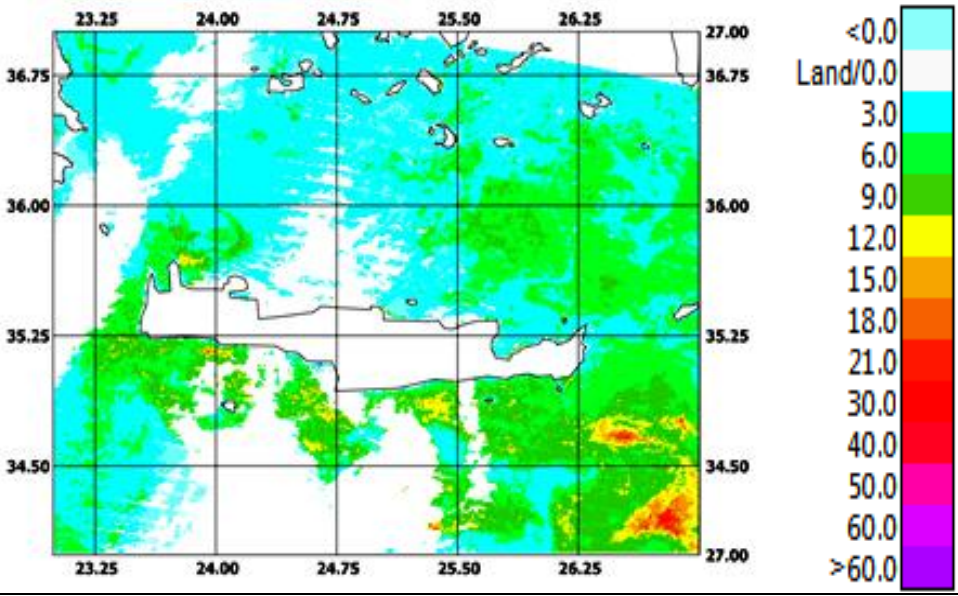

Figure 4.27 as figure 4.20 for MODIS acquisition of 27th April 2003 at 9:20am GMT

a)

b)

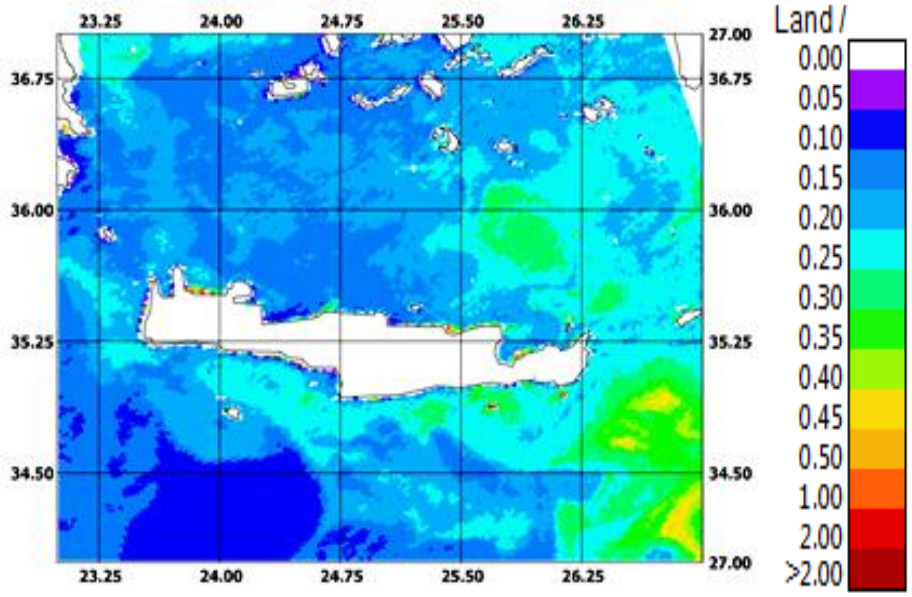

c)

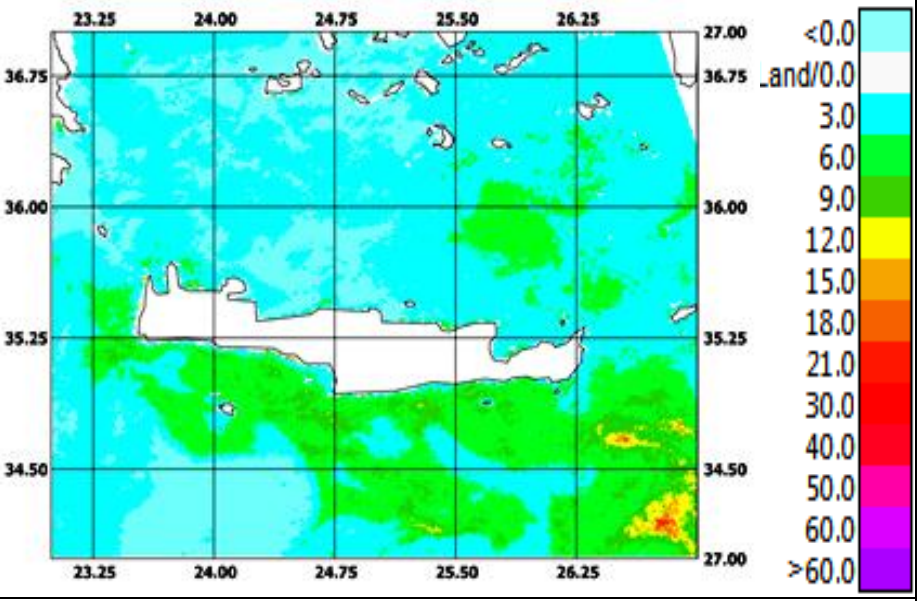

Figure 4.28 as figure 4.20 for MODIS acquisition of 27th April 2003 at 10:55am GMT

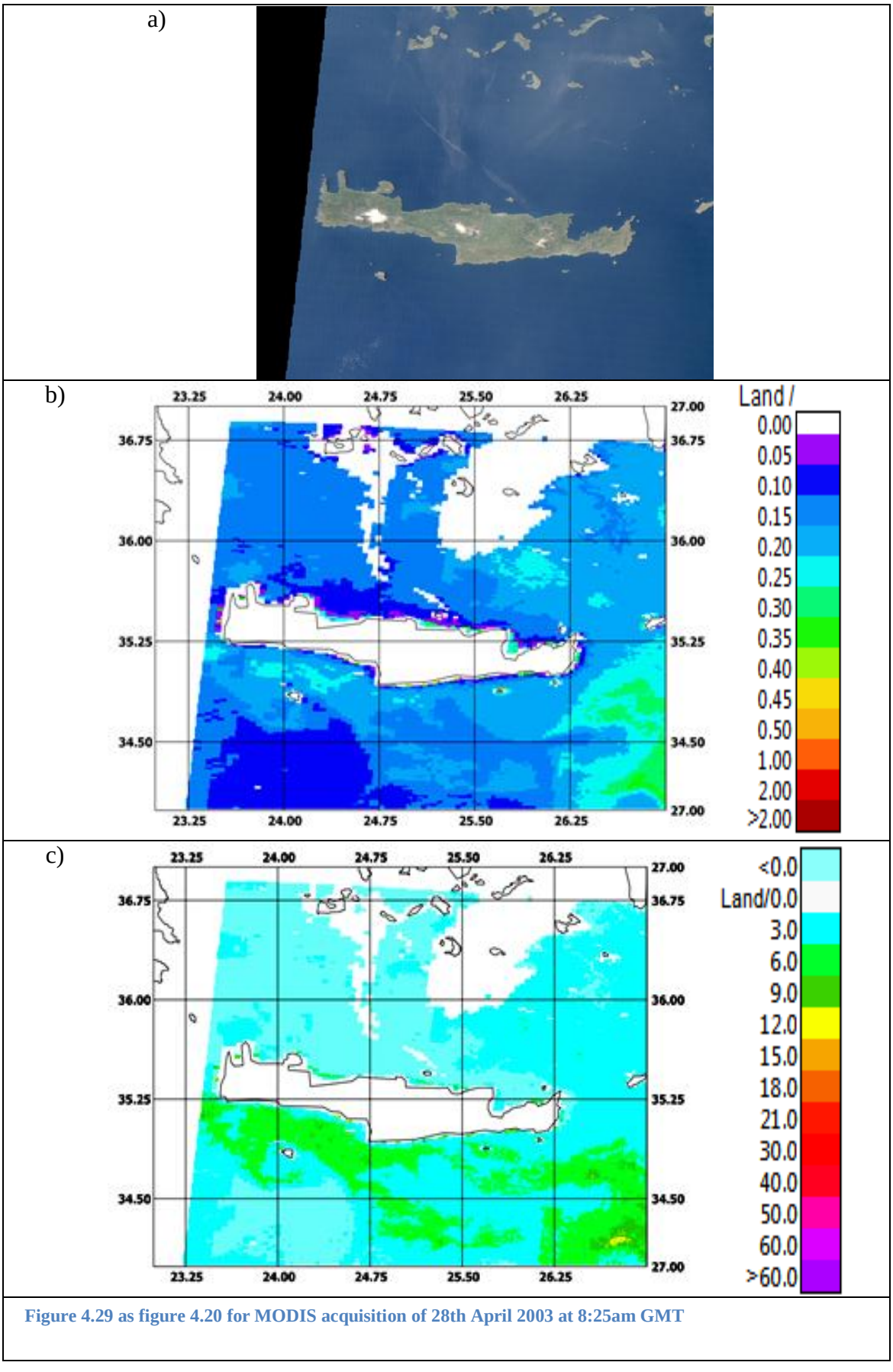

Figure 4.29 as figure 4.20 for MODIS acquisition of 28th April 2003 at 8:25am GMT

a)

b)

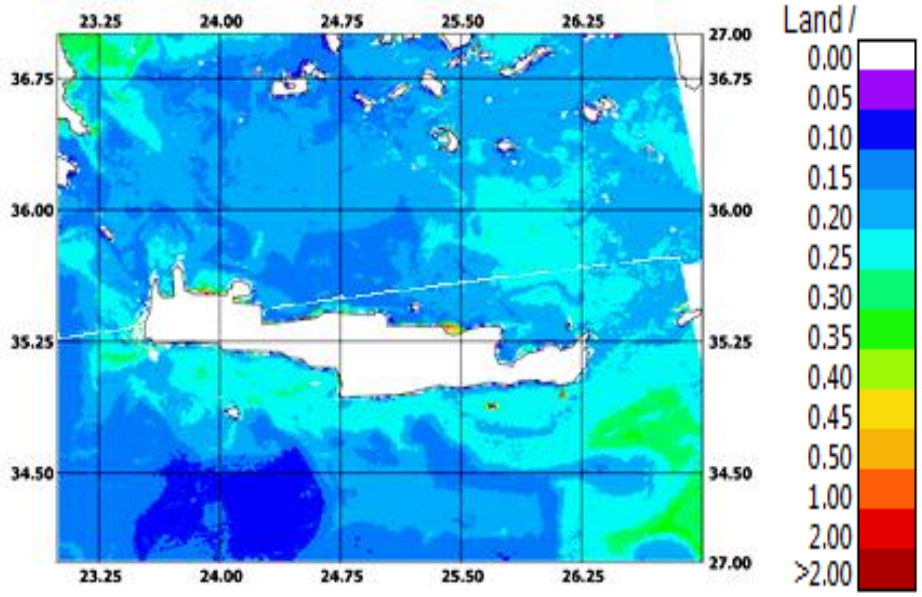

c)

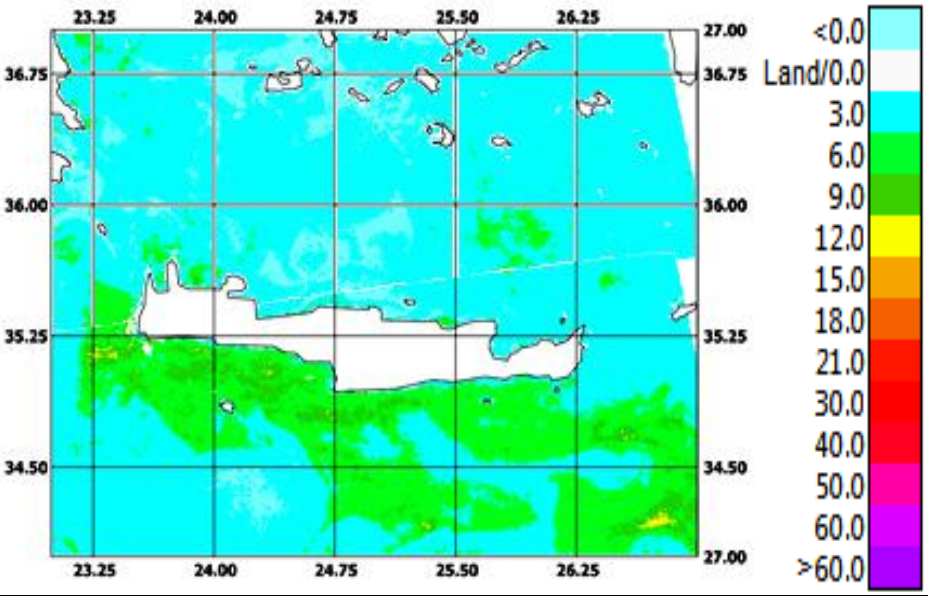

Figure 4.30 as figure 4.20 for MODIS acquisition of 28th of April 2003 at 11:35am GMT

a)

b)

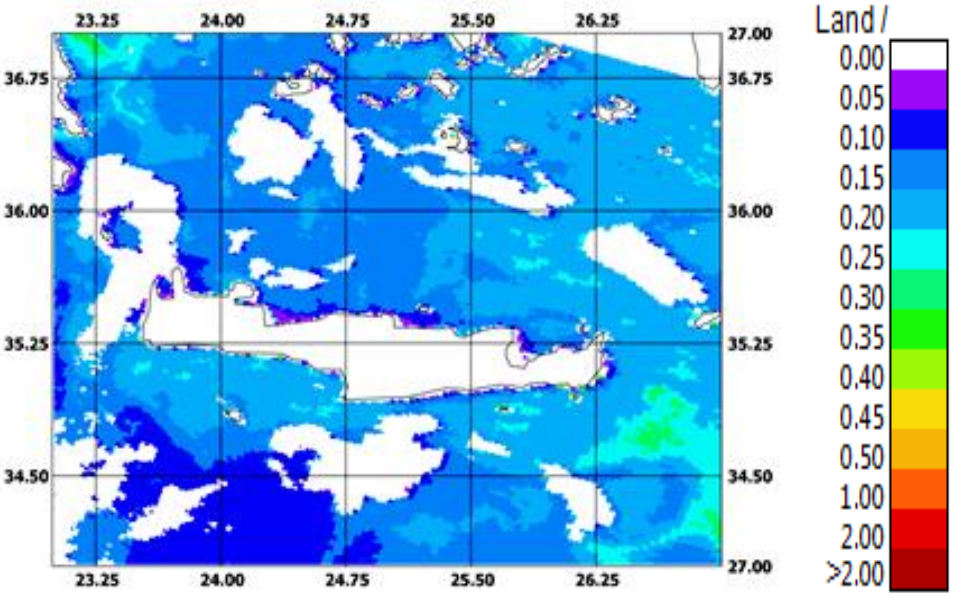

c)

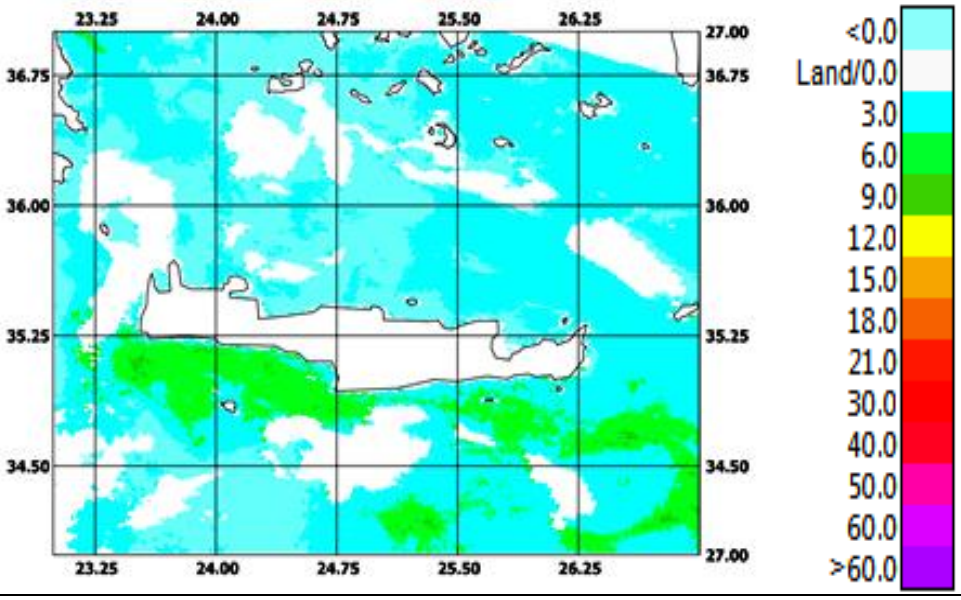

Figure 4.31 as figure 4.20 for MODIS acquisition of 30th of April 2003 at 9:50am GMT

The temporal analysis sequence of the maps provides several elements of discussion. Concerning chlorophyll-a maps, measured values in all the days seem to do not agree with the general trend we have discovered. In all the maps a lot of pixels show values quite high, up to 2 mg/m^3, which are extremely different from the one we measured in the multi-year study (0.07 – 0.17 mg/m^3), as well as from the one we achieved for April 2003 (0.167 mg/m^3). This result, first of all, confirms that April 2003 has a strange behavior in terms of chlorophyll-a concentration, and also that the operation of spatial average should be used carefully, because it could smooth high intensity peaks.

Looking at Chl-a ALICE maps, again the indications achieved by analyzing the monthly Chl-a ALICE map are confirmed: when the normal behavior of the investigated signal is very low and show a low range of natural fluctuation, its variations may produce very high relative increase. This is why we consider in this work, as statistically significant, the anomalies detected at values higher than 6. These values, as well as those at the following level (i.e. >9) have been detected almost in all the images, with an almost persistence in time and space. Tab. 3.3 reports the number of detected pixel at growing level of ALICE index.

Highest values have been detected for the image of 4 April at 09:15, where Chl-a ALICE values higher than 60 have been detected, again in correspondence of areas where chlorophyll values were higher than 0.20 mg/m^3. Similar values, but concerning a smaller fraction of pixels, have been also detected on the image of 19 April at 08:30. Finally, it seems that the strange behavior discovered for April 2003 may be due from a general increase of chlorophyll-a all along the month, even if few images, especially that of the 4 of April at 09:15, has an higher impact than the other on the final result.

Table 4.3 Number of ALICE pixels for different values levels and for every cases analyzed

Date	⊗>6	⊗>9	⊗>12	⊗>15	⊗>18	⊗>21	⊗>30	⊗>40	⊗>50	⊗>60
04/04/2003 09:15	32492	16897	7598	4049	2599	1863	901	409	164	63
09/04/2003 09:35	5926	493	88	23	9	3	0	0	0	0
09/04/2003 11:05	4973	617	126	35	12	4	1	0	0	0
12/04/2003 11:40	16550	2137	187	35	10	7	2	2	1	1
16/04/2003 09:40	3901	200	43	19	6	0	0	0	0	0
19/04/2003 08:30	4422	472	90	69	57	53	40	28	23	19
26/04/2003 11:50	6927	459	32	3	0	0	0	0	0	0
27/04/2003 09:20	13321	3267	919	251	72	18	2	2	0	0
27/04/2003 10:55	5786	1198	283	61	11	0	0	0	0	0
28/04/2003 08:25	1040	118	13	2	1	0	0	0	0	0
28/04/2003 11:40	3529	208	10	4	1	0	0	0	0	0
30/04/2003 09:50	292	7	1	0	0	0	0	0	0	0

Trying to understand these results, we looked for weather/hydrological situation of Crete island during 2003. In general, the period September 2002 - August 2003 was characterized by the highest level of precipitation (about 1423mm) in a thirty-year data period (1974-2005) (Vrochidou and Tsanis, 2012). In particular, April 2003 was extremely wet and cold with a lot of rain on Crete (data from "National Observation of Athens-NOA"): while for this month the millimeters of rain measured in Greece were between 20 and about 80 (Fig. 3.32), for the municipality of Chania this value arrived up to 124.6 mm, and was 389% higher than the corresponding rainfall value for the years 1961-1990 (NOA 2013). As indicated in Fig. 3.32, unfortunately the 36.7 mm of rain measured in Heraklion are not the final values for the investigated period for a failure occurred on 18 of April 2003, anyway they represents a value 122% higher than those observed during the years 1961-1990. The rain abundance, equally distributed on the month, leaded an increase of rivers discharge that were the mainly responsible of nutrients risen; in this way, as said, phytoplankton has access to more quantitative of nutrient and this involves an excess of chlorophyll concentration than normal which is underlined by high values of ALICE. The particular behavior of 4 of April is the finally result the last ten days of the March 2003, when the situation was the worst of the whole analyzed period (NOA 2013).

Figure 4.32 Millimeters of rain for April 2003 all over Greece ((http://cirrus.meteo.noa.gr/forecast/deltio_noa042003.pdf)

4.4 Confutation/falsification analysis

To better check for the reliability of the results showed up to now, a further investigation was carried out. In particular we looked for the presence of any significant and persistent anomalous Chl-a ALICE signals when analyzing "unperturbed" conditions. Looking at the April trend (Fig. 4.17), it can be seen as at least two months, April 2004 and April 2012 show spatially averaged values quite similar to the long period one, and so they can be considered as unperturbed one. As a confirmation of these quite conditions, the rain values measured for April 2004 were 13.4 mm for Chania and 24.7 mm for Heraklion (http://cirrus.meteo.noa.gr/forecast/deltio_noa042004.pdf), while for April 2012, 39.2 mm of rain were measured in Chania and 13.2 in Heraklion (NOA 2013). So that, the whole analysis already performed for April 2003, was done also for April 2012. First, the analysis at monthly level was performed, than the one at daily basis.

In Figure 4.32a) the Chl-a map of April 2012 is presented while the corresponding ALICE is shown in Figure 4.32b). As you can see, except that for few pixel in the South-West part of the image, Chl-a values ranges between 0.05 and 0.20 mg/m^3 in good agreement with the expected values. The same behavior is detectable in the monthly Chl-a ALICE map, where generally values lower than 6 have been detected, with a few exceptions not higher than 9.

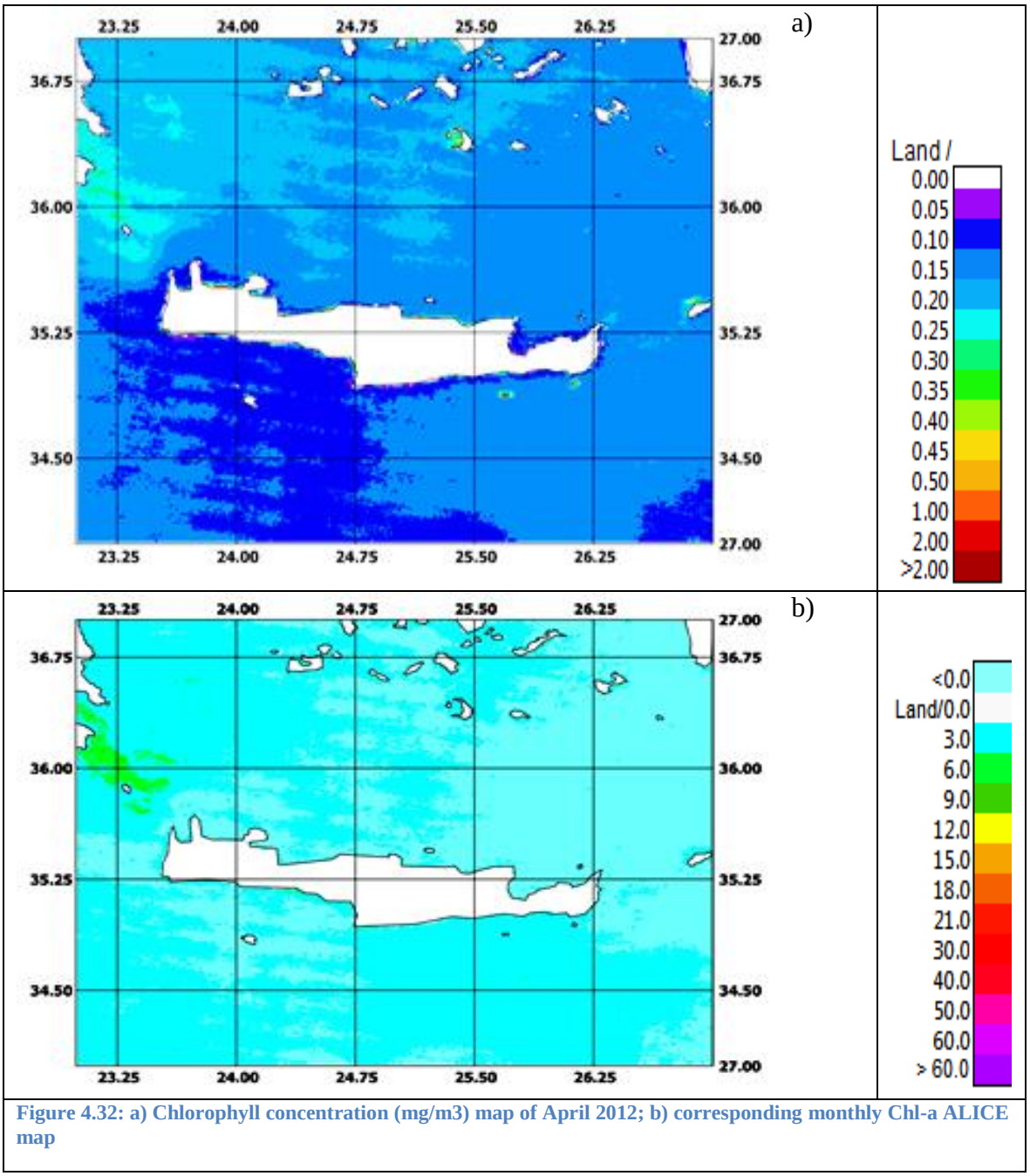

Figure 4.32: a) Chlorophyll concentration (mg/m3) map of April 2012; b) corresponding monthly Chl-a ALICE map

From Figure 4.33 to Figure 4.36 few of the daily maps (RGB, chlorophyll-a concentration and Chl-a daily map) of April 2012 are also presented.

a)

b)

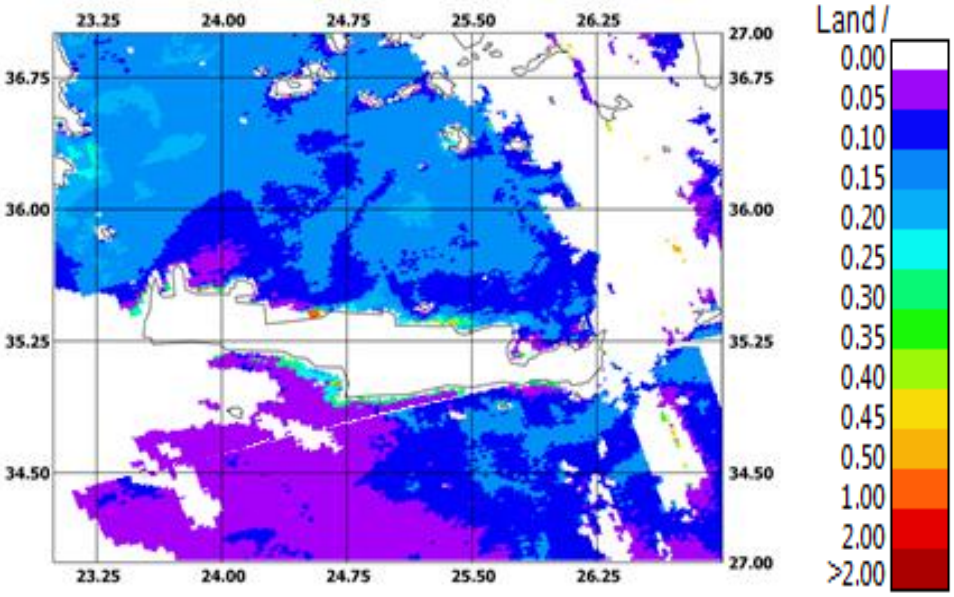

c)

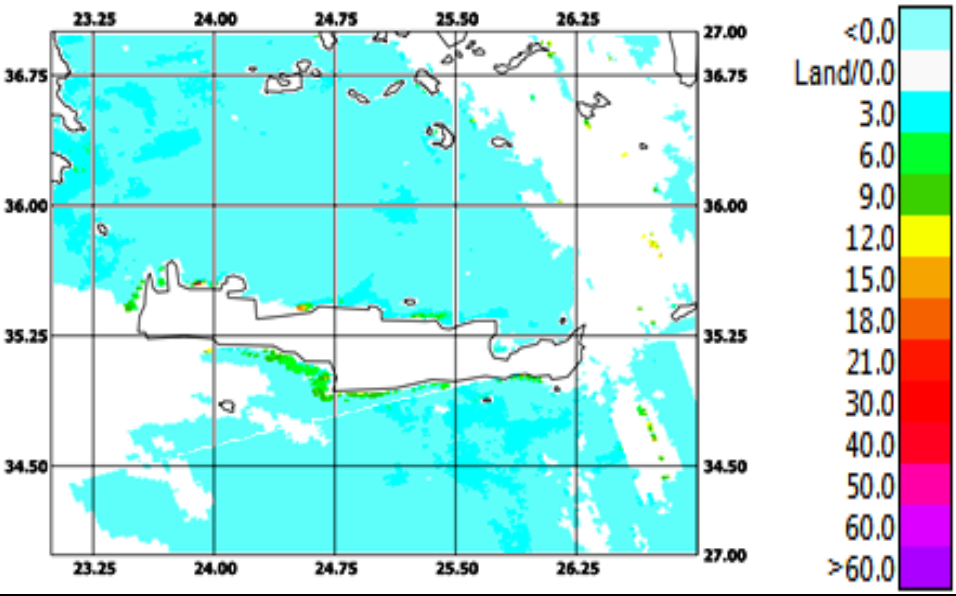

Figure 4.33a) RGB of the MODIS acquisition of 12th of April 2012 at 10:55am GMT; b) the chlorophyll map; c)ALICE map

a)

b)

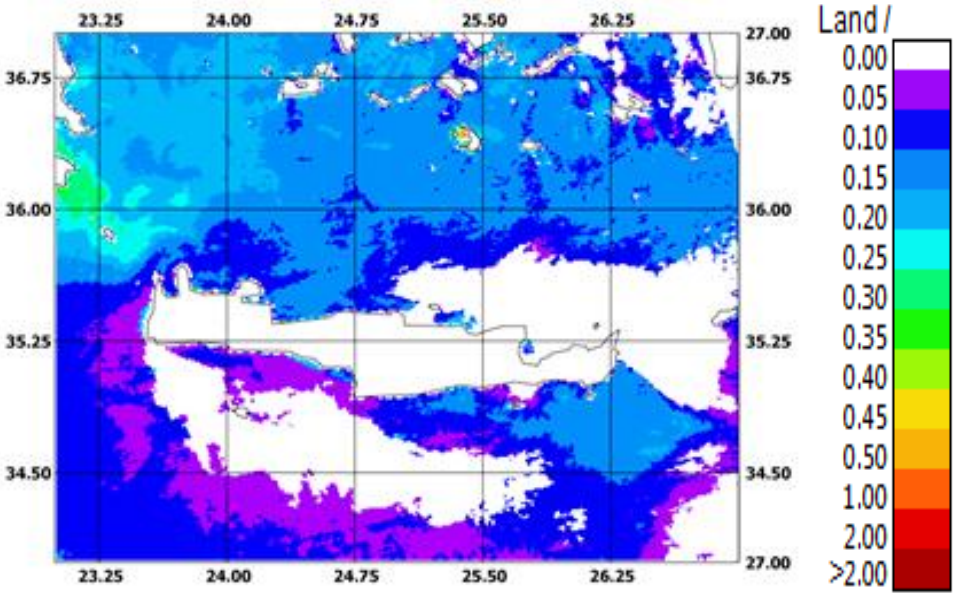

c)

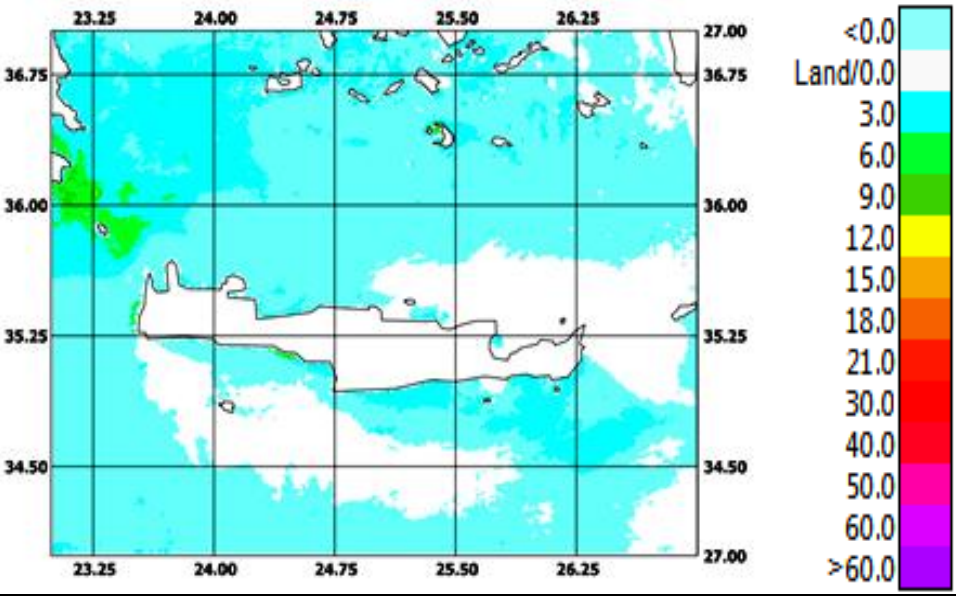

Figure 4.34 as Figure 4.33 for MODIS acquisition of 26th of April 2012 at 11:05 am GTM

a)

b)

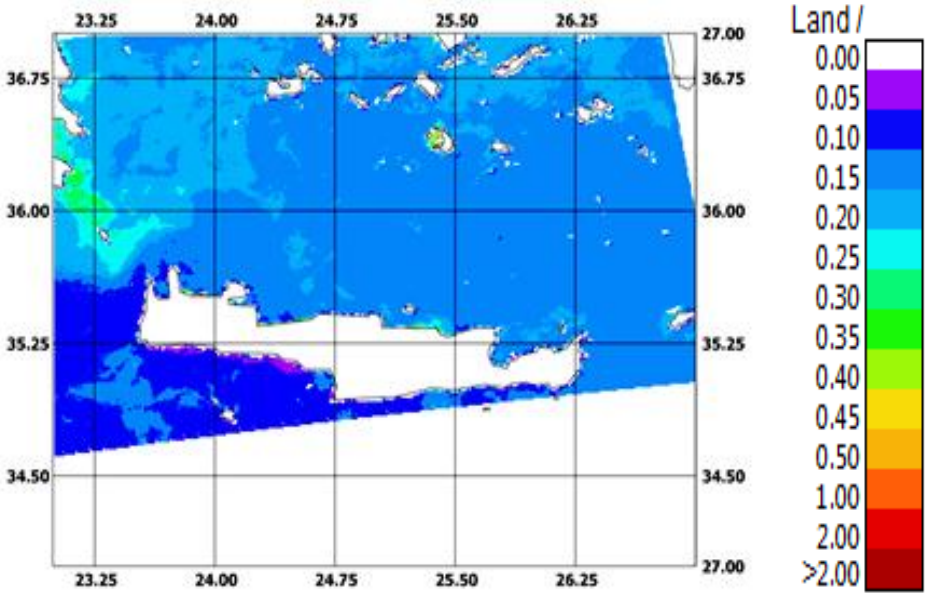

c)

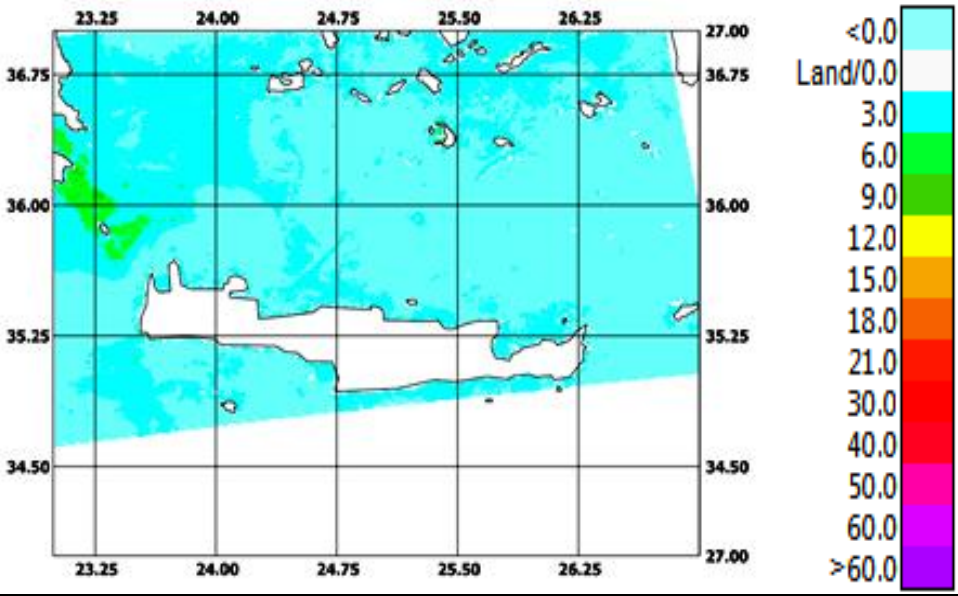

Figure 4.35 as Figure 4.33 for MODIS acquisition of 27th of April 2012 at 11:50am GTM

a)

b)

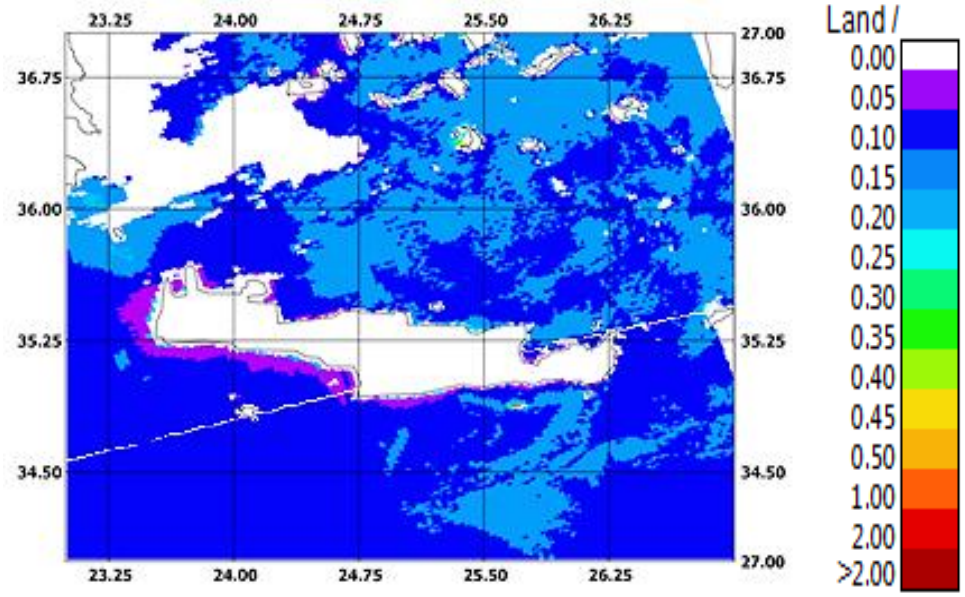

c)

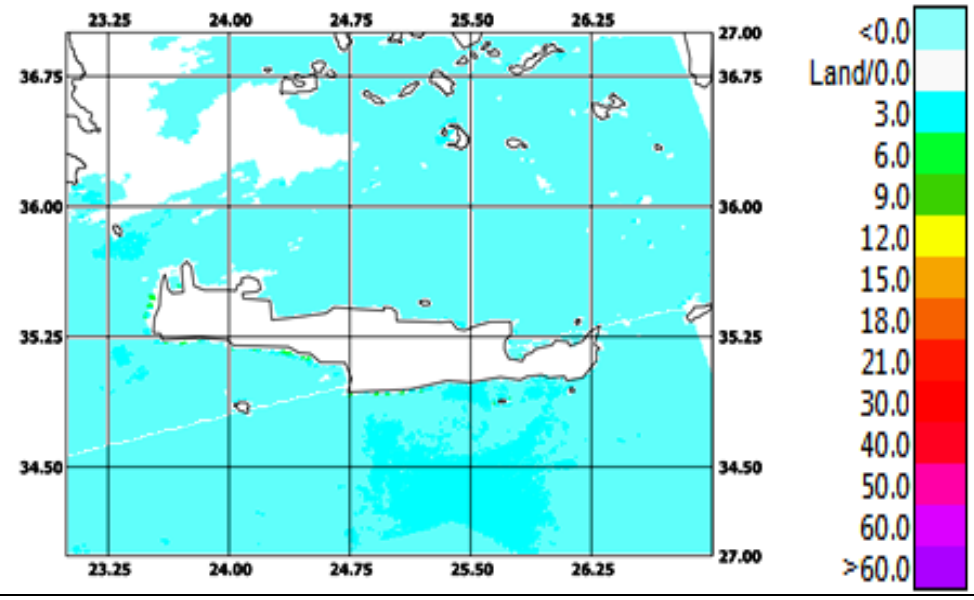

Figure 4.36 as Figure 4.33 for MODIS acquisition of 28th of April 2012 at 10:50am GTM

In Table 4.4 again the number of the pixels detected at increasing level of confidence by the Chl-a ALICE index are reported.

Table 4.4 Number of ALICE pixels for different values levels and for every cases analysed

date	⊗>6	⊗>9	⊗>12	⊗>15	⊗>18	⊗>21	⊗>30	⊗>40	⊗>50	⊗>60
12/04/2012 10.55	421	123	33	9	5	3	1	0	0	0
26/04/2012 11.05	119	5	0	0	0	0	0	0	0	0
27/04/2012 11.50	70	9	3	0	0	0	0	0	0	0
28/04/2012 10.50	6	1	1	0	0	0	0	0	0	0

By looking at these numbers, as well as to the figures just plotted, the different behavior in terms of chlorophyll variations between 2003 and 102 is clearly identifiable. For the "unperturbed" period, at least from a meteorological point of view, ALICE index values are largely below the previously identified limit. The highest values of the index have been identified in correspondence with those areas, close to the Greek coasts, already identified in the monthly map. Their spatial persistence seems to suggest that a perturbation of small intensity affected that area. This results further enhance the reliability of the proposed approach in automatically identify known or not chlorophyll-a variation.

CONCLUSIONS

Coastal ecosystems are very complex and dynamic habitats, which deserve monitoring systems adequate to provide both the identification of the water status as well as to timely identifying possible critical situation. In such a framework, remote sensing data, thanks to the capabilities to cover large areas with high temporal frequency and relatively low cost, may provide a useful support.

In this thesis the Robust Satellite Techniques (RST) approach was applied to MODIS data for investigating and monitoring sea water quality. Among the sea optical parameters retrievable by satellite, in this work the chlorophyll-a (Chl-a) concentration was analyzed in particular. This parameter was chosen as representative of the water body status due to its crucial role in the coastal sea water ecosystem. The study was focalized on the sea water surrounding Crete Island for which more than 10000 NASA MODIS Ocean Color Level 2 imagery covering the period 2003-2012 were analyzed.

The work was divided in two main activities: a long term trend and a medium/short-time analyses. The first one consisted in the generation and analysis at pixel level of the seasonal Chl-a concentration trend for the region of interest which allowed to understand the normal behavior of such a parameter, both in terms of expected values and natural variability. This trend was obtained by exploiting the above mentioned 10 years of MODIS data. Then the second analysis started investigating first the annual (i.e. for each year from 2003 to 2012) Chl-a concentration trends, looking for possible critical temporal/spatial features respect to the long term trends. Finally, once such a situation was assessed, an analysis at daily temporal scale was performed to better investigate the nature/source of the phenomenon.

Main results obtained by the first long term trend analysis are:

- The spatially averaged Chl-a concentration values around Crete Island range in a very short interval, between 0.05 – 0.2 mg/m^3, with very low fluctuations. These values are those typical measured for oligotrophic conditions, in good agreement with previous achievements concerning Mediterranean sea water;
- The highest Chl-a variability, as expected, is achieved close to the coasts, where human activities and the increased presence of nutrient influence inevitably the chlorophyll concentration. As expected, costal water in northern part of the island have a higher

dynamic in terms of chlorophyll-a concentration values: this is due by the high level of urbanization along the northern coastline.

- A clear difference between cold and warm season characterizes the chlorophyll trend: relatively high Chl-a concentration values are present during winter and fall, while low amount of chlorophyll have been detected during summer. Again, this results is well in agreement with the general behavior of Mediterranean sea and it is due to the high nutrient contribution by rivers as well the high vertical instability of water during winter season.

Results achieved by the RST based medium/short-time analysis allow to:

- Detect April 2003 as a period characterized by an anomalous behavior (i.e. from a statistical point of view) in term of Chl-a concentration variations. In particular, high values (up to 12) of the proposed index have been detected on a monthly analysis over large areas in the sea water in the southern part of the island.
- Identify, by the daily analysis, that even if all along the month high value of Chl-a concentration have been detected, the Chl-a map provided for the 4 April 2003 at 09:15 was the most perturbed one.
- Find the source of this strange behavior in the extreme rains which occurred in that period causing an extreme increase of nutrients and consequently an increase of the level of chlorophyll concentration.

Results achieved in this thesis demonstrated the potential of RST in providing useful information about sea water status, both in terms of normal status identification and timely detection of possible critical situation. The analysis at pixel level of historical series of chlorophyll products helped to reduce the negative impact of site effects on the achieved results, providing a wide characterization of the investigated area. Obviously, further studies need to be carried out, especially by integrating in situ measurements, to better assess its reliability. Anyway, considering that such an approach is completely automatic and intrinsically exportable both in different geographical areas and on different satellite sensors, it might be considered as a further useful tool for operational monitoring of sea water status.

References

Books- Papers:

A.-E. K. Vrochidou and I. K. Tsanis, " *Assessing precipitation distribution impacts on droughts on the island of Crete."* Nat. Hazards Earth Syst. Sci., 12, 1159–1171, 2012

A .Morel, and L. Prieur. *"Analysis of variations in ocean color"* Limnol. Oceanogr., 22(4), 709-722,1977

C. Filizzola, T. Lacava, F. Marchese, N. Pergola, I. Scaffidi, and V. Tramutoli, "*Assessing RAT (Robust AVHRR Techniques) Performances For Volcanic Ash Cloud Detection And Monitoring In Near Real-Time: The 2002 Eruption Of Mt. Etna (Italy)*", Remote Sensing Of Environment, 107 440–454, 2007

C. Filizzola, N. Pergola, C. Pietrapertosa, and V. Tramutoli, "*Robust satellite techniques for seismically active areas monitoring: a sensitivity analysis on September 7, 1999 Athens's earthquake*", Physics And Chemistry Of The Earth, vol n. 29 pag. 517-527, 2004

Claire J. Horwell and Peter J. Baxter, "*The respiratory health hazards of volcanic ash: a review for volcanic risk mitigation*", Springer- Verlag, Bull Volcanol 69: 1-24, 2006

C. Mobley, E. Boss, and C. Roesler "*Ocean Optics Web Book"*, available at http://www.oceanopticsbook.info/ Platt, T., N. (2013) Hoepffner, V. Stuart, and C. Brown [eds]. "*IOCCG Report Number 7: Why Ocean Colour?"* The Societal Benefits of Ocean-Colour Technology. 2008

C.D Mobley,., L.K. Sundman, C.O. Davis, J.H. Bowles, T.V. Downes, R.A. Leathers, M.J. Montes, W.P. Bissett, D.D.R. Kohler, R.P. Reid, E.M. Louchard, and A. Gleason. "*Interpretation of hyperspectral remote-sensing imagery by spectrum matching and look-up-tables*" Appl. Optics 44(17), 3576-3592, 2005.

C.D Mobley,., L.K. Sundman, C.O. Davis, J.H. Bowles, T.V. Downes, R.A. Leathers, M.J. Montes, W.P. Bissett, D.D.R. Kohler, R.P. Reid, E.M. Louchard, and A. Gleason. "*Interpretation of hyperspectral remote-sensing imagery by spectrum matching and look-up-tables*" Appl. Optics 44(17), 3576-3592, 2005.

C.D Mobley, "*Estimation of the remote-sensing reflectance from above-surface measurements*". Appl. Optics 38(36), 7442-7455, 1999.

C. R. McClain, "*Satellite Remote sensing: Ocean Color"*, Elsevier Science Ltd, p.114-126, 2009

Valerio Tramutoli, "*Robust AVHRR Techniques (RAT) for Environmental Monitoring: theory and applications*", SPIE, vol.3496 p. 101-113, 1998

C. S. L. Grimaldi, D. Casciello, I. Coviello, T. Lacava, N. Pergola, and V. Tramutoli, "*A MODIS Robust Satellite Techniques for near real time monitoring of oil spilled areas*", IEEE Gold Remote Sensing Conference. May 22-23 2008, Frascati (ESA-ESRIN), Italy, 2008.

Dale J. Van Donsel, Edwin E. Geldreich and Norman A. Clarke, "*Seasonal Variations in Survival of Indicator Bacteria in Soil and their Contribution to Storm-water Pollution*", Copyright: American Society for Microbiology, Vol.15, No.6, p 1362-1370, 1967

D.A Toole,., D.A. Siegel, D.W. Menzies, J.J. Neumann, and R.C. Smith. "*Remote-sensing reflectance determinations in the coastal ocean environment: impact of instrumental characteristics and environmental variability*". Appl. Optics 39(3), 456-469,2000.

D. Casciello, C. S. L. Grimaldi, I. Coviello, T. Lacava, N. Pergola, and V. Tramutoli, "*A Robust Satellite Techniques for oil spill detection and monitoring in the optical spectral range*", In Global Monitoring for Security and Stability (GMOSS), JRC Scientific and Technical Reports, Ed. G. Zeug & M. Pesaresi, EUR 23033 EN, pp. 294-305, 2007.

D. Casciello, T. Lacava, N. Pergola, and V. Tramutoli, "Robust Satellite Techniques (RST) for oil spill detection and monitoring", In Proceedings Multitemp 2007, Leuven, Belgio. Digital Object Identifier 10.1109/MULTITEMP.2007.4293040, 2007.

Dirk A. Aurin Heidi M. Dierssen. "*Advantages and limitations of ocean color remote sensing in CDOM-dominated, mineral-rich coastal and estuarine waters*", Remote Sensing of Environment Volume 125, Pages 181–197, October 2012 doi: http://dx.doi.org/10.1016/j.rse.2012.07.001

European Environment Agency, "*The European Environment: state and outlook 2010, marine and coastal environment*", Office of the European Union Publications, pages58, 2010.

European Commission, Guidance Document: The implementation of the Birds and Habitats Directives in estuaries and coastal zones, European Commission, pages 45, 2011.

Emmett W. Chappelle, Moon S. Kim and James E. McMurtrey III, Ration Analysis of Reflectance Spectra (RARS): An Algorithm for the Remote Estimation of the Concentration of Chlorophyll a, Chlorophyll b and Carotenoids in Soybean Leaves, Elsevier Science Ltd, REMOTE SENS ENVIRON vol. 39, p. 239-247, 1992.

Fabrizio D'Ortenzio, Salvatore Marullo, Maria Ragni, Maurizio Ribere d'Alcalà, Rosalia Santoleri, "*Validation of Empirical SeaWifs algorithms for chlorophyll-a retrieval in Mediterranean Sea A case study of oligotrophic seas"*, Elsevier Science Ltd, vol.82 p79-94, 2002.

G. Di Bello, C. Filizzola, T. Lacava, F. Marchese, N. Pergola, C. Pietrapertosa, S. Piscitelli, I. Scaffidi, and V. Tramutoli, "*Robust Satellite Techniques for Volcanic and Seismic Hazards Monitoring*", Annals of Geophysics, vol.47, no.1, 49-64, 2004

G. Mazzeo, F. Marchese, C. Filizzola, N. Pergola, and V. Tramutoli, "*A Multi-temporal Robust Satellite Technique (RST) for forest fire detection*", Proceedings of Multitemp 2007, Digital Object Identifier 10.1109/MULTITEMP.2007.4293060, 2007.

Giorgos Kallis and David Butler, "*The EU water framework directive: measures and implications*", Elsevier Science Ltd, p 125–142, 2001.

Gordon, H.R. and A. Morel, "*Remote Assessment of Ocean Color for Interpretation of Satellite Visible Imagery: A Review. Lecture Notes on Coastal and Estuarine Studies*", vol. 4, Springer-Verlag,1983.

Gordon HR, Morel AY, "*Remote Assessment of Ocean Color for Interpretation of Satellite Visible Imagery: A Review*", New York, 1983.

GUPTA, R. P, "*Remote sensing Geology*", Edit by Springer and Verlag, 1991

G. Volpe, R. Santoleri, V. Vellucci, M. Ribera d'Alcalà, S. Marullo, F. D'Ortenzio, "*The colour of the Mediterranean Sea: Global versus regional bio-optical algorithms evaluation and implication for satellite chlorophyll estimates*", Remote Sensing of Environment, 2007.

Jesper H. Andersen, Maria Laamanen et.al, "*Baltic Sea Environment Proceedings No. 115B Eutrophication in the Baltic Sea An integrated thematic assessment of the effects of nutrient enrichment in the Baltic Sea region*", Helsinki Commission, pages 148, 2009.

Longhurst A, Sathyendranath S, Platt T, Caverhill C, "*An estimate of global primary productivity in the ocean from satellite radiometer data*". J Plankton Res 17:1245–1271, 1995.

N. Genzano, C. Aliano, C. Filizzola, N. Pergola, and V. Tramutoli, "*A robust satellite technique for monitoring seismically active areas: The case of Bhuj–Gujarat earthquake*", Tectonophysics, 431, 197-210, 2007.

Noam Levin, "*Fundamentals of Remote Sensing"*, Pages 225, e-book (http://geography.huji.ac.il/personal/Noam%20Levin/1999-fundamentals-of-remote-sensing.pdf), November 1999.

N. Pergola, G. D'Angelo, M. Lisi, F. Marchese, G. Mazzeo, and V. Tramutoli, "*Time domain analysis of Robust Satellite Techniques (RST) for near real-time monitoring of active volcanoes and thermal precursor identification*", J. Physics and Chemistry of the Earth, doi: 10.1016/j.pce.2008.07.015, 2008

N. Pergola, C. Pietrapertosa, T. Lacava, and V. Tramutoli, "*Robust Satellite Techniques for Volcanic Eruptions Monitoring*", Annali di Geofisica, Vol. 44, N. 2, pp.167-177, 2001.

N. Pergola, F. Marchese, and V. Tramutoli, "*Automated detection of thermal features of active volcanoes by means of Infrared AVHRR records*", Remote Sensing of Environment, vol. 93, no.3, 311-327, 2004.

N. Pergola, V. Tramutoli, I. Scaffidi, T. Lacava, and F. Marchese, "*Improving volcanic ash clouds detection by a robust satellite technique*", Remote Sensing of Environment, vol.90, no.1, 1-22, 2004.

O'Reilly, J.E., S. Maritorena, B.G. Mitchell, D.A. Siegel, K.L. Carder, S.A. Garver, M. Kahru, and C. McClain. "*Ocean chlorophyll algorithms for SeaWiFS*". J. Geophys. Res. 103(C11), 24937-24953, 1998.

O'Reilly, J. E., Maritorena, S., Siegel, D., O'Brien, M. C., Toole, D.,Mitchell, B. G., et al. "*Ocean color chlorophyll a algorithms for SeaWiFS, OC2, and OC4: Version 4*". SeaWiFS Postlaunch Technical Report Series, Vol.11. SeaWiFS postlaunch calibration and validation analyses: part 3, 2000.

Patrick Steyaert and Guillaume Ollivier, "*The European Water Framework Directive: How Ecological Assumptions Frame Technical and Social Change*", Ecology and Society 12(1): 25. [online] URL: http://www.ecologyandsociety.org/vol12/iss1/art25, 2007;

P. Lazzari, C. Solidoro , V. Ibello, S. Salon, A. Teruzzi, K. Beranger , S. Colella, and A. Crise ."*Seasonal and inter-annual variability of plankton chlorophyll and primary production in the Mediterranean Sea: a modelling approach*", Biogeosciences, 9, 217–233, 2012 doi:10.5194/bg-9-217-2012

R. Anne Jones and G. Fred Lee, "*Chlorophyll-a raw water quality parameter*", American Water Works Association, p490-494, 1982.

R. Corrado, R. Caputo, C. Filizzola, N. Pergola, C. Pietrapertosa and V. Tramutoli, "*Seismically active area monitoring by robust TIR satellite techniques: a sensitivity analysis on low magnitude earthquakes in Greece and Turkey*", Natural Hazards and Earth System Sciences, vol n.5-1, pag.101-108, 2005.

REES, W. G., "*Physical Principles of Remote Sensing*", Edit by Cambridge University Press, 1990;

Remote Sensing of Ocean Colour in Coastal, and Other Optically-Complex, Waters-IOCCG Report Number 3, 2000.

R. M. Pope and E. S. Fry, "Absorption spectrum (380–700 nm) of pure water. II. Integrating cavity measurements," Applied Optics 36(33), 8710, 1997.

T. Lacava, V. Cuomo, E.V. Di Leo, N. Pergola, F. Romano, and V. Tramutoli, "Improving soil wetness variations monitoring from passive microwave satellite data: The case of April 2000 Hungary flood", Remote Sensing Of Environment, vol n.92-2, pag. 135-148, 2005.

T. Lacava, E.V. Di Leo, N. Pergola, and V. Tramutoli, "Space-time soil wetness variations monitoring by a multi-temporal microwave satellite records analysis", Physics And Chemistry Of The Earth, vol n. 31, pag.1274 -1283, 2006.

T. Lacava, M. Greco, E.V. Di Leo, G. Martino, N. Pergola, F. Sannazzaro, and V. Tramutoli, "Monitoring soil wetness variations by means of satellite passive microwave observations: the HYDROPTIMET study cases", Natural Hazards and Earth System Science, vol. n.5-4, pag.583-592, 2005.

T. Lacava, M. Greco, E.V. Di Leo, G. Martino, N. Pergola, F. Romano, F. Sannazzaro, and V. Tramutoli, "Assessing the potential of SWVI (Soil Wetness Variation Index) for hydrological risk monitoring by means of satellite microwave observations", Advances in Geosciences, vol. 2, pag.221-227, 2005.

Valerio Tramutoli, Robust Satellite Techniques (RST) for natural and environmental hazards monitoring and mitigation: ten year of successful applications, 2008

V. Tramutoli, V. Cuomo, C. Filizzola, N. Pergola, and C. Pietrapertosa, "*Assessing the potential of thermal infrared satellite surveys for monitoring seismically active areas: The case of Kocaeli (I˙zmit) earthquake, August 17, 1999*", Remote Sensing of Environment, 96 409 – 426, 2005.

V. Tramutoli, G. Di Bello, N. Pergola, and S. Piscitelli, "*Robust satellite techniques for remote sensing of seismically active areas*", Annals of Geophysics, vol.44, n.2, 295-312, 2001.

YSI tech note, The Basis of Chlorophyll Measurement, 0113 T606-01, Web: www.ysi.com/ www.EXOwater.com/

Zaneveld JRV, "*Optical Aspects of Oceanography*",ed Jerlov NG (Academic, San Diego), pp 121–134,1973.

Web pages:

CB 2013(visited last: August 2, 2013)

http://www.cretanbeaches.com/p%CE%BFtamia/p%CE%BFtamia/potamos-anapodaris-demati/

http://www.cretanbeaches.com/p%CE%BFtamia/p%CE%BFtamia/giofyros-potamos/

Encyclopaedia Britannica (visited last: July 28, 2013)

http://www.britannica.com/EBchecked/topic/531121/seawater#toc301660

Interkriti (visited last: August 7, 2013)

http://www.interkriti.org/crete/introduction_to_crete.html

NASA Ocean Color page (visited last August 7, 2013)

http://oceancolor.gsfc.nasa.gov/SeaWiFS/TEACHERS/sanctuary_3.html

http://oceancolor.gsfc.nasa.gov/SeaWiFS/TEACHERS/sanctuary_4.html

http://earthobservatory.nasa.gov/Features/Phytoplankton/

http://kids.earth.nasa.gov/seawifs/phyto3.htm

http://oceancolor.gsfc.nasa.gov/forum/oceancolor/topic_show.pl?tid=2332

www.oceancolor.gsfc.nasa.gov

NOA 2013 National Observatory of Athens (visited last August 6, 2013)

http://cirrus.meteo.noa.gr/forecast/deltio_noa042003.pdf

http://cirrus.meteo.noa.gr/forecast/deltio_noa042004.pdf),

http://cirrus.meteo.noa.gr/forecast/deltio_noa042012.pdf

Earth's cartography (download *.shp file) (visited last: April 2013)

http://geocommons.com/overlays/5603

Wikipedia (visited last: August 2, 2013)

http://el.wikipedia.org/wiki/%CE%9A%CF%81%CE%AE%CF%84%CE%B7

Annex

List of Tables

List of Figures